Carbonaceous materials for their use as aircraft lightning strike protection

Guillermo Mokry López

Tesis depositada en cumplimiento parcial de los requisitos para el grado de Doctor en

Ciencia e Ingeniería de Materiales

Universidad Carlos III de Madrid

Director/a (es/as):

Juan Baselga Llidó

Zulima Martín Moreno

Javier Pozuelo de Diego

Tutor/a:

Javier Pozuelo de Diego

[Mes de la defensa de tesis]

AGRADECIMIENTOS

Este trabajo no podría haber sido realizado, sin la ayuda y apoyo que todos me habéis brindado durante los últimos años. En primer lugar, agradecer a Airbus Group la concesión del contrato suscrito al "Convenio Específico de Colaboración entre la UC3M y AIRBUS GROUP para la realización de tesis doctorales conjuntas" definido en el acuerdo Marco de Colaboración Científica y Tecnológica que ambas entidades tienen suscrito, y que ha hecho posible la realización de este trabajo de investigación.

Gracias al departamento de materiales, al grupo de polímeros y composites y a Airbus, en especial a mis directores de tesis, Juan Baselga Llidó, Zulima Martín y Javier Pozuelo de Diego. Gracias a mis padres y abuelos, sin los cuales habría tirado la toalla después de tanto intento fallido. Gracias por haberme dado esta oportunidad con vuestro esfuerzo y trabajo, por haberme permitido llegar hasta aquí, y por haberme apoyado en cada momento del camino. Sois un pilar incuestionable, perenne, perpetuo y no podré agradeceros nunca todo lo que hacéis por mi diariamente.

Gracias también a todas esas personas que me han ayudado en el día a día haciendo mi camino mucho más fácil; Ángel Manuel Solanilla y Javier Sanz Feíto, cuya ayuda ha resultado inestimable para no morir electrocutado en más de mil ocasiones; a María Vila y Juan José Vilatela, que dieron una segunda vida a esta tesis con su ayuda y sus ideas; Ana Laura Elías y Mauricio Terrones, que me acogieron en un país extranjero y me hicieron sentir en casa; a Valentín García y Pedro Nogueroles, por creer en mi trabajo y ver las mil posibilidades que yo no era capaz de visualizar; a mis amigos y compañeros de sufrimiento, paño de lágrimas, quejas, risas y buenos momentos, muy especialmente a Pedro, María, Morena, las Andreas y Eric "meu" Macía. Sin vosotros esto no habría salido adelante; gracias a todo el resto de compañeros de departamento, los que están y los que se han ido, entre los que incluyo a profesores, estudiantes y técnicos que habéis hecho de las comidas muchísimo más divertidas y amenas; gracias a mis compañeros, y amigos, del máster de biotecnología, que después de casi 10 años seguís a mi lado incansables (y eso tiene mérito) y restregándome los beneficios de ser doctores, en especial a Ruth y Yovanny sin olvidar a Flori, Parras, Marcos, Ana y por supuesto a una persona muy especial en mi vida, Irene; a mi amiga incondicional Noe, que siempre está ahí cuando la necesito. A Jozelo, Andreh, Chara y Siya, compañeros de otra vida, otras tesis. Un agradecimiento aparte para Gabino, que me dijo hace casi una

década, que no todas las personas servíamos para la ciencia. Quien la sigue la consigue.

Por último, un GRACIAS con mayúscula a mi pareja, Sara. Desde que te conozco has sido un mar de bondad, ánimos, sonrisas y buenos momentos. Se dice que, si no sabes a que puerto te diriges, ningún viento te es favorable; pues ese puerto, ese remanso de paz cuando la tormenta arrecia, eres tú. Gracias.

CONTENIDOS PUBLICADOS Y PRESENTADOS

Patentes

Referencia de patente: 19382471.1-1103

Fecha: 30/07/2019

Propietario: Airbus Operations, S.L.U.

Título: Method for manufacturing a hybrid material for conducting electrical currents.

Inventores: Guillermo Mokry López, Juan Baselga Llidó, Zulima Martín Moreno, Javier Pozuelo de Diego, Javier Sanz Feíto, Juan José Vilatela, Pedro Nogueroles Viñes, Valentín García Martínez

La patente está incluida parcialmente en la tesis en los capítulos uno y cuatro. El material de esta fuente incluido en la tesis no está señalado por medios tipográficos ni referencias.

Artículos científicos

Título: High Ampacity Carbon Nanotube Materials

Autores: Guillermo Mokry, Javier Pozuelo, Juan J. Vilatela, Javier Sanz, Juan Baselga.

Revista: Nanomaterials (Basel, Switzerland), 2019, Vol 9 (3)

DOI: 10.3390/nano9030383

Url: https://www.ncbi.nlm.nih.gov/pmc/articles/PMC6474024/

El artículo está incluido parcialmente en la tesis en los capítulos uno y cuatro. El material de esta fuente incluido en la tesis no está señalado por medios tipográficos ni referencias.

Index

Abbreviations

Abbreviation	Meaning
AFM	Atomic force microscopy
BET	Brunauer-Emmett-Teller
BSE	Back scattered electrons
CFRP	Carbon fiber reinforced polymer
CNT	Carbon nanotubes
CVD	Chemical vapor deposition
DC-EPD	Direct current electrophoretic deposition
ECF	Expanded copper foil
EDA	Ethylenediamine
EDX	Energy Dispersive X-ray spectroscopy
EPD	Electrophoretic deposition
FESEM	Field effect scanning electron microscopy
GFRP	Glass fiber reinforced polymer
GO	Graphene oxide
ICs	Interconnects
LSP	Lightning-strike protection
MWCNT	Multi-walled carbon nanotubes
PREPD	Pulse reverse electrophoretic deposition
PTFE	Polytetrafluoroethylene
PVD	Physical vapor deposition

Abbreviation	Meaning
r-GO	Reduced graphene oxide
SE	Secondary electrons
SEM	Scanning electron microscopy
SWCNT	Single-walled carbon nanotubes
TEM	Transmission electron microscopy
XPS	X-Ray Photoelectron Spectroscopy
XRD	X-ray diffraction

Motivation of this thesis

The main motivation behind this work, was to substitute the current technology used as lightning strike protection in the aircraft industry. This protection is composed of metallic meshes of foils, normally bronze, copper, and in some exceptional cases, for example in some fairings, aluminum in which cases, Glass Fiber Reinforced Polymer (GFRP) material will be added to avoid corrosion that direct contact between the Carbon Fiber (from the structural Carbon Fiber Reinforced Polymer material (CFRP)) and the Al might cause [1]. The bronze mesh adapts better to parts with complex geometries and is cheaper than cooper materials, however, its electrical conductivity is lower than the ones exhibited by copper meshes or foils. For those areas that need, not only Lightning Strike Protection (LSP), but also electromagnetic shielding, copper mesh or foils will be used such as Expanded Copper Foils (ECF), which is an epoxy pre-impregnated expanded copper foil that allows automated placement on the CFRP part.

ECF weights vary from 73 gm^{-2} to 815 gm^{-2}. The selection of the ECF weigh will depend on the substrate (type of CFRP with which the part is manufactured), the presence of other materials in the part (e.g. insulating GRFP), the thickness of the part, the zoning of the aircraft (components are classified into different zones according to the probability of receiving a lightning strike and to the current flow allowed by the component design) [2], and on the function of the part in the aircraft. The weight will be chosen in order to reach the best electrical requirements with the minimum weight.

However, copper being such a dense element (8.9 gm^{-3}) makes this technology relatively heavy. Being one of the main goals in the aerospace structures design, the reduction of weight and thus, the lower fuel consumption, a new material lighter than those currently in use for lightning strike protection appears as a great and interesting opportunity for the aircraft industry.

The material to replace the current solutions shall meet the following criteria: The overall density had to be smaller than the one of copper. If aircraft industry searched for an alternative, it would be to improve on the existing materials. A lower density material would reduce the overall weight of the protection system and would therefore reduce fuel consumption. Other metals with a lower density have been tried in the past, such as aluminum. However, it has been found that this metal in contact with the

carbon fibers in the airframe structure, causes a severe galvanic corrosion which makes its use not recommended for lightning strike protection [3].

Conductivity had to be the same as copper: Copper being one of the best conductors, with a conductivity close to $6 \cdot 10^7$ Sm^{-1} [4], is the perfect material for lightning strike protection. When lightning strikes, this mesh or foil is able to conduct the current away from the striking point towards electrostatic dischargers and diversion traps. If a new material was to be found, it would have to be at least as conductive as pure copper.

The maximum current density of the material had to be at least the one of copper: when a lightning pass through a conductor, this conductor is subjected to a big current density across a small cross section area. If the maximum current density this material could withstand (ampacity) was to be higher, it would allow a reduction of the cross section of the conductor, reducing like this the overall weight and space required for the lightning strike protection system.

During the course of this project, several limitations have oriented this work in very concise directions; scalability, being this an important factor when deciding which techniques to use for the synthesis of the new material, as it had to be possible to produce the material for industrial use; cost, as any expense increase in the production step, would make the main motivation of reducing costs in the final airplane implementation step futile; manageability, being very important for the material to be easily handled and resistant, to allow and easy, and as much as possible automated, integration in the airframe structure. Finally, the choice of materials was also a very important factor to take into account during this project. As it has been stated, aluminum exhibited lower densities, but caused galvanic corrosion when they are in contact with carbon fibers. Using carbon fibers on their own might prove light and cheap, but the conductivity values are below the requirement to withstand lightning strikes, especially since carbon fibers in the aircraft structure are impregnated with polymeric resins. These factors suggested that using copper as a part of a hybrid material, could be the best alternative to the problem at hand. This thesis presents the work of how a hybrid material consisting of copper and carbon was synthesized, and the many combinations and techniques that were tried.

Chapter 1: State of the art

Lightning strike protection systems

Lightning strikes mostly occur at altitudes between 5000 - 15000 feet (1,524 to 4,572 meters), when aircrafts pass through cumulonimbus clouds in which static charges are built up. Lightning initially attaches to an airplane extremity in one spot (random, forward fuselage, nacelle, empennage, or wing tip) and exits from another. In addition, it manifests as a brilliant flash of light, smell of burning material and noise. In airplanes, damage can occur to avionics and fuselages although significant structural damage is rare. The damage caused by lightnings in aircrafts, can be classified into two main categories; direct effects, associated with the physical damages which occurs at the attachment point, and indirect effects, that are related to the electromagnetic coupling with the cables and the system [5]. Direct effects can be subdivided into thermal and mechanical constraints. After the lightning attaches, the current will cause the increase in the temperature of the material, causing melting and puncturing. Mechanical constraints are usually caused by the explosion induced by the very sharp temperature increase within microseconds. This overpressure causes the propagation of a strong shock wave which is the cause for mechanical strains. On the other hand, indirect effects are usually observed as an overvoltage, and some other phenomena (such as edge glow) which are not fully understood up to date.

To understand how lightning strikes might affect an aircraft, it is first very important to understand how these strikes evolve in time [6]; first, a step leader occurs. It starts in the cloud and moves in small steps of around 50 meters each. In this step leader there is a high concentration of negative charges which come from the cloud. The air becomes ionized along the path of the leader. This causes the air to become effectively, a conductor. The moment the leader touches ground there is a connection made between the cloud and ground, which causes the negative charges to be dumped through the bottom of the step leader which, in turn, leaves positive charges behind attracting even more negative charges from higher up the leader. This returning positive charge is known as "return stroke", which is the brightest and the one usually observed in stormy days. When the return stroke has disappeared, a new step leader goes down through the old path.

However, this time, there are no steps and instead moves directly towards the ground in a strike known as dark leader. It happens again and again and as many as 42 times though the same path. The current that is produced in a lightning strike is around 200,000 Amperes and it carries around 20 Coulombs [7]. In an aircraft, this lightning attaches at one point and is conducted towards an exit area, such as diversion traps or electrostatic dischargers, and therefore, the protection system must withstand extremely high current densities in small time periods. The maximum current density a material can withstand without failing is known as ampacity, as it was defined by Subramaniam et al [8]. This thesis, appeared from the need to find new materials, which could conduct lightning strikes as effectively as copper, and with an ampacity which could rival or excel the one shown by the metal. However, for understanding how this ampacity works for any material, it is important to define and explain the process that governs at the point where extremely high current densities are able to alter matter. This process is known as electromigration.

Electromigration

Electromigration has been occurring for hundreds of years, but it was not until the appearance of integrated circuits in 1966 when the problem became a concern for industry [9]. Electromigration occurs whenever there is a current flow through a conductor, but the conditions for electromigration to cause failure in a conductor could not be met at the time; for instance, the bulk wires used for conducting current at home would have a maximum current density of about $1 \cdot 10^4$ Acm^{-2}, but the failure of these cables would occur due to Joule heating and not to the electromigration process as such. However, with the irruption of integrated circuits [10], came new problems which no one had predicted, and as the conductor strips where being placed in contact with heat sinks, Joule heating failure mechanism was relegated to a second place, which gave way to the main failure mechanism we still experience today; electromigration.

The first integrated circuits were made out of very thin aluminum lines, a material which due to its low melting temperature (660 ºC) and to the many small grain boundaries it possessed, caused very rapid metal diffusion when enough current densities were passed through. This was the effect of electromigration, although at the time it was still not completely understood.

But to understand why electromigration is such an important phenomenon in metallic interconnects it is important to understand the whole process and failure mechanism. When a current is passed through a conductor, the metal ions are exposed to two different forces which act in opposite direction to each other [11]. One of these forces is due to the electric field and the charge of the metal ions, which causes the positively charged metal ions to be attracted to the negatively charged electrode. However, the shielding of the electrons in the conductor, makes this force neglectable for most of the models which have been considered through the years. This, therefore, leaves us with one force which acts in the same direction as the current flow, and occurs due to the exchange of momentum between the moving electrons and the metal ions. In the case of a perfect lattice, such as those which occur in a homogeneous crystalline structure near 0 Kelvin, there is hardly any exchange in the momentum between the moving electrons and the metallic ions.

However, above 0 Kelvin, this perfect lattice cannot occur due to the many defects that can be found [12]. Point defects, such as vacancies, caused by the movement of atoms in the lattice, or impurities, due to the material purifications methods which are not 100% effective; planar defects, such as grain boundaries which are caused by two separately growing crystals coming into contact, and causing two different crystallographic directions at the juncture; linear defects, such as dislocations (both edge and screw type) due to the misalignment of the lattice atoms. Apart from those defects, there is also the fact, that above 0 Kelvin atomic vibration occurs, and the metal atoms are placed out of their perfect lattice position about 10^{13} times each second [13]. This causes the metal ions to move into the path of the electrons periodically, causing the momentum exchange due to electron scattering, and in term initiating diffusion of metallic atoms away from that point. This causes eventually a thinning of the conductor, leading to a short-circuit. In places such as grain boundaries, or vacancy defects, where there is free space available for the moving atoms. At the same time, in grain boundaries there is a change in the symmetry which characterizes the bulk crystal lattice, which makes the collisions between the moving electrons and the metallic atoms much more frequent. Grain boundaries are also known for having weaker bonds than the rest of the crystal, so all these factors just makes grain boundaries to be the preferential sites for electromigration to occur.

Although metal behavior is the one being referred to constantly, it is important to mention that electromigration has also been seen to occur in

semiconductors which have been heavily doped [14]. In n-type semiconductors, where the electrons are the main charge carriers, the diffusion occurs in the same direction as the current flow, whereas in p-type semiconductors, where the charge is being carried mostly by holes, the diffusion phenomenon occurs in the opposite direction to the flow.

Interconnects, as it is possible to deduce from the explanation above, being the place where the current pathways change from being macroscopic to being usually smaller, is one of the first places for failure to happen. The conductor dimensions usually change at this point, making the current density to be much higher once it enters the smaller circuit's cross section areas. If the power required for these electronical devices is always increasing, and the dimensions of the conductors are constantly being decreased, it is easy to figure out that a limit will be soon reached and won't be long until electromigration becomes the limiting factor.

As well as miniaturization, there has been an increased research interest in finding materials that can withstand huge current densities in the aeronautical industry. Current lightning strike protection systems are made of copper expanded foils in most cases, and if they are to withstand the 200 kA that a lightning can produce [7], they must have a thick cross section area. Trains and commercial aircrafts contain several tons of copper, if a different material could reduce the weight by one third, it would mean a reduction of 25,000 tons of fuel saving and 78,000 tons of CO_2 emission to the atmosphere per year [15]. According to the international roadmap for devices and systems [16], it is of utmost importance to find non-Cu solutions to cope with the increased electromigration risk due to the decreased volume of metal and the ramping of the current densities used, and one of the proposed lines of research, focuses on the use of carbonaceous materials. This thesis presents the results that have been achieved, during the four-year studies, following the use of carbonaceous materials for achieving low density high "ampacity" hierarchical hybrid composite materials.

Defining ampacity

The previous section states, that the main goal of this thesis is to find a low density high "ampacity" material. However, the term "ampacity" has not been defined. So, what is ampacity exactly? Ampacity is just a way of calling the maximum current density that a material can withstand before failure

occurs. Electromigration, as it has been explained before, starts the moment the first electron passes through. However, there must be sufficient "wind force" [17] to create enough momentum exchange to make the lattice atoms move. The term ampacity therefore refers to this point, at which movement of lattice atoms occur, and therefore resistivity begins to increase. This was defined perfectly by Subramaniam [8], where ampacity was defined as "the maximum current density at which the resistivity remains constant".

There are usually two ways that can be used for calculating ampacity. The first one is a theoretical approach, where formulas are resolved to determine the maximum current a material could withstand. However, for this approach, information about the material being studied must be known beforehand as it will be explained in the following paragraphs. In the case of unknown materials, or composites made of two or more materials, the use of these formulas is limited to mere estimations, and not real values of ampacity. For these cases, the second approach is required. This approach consists of the calculation of the ampacity by applying high currents to a line made of the studied material. By knowing the cross section of the conducting line, it is possible to determine the ampacity. These two methods are explained in detail in the sections below.

Calculating ampacity theoretically

In 1961 Huntington and Grone [18] reported the electromigration phenomenon for the first time by using light scratches on the surface of a gold wire, to which they applied a current density of 10 kA for days and observed how these markers moved. This was evidence enough to believe there was a driving force which had to do with the current density and the self-diffusion constant.

This gave birth, to the famous Huntington and Grone's equation (equation 10 below) which is one of the main equations used today for calculating ampacity. To understand this equation however, it is necessary to understand how Huntington and Grone came to this final form. Atomic diffusion can be thought, as the movement of ionized particles in a lattice. This diffusion, has a velocity caused by an external force, which can be expressed as follows:

$$\mathrm{v} = MF \qquad \textit{Equation 1}$$

Where *M* is the mobility, having units of velocity per unit of force, *v* is the diffusion velocity and *F* is the driving force. According to the Nernst–Einstein equation by which diffusion coefficients can be calculated, it is possible to stablish a direct relation between diffusion coefficient *D* and mobility, being both proportional to each other and therefore giving rise to the following equation:

$$M = D/kT$$ *Equation 2*

Where *D* is the diffusion coefficient; *K*, Boltzmann constant and *T* the temperature in degrees (Kelvin). Diffusion coefficient obeys a relation close to an exponential Arrhenius plot and can therefore be written as

$$D = D_0 \exp\left(\frac{\phi}{kT}\right)$$ *Equation 3*

Where ϕ is the activation energy of diffusion and D_0 is a prefactor that expresses the frequency of the collisions. On the other hand, we can stablish a relation between the number of particles passing through a certain cross section at a given time, with the velocity of the particles by the formula shown below, where *J* is the particle flux, *v* the velocity of the particle and *N* is the particle density.

$$J = Nv$$ *Equation 4*

By joining equations 1, 2 and 4 we can obtain that the flux of ionized particles caused by an external force will be given by

$$J = \frac{ND}{kT}F$$ *Equation 5*

As it has been stated in the section above, the driving force *F* in the case of electromigration, consists of two main forces; one, acting on the electric charge in an electric field *E*, and the second force which will be due to electron collisions. If we understand that an electric field is the force exerted per unit of charge, then we can write it as

$$F_c = qE = C_1 eE$$ *Equation 6*

And the force transmitted by the collisions with electrons as

$$F_e = C_2(-e)E$$ *Equation 7*

Where in both cases C_1 and C_2 are constants, q is the ionic charge and e, is the charge of an electron. If electric field (E) is proportional to the current density (j), and resistivity (ρ) is inversely proportional to current density, then we obtain that

$$j \propto \frac{1}{\rho} \; and \; J \propto E \rightarrow j = \frac{E}{\rho}$$ *Equation 8*

Therefore, it is possible to state that the driving force will be given by

$$F = F_c + F_e = (C_1 - C_2)eE = Z^* e\rho j$$ *Equation 9*

Where Z^*, is the effective valence also known as the effective charge. The value of the effective valence is the sum of the wind valence, which represents the sign and magnitude of the exchange of energy between the moving electrons and the direct valence, which is the nominal valence of the conductor. If we merge equation 9 with equation 5, we obtain Huntington and Grone's equation as shown below:

$$J = \frac{ND}{kT} Z^* e\rho j = \frac{ND_0}{kT} \exp\left(-\frac{\phi}{kT}\right) Z^* e\rho j$$ *Equation 10*

Where J is the particle flux, N is the particle density, D the diffusion coefficient, K and T Boltzmann constant and absolute temperature respectively. Z^* is the effective valence also known as the effective charge, e the charge of an electron, ϱ resistivity and j current density. Lastly, ϕ is the activation energy of diffusion and D_0 is a pre-factor that expresses the frequency of the collisions. From equation 10 it is possible to deduce, that the sign of the effective valence will give the direction of movement for the atomic migration. If migration occurs for example in the same direction as the electron flow, then the effective valence value will be negative. From equation 1, it is possible to observe that the mass flux caused by electromigration is directly proportional to the current density, the diffusion coefficient and the concentration of diffusing atoms.

This equation was used for years, until 1968, when James R. Black [19] found that the electromigration driving force was not proportional to the current density, but to the square of current density. In his opinion, the first

models that had appeared for electromigration were not sufficiently exact, as they had used a very narrow distribution of current densities, so he tried to replicate the measurements with a wider range of current densities and soon realized that the mean time for failure of the conductors depended inversely on the square of the current density. This gave way, for Black's law as seen in equation 2, which is the one used up until today for electromigration measurements:

$$\frac{1}{MTF} = Aj^2 \exp(\frac{\phi}{k_b T})$$ *Equation 11*

Where *MTF* is the median time to failure in hours; *A*, the cross-section area of the film; *j*, the current density in amperes per square centimeter; ϕ, the activation energy in electron volts; k_b Boltzmann constant and *T* the film temperatures in degrees.

In this same study it was also observed, that the mass transport during electromigration occurred preferentially through the grain boundaries and the surface of the conductor and could be measured through the activation energies of these: In the case of an aluminum conductor with fine grains, the activation energies that were calculated from the equation above were in the order of 0.48 eV, whilst in well ordered, large grained aluminum the activation energy raised to 0.84 eV. This increase in the activation energy was quickly attributed to the higher energy surface and bulk diffusion pathways which the atoms had to follow when the low energy grain boundary diffusion pathways had been severely reduced. It was also noticed, that above 275 degrees Celsius the predominant diffusion was through the lattice and therefore grain and surface diffusions were not important.

However, things were not that simple, and it was soon realized that both Black's law and Huntington's law were right, and it all depended on the type of failure that occurred, if it was nucleation or growth dominated which depends strongly on the method used to construct the line. Most aluminum lines for instance, are often placed on top of a refractory metal known as shunt. Through these shunt layers the electric current can bypass the void formed in the conducting line when electromigration occurs, and in these cases the failure mechanism is growth dominated, and failure occurs once the void is too big and breaks connection, and in this case a 1/j kinetic must be used. However, if there is no shunt layer then the failure is nucleation and migration dominated and follows Black's law instead. On some

occasions it is even possible to have both nucleation and growth kinetics at the same time, and a power on the current density cannot be used to explain it. These two mechanisms are represented on Figure 1.

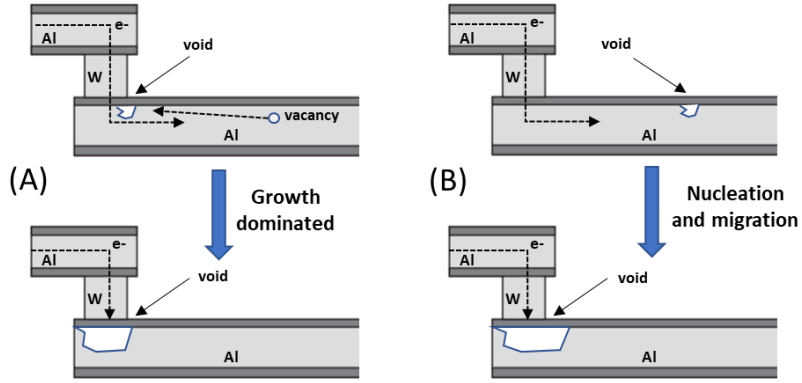

Figure 1: Two different mechanisms of void formation in copper during electromigration stress for (A) which is due to growth dominated failure, and (B) which corresponds to nucleation and migration [20]

There are several diffusion paths available through a conductor, namely lattice, grain boundary, material interfaces and dislocation cores. Lattice diffusion has the highest activation energy [21], it means that the mass transport through this pathway will be the slowest, whilst grain boundaries and interfaces have lower activation energies, which means that mass transport will predominate through these paths. On the lowest activation energy level, we have surface diffusion. However, it is interesting to see that this diffusion mechanism is blocked whenever there is a passivation layer on the surface of the conducting line, so it will not be available for metals, such as aluminum or titanium, that form passivation layers whenever exposed to air. Therefore, to account for the effective diffusion (total diffusion occurring) it is necessary to add all of these individual diffusion pathways with their corresponding fraction of atoms that diffuse through them. This can be seen in equation 12 below:

$$D_{eff} = D_{lattice} + f_{gb}D_{gb} + f_i D_i + f_c D_c \qquad \textit{Equation 12}$$

For a dual damascene interconnect the effective diffusivity according to bibliography [22] can be expressed in terms of thickness of grain boundaries (δ_{gb}) and interfaces (δ_i), average grain diameter (d), dislocation density (ρ_c), cross section area of the dislocation core (a_c), line width (w) and line height (h).

$$D_{eff} = D_{lattice} + \delta_{gb}\left(\frac{w-d}{wd}\right)D_{gb} + \delta_i\left(\frac{w+h}{wh}\right)D_i + \rho_c a_c D_c \qquad \textit{Equation 13}$$

The diffusion coefficients are expressed by a simple Arrhenius law. From equation 13, one can observe that the effective diffusivity depends strongly on factors such as the microstructure, temperature and the quality of the interface between the conducting layer and other layers. At higher temperatures, the diffusion rate increases whilst the opposite happens with lower temperatures. Also, if there is a temperature gradient along the line there will be regions with different diffusion rates resulting in hillocks and void formation indistinctly. So, temperature has a huge effect on the mass diffusion during electromigration. On the other hand, microstructure is another factor which greatly affects the mass transport. A film with a uniform size of grain will have a network of grain boundaries which will meet at triple points [12]. A representation of this triple points can be observed in Figure 2.

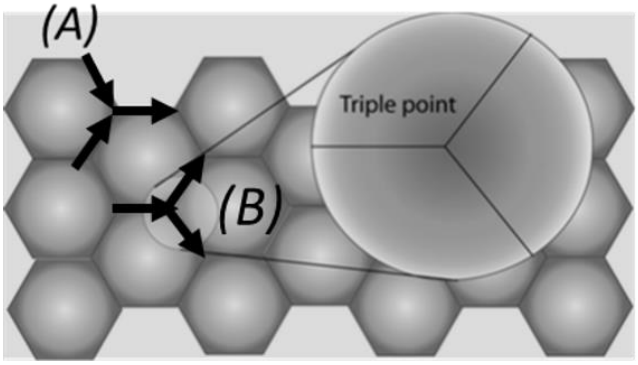

Figure 2: A) and B) are triple point regions, places where crystallographic directions change from one grain to the next. These points are the usual spots where regions of depletion or accumulations occur, and it depends on the structure of the triple point. (B) If one grain boundary leads to two grain boundaries, there will be an area of depletion of mass causing voids, whilst two grain boundaries leading to a single grain boundary will lead to mass accumulation and therefore a hillock formation (A) [20]

At this triple points, crystallographic directions change from one grain to the next, so it is easier to find divergences in mass transport at these points. Depending on the type of triple point found, being possible that one grain boundary leads to two other grain boundaries, in which case there will be more mass leaving the triple point than entering so a void will form (causing eventually an open circuit if no shunt layer is present), or two grain boundaries joining with a single grain boundary, leading to a mass accumulation and a hillock formation (causing a short circuit between adjacent lines). Following this idea, smaller grain sized metals will lead to

the formation of more grain boundaries (and therefore triple points), than bigger grained metals.

From equation 4, it is also possible to observe some design rules that should be taken into consideration. As illustrated in Figure 3, if the line width is larger than the grain size it will contribute to the overall electromigration by creating pathways of grain boundaries throughout the line (polycrystalline line), but oppositely, interfacial diffusion will become the preferred diffusion pathway when the linewidth is smaller than the average grain size, as there will be no continuous path of grain boundaries throughout the line (bamboo-like structure).

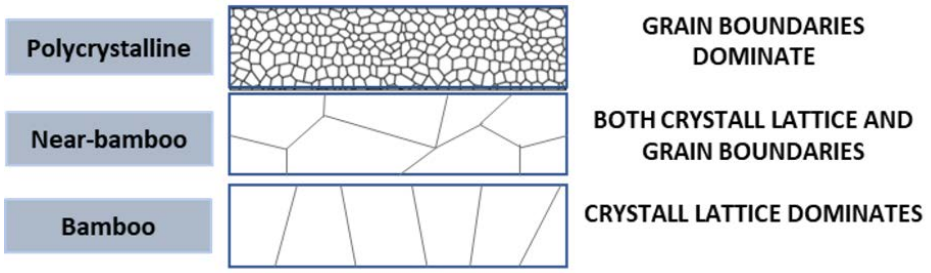

Figure 3: Different kinds of crystal structures which contribute to different preferred diffusion pathways during electromigration. Polycrystalline lattice has many small grain boundaries and therefore diffusion would be dominated by grain boundary diffusion although other types of diffusion also occur. On the other extreme, near-bamboo or bamboo structures will have lattice diffusion as its primary diffusion pathway, although near bamboo would also present grain boundary diffusion depending on the size of the line diameter with respect to the grain size [20]

Gradients might also occur when two or more metals are used (or two different materials), as there will be regions with different grain sizes leading to mass diffusion changes throughout a line.

This fact is specially observed in contacts and vias, as there is an impossibility of the diffusing metallic atoms to cross the materials used in them, and therefore there are voids and hillocks formed at the contact. An example of hillocks formation during an experiment with carbonaceous-copper composites, when the ampacity of such material was reached, can be observed in Figure 4.

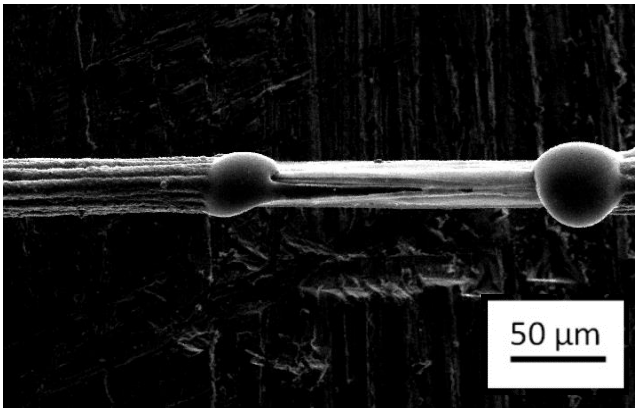

Figure 4: SEM micrograph depicting a copper-graphene oxide fiber. Hillock formation during electromigration process can be observed at both edges, as lumps of accumulated copper. Scale bar 50um.

Electromigration however does not only depend on the current density as it was shown by Blech [23], and depends also on a critical length of the line being used. The equations for Blech effect are out of the scope of the review, but we can summarize it by saying that the Blech effect consists of three separate concepts; Blech product, Blech length and Blech condition, all of them are related to the stress gradients which opposes the mass flow during electromigration. As stress gradients build up in the lines to oppose the electromigration force, hillocks and voids help relieve these stresses (also known as back stress). However, after some time, the formation of a void might cause an open circuit if a shunt layer is not present to bypass this point, and a hillock might cause two separate lines to come into contact causing a short circuit. This stress factor was therefore incorporated into the equation 1 to account for this new observed parameter and this way, equation 14 was obtained.

$$J = \frac{ND}{kT}(Z^*epj - \Omega\frac{\Delta\sigma_{nn}}{\Delta\sigma_l}) \qquad \textit{Equation 14}$$

Where Ω is the atomic volume, σ_{nn} the stress normal to the grain boundaries and l is the distance along the line. Blech observed that whenever the line length was below a critical value, electromigration could be avoided. In these cases, stress forces would grow and eventually would have the same dimension but opposite of the electric field (equation 15).

$$Z^*epj = \Omega\frac{\Delta\sigma_{nn}}{\Delta\sigma_l} \qquad \textit{Equation 15}$$

In this case, as the stress gradient would be stable at the value for balancing the electric force, there will be no gradient whatsoever, therefore approximating equation 15 to the one shown by equation 16, which is known as the critical Blech length, or the longest conductor possible where electromigration would not happen.

$$(jl)_{critical} = \frac{\Delta\sigma_{nn}\Omega}{Z^* e\rho} \qquad \textit{Equation 16}$$

Measuring ampacity experimentally

Ampacity, as it has been explained above, could be theoretically calculated using the above formulas, but for most of the new emerging materials, some of the parameters such as activation energies would be unknown. Therefore, there is an emerging necessity to develop methods, that would allow to measure ampacity at any size scale.

Generally, with microwires, the way to measure ampacity is straight forward. However, a 4 point-probe measuring method would always be recommended, as this would remove any error that could arise from the cabling being used. By running a current-voltage cycle, one would be able to determine (by using Ohm's law) the resistance of the material at each different current. This would allow the user, to determine resistivities for each current measured during the test. The current at which the value for this resistivity increases would be the one to use for calculating the current density, by dividing by the cross section of the material as seen in Figure 5.

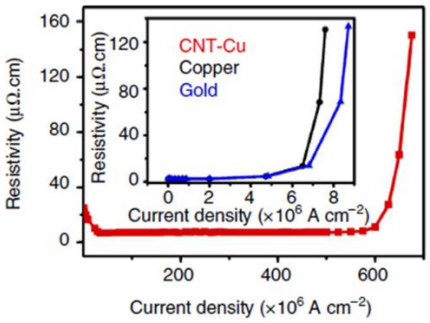

Figure 5: The way for determining ampacity experimentally is to present resistivity vs current density. The resistivity should remain constant up until the ampacity point, which would be the moment when resistivity rises abruptly by more than 20% [8].

This kind of measurement has been done with the micrometer and sub-micrometer scale before, and even simultaneous characterization of the

material can be done by using techniques such as STM or AFM, which allows for the live visualization of how the morphology changes with current [24].

A good guidance for determining the kind of diffusion that is occurring (lattice, surface or grain diffusion) would require to know the activation energy of the composite material. Higher activation energies would suggest that the diffusion pathways chosen by atoms for electromigration would be the less energetically favorable such as lattice diffusion, whilst smaller values would suggest grain diffusion. Determining activation energies can be done with any conducting material, by plotting an Arrhenius plot in which the slope would correspond to the activation energy.

However, it is important to notice that size would be a big limitation when choosing the right power unit, as bigger cross sections would require more current to be able to reach the ampacity point. If we take bibliographical values for copper ampacity [25] we would need to apply a current of approximately 75 KA to reach the failure point of a line with a cross section of 400 micrometers. One way to avoid these huge currents would be to diminish the cross section of the desired material, but then other phenomena could come into play, such as changes in crystalline structure (from polycrystalline to bamboo type for instance) or changing the length of the conductor, reaching the critical length defined by Blech's length, preventing electromigration all together. On the other hand, if instead of using a line, there was a requirement for measuring the ampacity of a larger 2D material, the difficulty would be even higher as there are no measuring systems nowadays, that allow this kind of measurement in macroscopic laminar like materials. However, during the duration of this thesis, we have begun working on a new device, that would theoretically allow for the experimental measurements of laminar materials. This will be explained in later chapters.

Evolution of high ampacity materials

Metals as high ampacity materials

Ampacity, as it has been explained in the electromigration introduction section, was not always observed, as most of the times the failure mechanisms consisted of Joule Heating. However, with the irruption of integrated circuit, Joule heating gave way to electromigration failure, and soon many different materials were being tried, in search of a higher ampacity material. As a way of illustrating this fact, a short summary of the main materials that were used during the years of electromigration zenith is presented below:

The first interconnects, as it was explained at the beginning of this chapter, were fabricated with aluminum, but by the end of the 1960s Blech exposed the idea that aluminum ICs were failing due to electromigration [26]. Several years later Black [19], systematically studied the phenomenon varying several parameters and came up with an equation by which, theoretically, one could construct aluminum lines with infinite lifetime, by taking into consideration current densities, conductor temperatures and conductor cross sectional areas. However, it was soon discovered that these infinite lifetime lines could not really avoid electromigration due to grain structures and other defects, and soon many articles related to this electromigration phenomenon topic appeared [26]–[28], explaining the relation that was observed between the aggregates that were being formed at exactly the different grain sizes transition points. Exactly two-thirds of the defects that were being found in the aluminum lines were at these transition points. This can be easily understood by looking at the activation energies for the different kinds of diffusion in aluminum; bulk diffusion had an activation energy of 1.2 eV whilst surface diffusion was 0.8 eV. On the other hand, grain boundary diffusion had an activation energy of 0.7 eV which meant that this diffusion path was the most favorable energetically speaking [29].

Soon, copper was found to be a good replacement for aluminum, both by doping aluminum with copper (legend says it was done by IBM by error, due to a misaligned electron beam depositing aluminum and it was soon discovered to have better ampacity than pure aluminum), and by using pure copper as the line material. Copper, in comparison to aluminum has different diffusion activation energies, being in its case bulk, grain-boundary and surface diffusion the order of highest to lowest activation energies,

making surface diffusion the preferred mechanism in copper (2.3, 1.2 and 0.8 eV respectively) [29]. However, copper in contact with air rapidly oxidizes which prevents diffusion through the surface, and therefore grain boundary becomes the primary diffusion pathway. Copper, nevertheless, is only a temporary measure as miniaturization is pushing the cross-section areas of the copper lines to new limits, which exceeds the ampacity values of the metal. As a point to consider, technology used for the fabrication of copper, namely damascene technology [23], has also been seen to affect the quality of the copper lines produced, as due to the high temperatures used diffusion of copper ions into the neighboring silicon or silicon dioxide has been observed [30]. Therefore, further steps are necessary to prevent this diffusion problem which would mean an increase in the total costs for the process.

However, and as it will be explained in the next sections, there has been an increased interest in searching for new materials that would replace the ones that have been mentioned. Copper, whilst being one of the best conductors in the world, has also a very high density and its ampacity, as it has been mentioned, is relatively low.

With miniaturization, this ampacity point is being rapidly reached, and for "macroscopic" uses, such as lightning strike protection, its density makes it inefficient, as the addition of weight is considerably high. So why not look for new materials, which could provide the same values of ampacity but exhibiting at the same time much lower densities? This question was the origin of the thesis. A simple question, but at the same time one so difficult to answer. As Subramaniam et al stated [8], having a high ampacity and a high conducting material is usually mutually exclusive, as the former requires a strongly bonded system, whilst for the latter, free electrons are needed to transport current with efficiency, and therefore a weakly bonded system is required. If we analyze the materials, shown in Figure 6, it is easy to find a pattern were most metals have very high conductivities, but very low ampacity points. And strongly bonded systems, such as carbonaceous materials, have incredible ampacities, but extremely low conductivities when compared to the same metals.

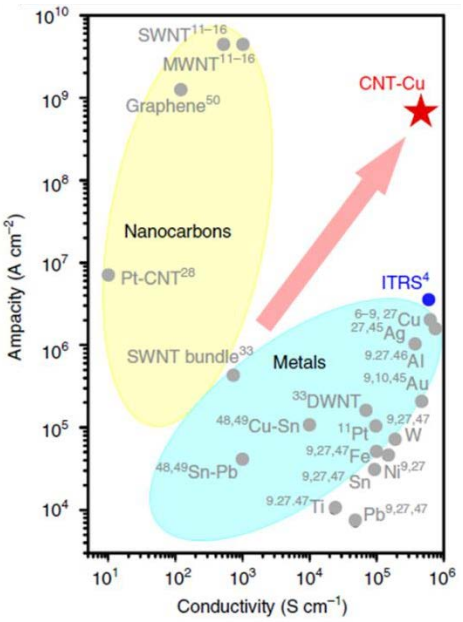

Figure 6: Graphical comparison of ampacity against conductivity for metals and nanocarbons. Metals usually exhibit high conductivities and low ampacities, whilst nanocarbons exhibit the opposite. Subramaniam et al. [8] *managed to synthesize a material combining both the outstanding properties of metals and nanocarbons.*

At the beginning of this thesis, the number of publications regarding composite materials with outstanding ampacity/conductivity were limited. However, with the passing of the years, there has been an increase in the number of groups and publications which pursue the search for this composite by using carbonaceous materials and copper as their working base. The next two sections will try and summarize the state of the art of carbon-metal composites that were published in the last few years. It is important to notice, that most of the articles which will be mentioned, were written after the thesis was nearly at its end.

Carbon allotropes as high ampacity materials

The first step to understanding why carbonaceous materials are being used as high ampacity materials, is to understand how something so simple as carbon, can form so many different structures with outstanding properties. Carbon may form different kinds of allotropes, with sp^2 and sp^3 hybridizations. Graphite, graphene, carbon nanotubes and fullerenes are all sp^2 hybridized, whilst only diamond presents sp^3 hybridization [31], [32]. The first of these allotropes, was observed in 1985, when Sir. Walter Kroto

[33] discovered a new form of the usual carbon structures, different to diamond and to pure carbon, and which was named Fullerene, in honor to the architect Richard Buckminster Fuller and his geodesic spheres. Fullerenes (or Buckyballs) together with metals, have not been explored up to date for electronical purposes. For this reason, this allotrope of carbon will not be explained further. The structure of a fullerene can be observed in Figure 7, together with the other allotropes of carbon.

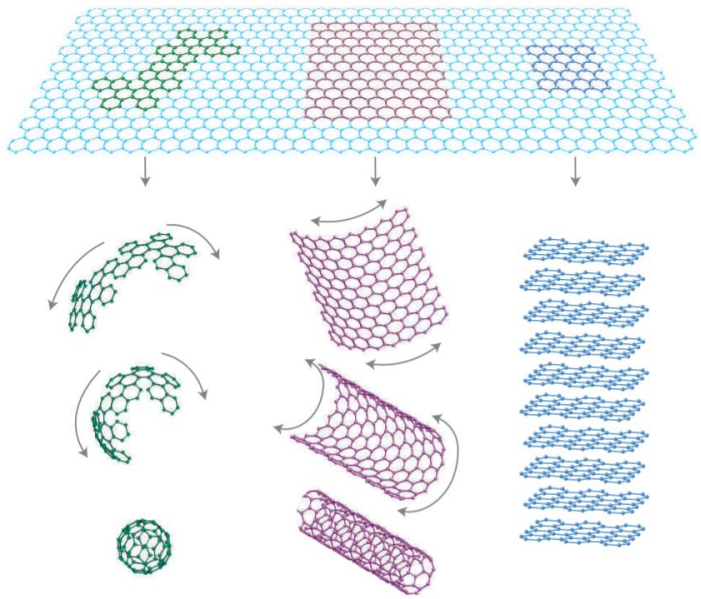

Figure 7: Allotropes of carbon, made from the building black known as graphene. Image extracted from "The rise of graphene" [34]. *Left, buckyball, middle, nanotube, right graphene stacked to form a graphite 3D structure.*

The second allotrope of carbon was observed, for the first time, in 1991 by Iijima, when he observed a new kind of tubular structure [35] made of carbon, which he named carbon nanotubes. These 1-D structures, are made up of carbon layers which are rolled up to form a unidimensional cable, with a few nanometers in diameter, and sizes which can range between micrometers and centimeters [36], [37]. These first nanotubes consisted of several tens of graphitic shells, which nowadays are known as multi walled carbon nanotubes (MWCNT), which possess a shell separation of around 0.34 nm. Two years later, [38] Iijima and Ichihashi first, followed by Bethune et al [39], managed to synthesize effectively the first single walled carbon nanotubes (SWCNT). Nowadays, most of the groups synthesize carbon nanotubes, both multiwalled and single walled by arc-discharge,

laser-ablation and catalytic growth, although many other techniques have been developed to produce other forms of carbon nanotubes; multi walled carbon nanotubes [40]–[42], single walled carbon nanotubes [43]–[45], carbon nanotube yarns [46]–[48], films [49], [50] and composites [8], [51]–[56] to name just a few of the many different possible forms of the same type of 1D carbonaceous material.

Carbon nanotubes mechanical properties are one of the factors which make them so interesting to researchers. They are usually known for being stronger than steel and harder than pure diamond, and at the same time, present very high values for Young's modulus [57] and tensile strength [58], which makes them one of the best reinforcement material up to date. Nanotubes have been used as electron field emitters [59], for fuel cells [60] , battery electrodes [61] , high capacity hydrogen storage media [62], field effect transistors, single-electron transistor, rectifying diodes [63] and logic circuits [64].

As it has been stated above, a carbon nanotube can be obtained by rolling a single sheet of graphene. However, a sheet of graphene can be rolled in different ways causing, different kinds of carbon nanotube, being the two main types chiral and non-chiral arrangements [65]. In the non-chiral arrangement, there is an overall order of the honeycomb lattices, along the direction of the tube. From these non-chiral arrangements, it is possible to find the zig-zag type and the armchair type which can be observed in Figure 8 below. On the other arrangements, where the carbon bonds lie at an angle to the tube direction are known as chiral arrangement also depicted below.

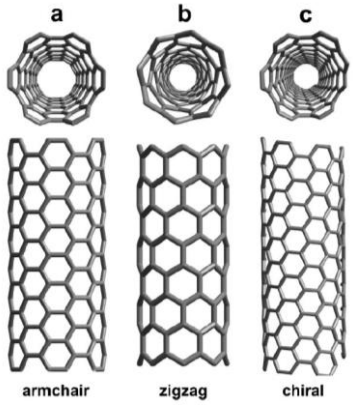

Figure 8: Different ways that a nanotube can arrange itself into. Armchair and zigzag arrangements are known as non-chiral arrangements, where there is an overall order of the honeycomb lattices along the direction of the tube. On the chiral arrangement, the carbon bonds lie at an angle to the tube direction.

This chirality can be defined in terms of a vector, known as the chiral vector C_n, expressed by the formula in equation 17:

$$C_n = ma_1 + na_2 \qquad \textit{Equation 17}$$

This vector is used to define the direction of the rolling of the graphene sheet, where m and n are superimposed with an origin defined as (0,0). This can be easily understood by looking at Figure 9. The diameter of the tube can also be defined by using these same units, and by using them in the following formula (equation 18):

$$d = a\sqrt{\frac{m^2 + mn + n2}{\pi}} \qquad \textit{Equation 18}$$

Where *a* is the lattice constant in the graphene sheet. The deviation from C_n from a_1 is known as the inclination angle. This inclination angle can be used, together with the values of *m* and *n*, to determine whether the structure will be zigzag or armchair, as long as the following criteria are met:

When $\theta = 0,\ (m,n) = (p,0)$ and where p = integer the obtained nanotube will have a zigzag structure.

When $\theta = \pm 30,\ (m,n) = (2p,-p)\ or\ (p,p)$ the obtained nanotube will have an armchair structure.

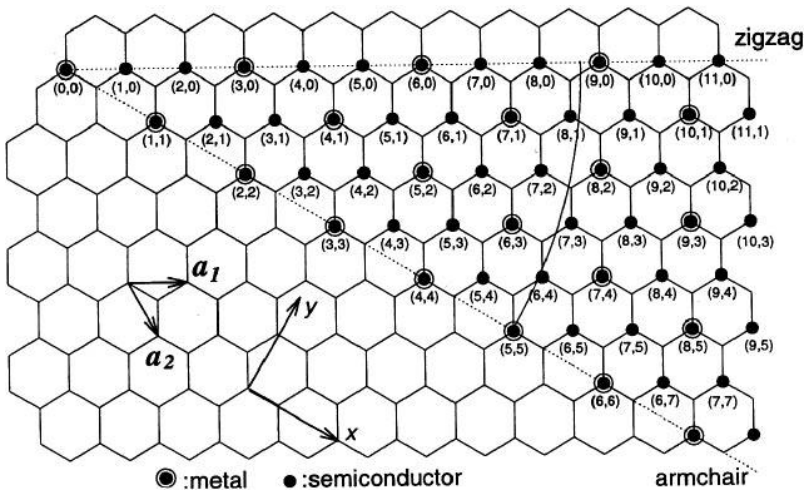

Figure 9: Chirality can be defined in terms of a vector, known as the chiral vector. This vector is used to define the direction of the rolling of the graphene sheet with respect to two coordinates (x,y) superimposed with an origin (0,0). This gives rise to the three kinds of chiralities present in nanotubes.

The chiral angle, (the angle between C_n and the zigzag direction can be defined by equation 19:

$$\theta = \arctan\left[-\frac{\sqrt{3n}}{2m+n}\right] \qquad \textit{Equation 19}$$

The electronic properties of the carbon nanotubes have been deeply studied, as it will be explained in the following sections. However, one of the parameters that defines these electrical properties the most, is the chiral vector which has been explained. All armchair nanotubes have been found to show metallic behavior (and therefore have outstanding electrical properties), as well as all zigzag tubes which have values of m and n which are multiples of the integer 3, as well as those tubes with indices that satisfy the condition $m - n = 3$

In the case of multi-walled carbon nanotubes, there are two main structures recognized in literature [66]: spiral type structure, also known as "swiss-roll", where the nanotubes are composed of rolls of graphene sheets, and the "Russian doll" structure, where the tubes are made of concentric cylinders of graphene. Examples of these structures can be seen in Figure 10. The Russian doll type is the most frequently observed.

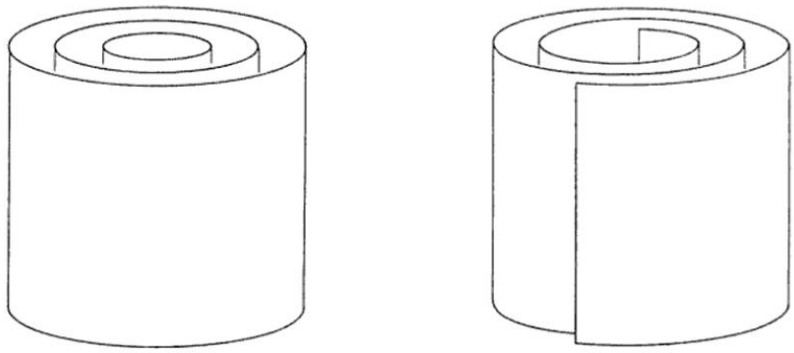

Figure 10. The two types of multi-walled carbon nanotube. Left, "Russian doll" structure, where the tubes are made of concentric cylinders of graphene Right, spiral type structure, also known as "swiss-roll", where the nanotubes are composed of rolls of graphene sheets.

As it has been mentioned, nowadays carbon nanotubes are produced by three main techniques: electric arc discharge technique [67], [68] used for the first time by Bacon et al in the sixties; laser ablation technique [69], used for the first time by Smalley et al [70] and finally by chemical vapor deposition [71], [72], used for the first time by Radushkevich and

Lukyanovich. These techniques, although very effective for producing carbon nanotubes, are useful only at small scale synthesis, making the search for big-scale synthesis, one of the main targets during the last years. Salvetat et al [73], demonstrated that this orientation of the carbon nanotubes had a great impact on their mechanical properties. Highly ordered nanotubes, produced by arc discharge method, were seen to possess high elastic moduli of around 810 GPa. However, other nanotubes which had been produced by catalytic methods, showed a steep decrease towards values close to 50 GPa. The explanation was that the elastic behavior of disordered nanotubes could involve shear deformation, which is much more sensitive to any defects or dislocations present that the highly ordered nanotubes. These highly ordered nanotubes showed no change in elastic modulus even when subjected to thermal anneals to reduce point defects. This led the author to the conclusion, that in highly ordered carbon nanotubes, point defects have no effect on the mechanical properties. It is important to mention, that in such ordered cases, the diameter of the nanotubes seem to have no effect on the elastic modulus neither. Other papers, such as the one by Yamamoto et al [74], also showed that the elastic modulus could be enhanced by using thermal annealing methods. MWCNTs were annealed at 1800, 2200 and 2600 °C and these showed improved strengths by a factor of 5.4, 5.1 and 15.6, and their elastic moduli by a factor of 5.9, 13.2 and 18.9 respectively. Their conclusion was that by annealing at such high temperatures, the degree of orientation of the 002 graphitic planes was improved, and the number of defect concentrations was severely reduced. These factors, as well as affecting the mechanical properties, also affect the electrical properties, as perfect lattices improve conductivity greatly as there is no defects to oppose the flow of electrons through the nanotube structure. As it has been previously explained in the sections above, defects are usually the points at which electromigration preferentially occurs, therefore reducing defects would reduce electromigration process severely.

Carbon nanotubes exhibit a high tolerance to electromigration, due to the strongly bonded system that occurs naturally between carbon atoms [75]. To give an exact number, the ampacity of carbon nanotubes has been found to be close to $1 \cdot 10^{9}$ Acm^{-2}, three order of magnitude above those of copper or gold ($1 \cdot 10^{6}$ Acm^{-2} approximately) [76]. Not less import is the fact that the thermal conductivity of carbon nanotubes exceeds that of copper by a factor of 15, which makes them the perfect option for dissipating heat from sensitive areas such as interconnects [77]. However, these conductivities

may vary greatly with the structure of the carbon nanotube, as it was observed in 1996 by Ebbesen et al [78], when they discovered that even carbon nanotubes that had been prepared at the same time (by arc discharge method), exhibited different electrical properties from one tube to the next. This came as a big surprise as the tubes even behaved differently when subjected to temperature variations. Some tubes had a metallic temperature dependence whilst others were clearly semiconducting, and it was concluded that helicity and interlayer interactions played an important role on these electrical properties.

Carbon nanotubes present a type of conduction which can only be compared to superconductors, as it has been proved that electrons move through them by ballistic transport, meaning that there is no resistance to the flow of electrons [79]. Ballistic transport occurs when the length of a conductor is smaller than the electron mean free path (approximately 40nm), and in these cases each conducting channel would contribute to the total conductance with a unit known as conductance quantum and usually denoted by G_0 ($G_0=2e^2/h$, where e, is the charge of an electron and h, Plank's constant) [79]. This has been proved in single walled carbon nanotubes easily by standard measuring methods (2 and 4 terminal sensing) and shows that as single walled carbon nanotubes have two bands crossing the Fermi level, the total conductance would be given as expected in a metallic nanotube, by $2G_0$. However, some measurements in MWCNTs have shown that the conductance of SWCNTs cannot be applied to each shell of a MWCNT individually, as the last have shown a conductance below $2G_0$ in most cases. The cause for these low conductance quantum measurements can be found in the current probing methods, as these will only take into account the outer shell of the MWCNTs and not every layer [80], [81], and it is well documented that the interaction between successive walls of the tube reduces the total conductance [82].

This fact would make SWCNT the best option, due to their high conductivity and their metallic behavior, for any electrical related use. However, as it has been stated above, chirality of the tubes affects the electrical properties of the tubes greatly, and at the same time, this chirality depends strongly on the synthesis technique used. Even when using the same kind of synthesis technique, one could obtain both semiconducting and metallic type single walled carbon nanotubes [78], [83]. On the other hand, multi walled carbon nanotubes usually show a metallic behavior with most of the synthesis methods that are used [84]. It is interesting to notice, that multiwalled carbon nanotubes do not fail at high current densities via

electromigration as it has been explained before, but fail in a series of sharp steps associated with the destruction of individual nanotube shells [76], as it has been observed via AFM showing how multi walled carbon nanotubes changed their diameter with increased current densities.

These outstanding properties, have made carbon nanotubes the way forward in electrical interconnects for integrated circuits, being however their use severely limited to these microscopic sizes, due to the inherent scaling limits that the synthesis methods possess. However, this is not the only problem when using these carbon nanotubes for electrical purposes. Briefly, some of the most recent problems that have been encountered when using carbon nanotube for electrical purposes are presented.

First, the high temperatures required for their synthesis and deposition of the carbon nanotubes: this is one of the main drawbacks of using carbon nanotubes, as the high temperatures usually affect any devices present or even the substrate where they must be deposited. Using the example of integrated circuits, these high temperatures usually affect any transistors and even the doping profiles. Many efforts are directed towards process engineering in order to try and reduce the temperatures being used, and some recent advances have reached synthesis temperatures close to 350 °C [85]. However, resistivities of these tubes are still above those exhibited by the homologous high temperature synthesis.

Second, high contact resistances exhibited: these high contact resistances between CNTs and a metallic components, are usually caused by the fermi energy differences between both and to the metal-carbon nanotube interface chemistry [86]. Carrier tunneling across the interface of nanotubes and metals due to the very different work functions between the two, is the main cause of these high contact resistances, which has been found to be greater than 6.5 KΩ for SWCNTs [87], which reduces the lifetime of these connections severely.

Third, the semiconductor and metallic behavior in carbon nanotubes: as it has been mentioned above, this factor depends greatly on the synthesis method used, however, metallic type carbon nanotubes are required for electronical purposes. Although usually for this end, and due to ease of production, multi walled carbon nanotubes are used, it has been found that although contact resistance is indeed reduced with metallic type nanotubes, the resistivity remains two orders of magnitude above the one of copper [77], as it was mentioned above, due to the interaction of each of the MWCNT walls. Some advances have been made on this behalf in recent

years, where using titanium particles as the catalyst precursor, it is possible to bring all the different layers into electrical contact, as the metal remains at the tip of the nanotube after the growth process.

Finally, but not less important, longer lengths than the ones exhibited by a single nanotube must be connected, therefore needing not a single nanotube which is far too short, but a bundle of nanotubes instead. As it has been mentioned, controlling chirality in carbon nanotubes is very difficult, therefore in a bundle it is possible to find both metallic and semiconducting nanotubes, which would not contribute to the overall current conduction. This, together with the fact that in between the nanotubes there will also be a contact resistance makes longer CNT bundles less efficient than shorter CNTs if a higher ampacity is searched for. However, and even with this problems, there are some authors which claim to have developed high ampacity power cables, made of closely packed and aligned carbon nanotubes [88], with values of ampacity close to $1 \cdot 10^5$ Acm^{-2}. Other recent results have shown that using a radial densification process it is possible to obtain cables with a diameter up to 1 cm in size [89]. A densified core of CNTs is first produced, and then successive layers of CNTs are wrapped and densified on top. This method produced a conducting cable that could withstand much higher Joule heating temperatures than normal copper cables which would make it an outstanding material for high current cables in air.

Therefore, even though carbon nanotubes might seem like an ideal substitute for any metallic component, the viability, nowadays, of using them on their own is quite low. For this reason, a step in between is required when looking to obtain materials with good conductivity and good ampacity. The possibility of using the outstanding conductivity values of metals, together with the great ampacity behavior of carbonaceous materials, might prove the solution to cope with the future needs in electronics. However, there are some issues when synthesizing carbon nanotubes – metal composites due to the poor adhesion that metals have exhibited with CNTs [90]. Due to the very strong covalent bonds that carbon atoms show towards each other, there is small possibility of carbon atoms bonding to other kinds of atoms, such as those present in metals. However, treating these carbonaceous materials with a pre-oxidation, acid or a heating stage after producing them have shown some benefits in improving adhesion [52]. Metals surface tension plays a very important role when trying to wet the carbon nanotubes, and only liquids with surface

tensions below 100-200 mNm^{-1} are able to wet this carbonaceous materials [91].

For achieving these composite materials, several techniques have been used up to date [55]; The technique that is most utilized is powder metallurgy [92]–[94], followed closely by electrodeposition and electroless deposition (being nickel and copper the two metals which have been most used) [95]–[102]. For metals with a low melting temperature a viable option is melting and solidifying them in the presence of carbon nanotubes [103]–[105]. Of all the metals that have been used together with carbon nanotubes, there is one which seems as the most promising when it comes to achieving a composite material with high conductivity and high ampacity. These are the composites made up of carbon nanotubes and copper, which is the metal that has proven to exceed any others in conductivity, and the one that has been used up until today for interconnects and most of the current conductors.

Although CNT-Copper composites were synthesized several times with success [101], [106]–[110], it was not until 2008 [111] when the idea of how this composite could behave under high current densities was presented. In this paper, a low-density CNT matrix was synthesized by CVD, and the voids in between tubes were filled up with copper by electrodeposition. After the annealing of the composite material it was observed that the average growth rate of voids caused by electromigration was 4 times smaller than the one observed for pure copper. Several years later, in 2013 [8], Subramaniam et al went even further, and stated that their copper-SWCNT composite showed a 100-fold increase in the ampacity when compared to pure copper and showing no decrease in conductivity. Their composite material was made by depositing vertically aligned carbon nanotubes (densified by liquid densification technique) which subjected to shear force became horizontally oriented. Then, in a two-stage growth process, organic electrodeposition followed by a second phase of aqueous electrodeposition, SWCNT-copper composite was achieved. It is very important to explain, that the organic phase was used to wet the CNTs so that the copper would be able to adhere and nucleate on the nanotubes. A second important lesson was obtained from this article, and this is that the rate-limiting step had to be the copper nucleation and not ion diffusion during electrodeposition. To this end, a slow deposition rate had to be used in order to achieve ion diffusion towards the interior of the CNT structure and prevent like this deposition on the outside only (as that would have made a coating of copper and not a proper composite material). As it was

stated, CNTs seemed to prevent the low energy diffusion pathways or, in other words, diffusion through surface and grain boundaries, forcing diffusion through the bulk of the lattice. This was proved by plotting experimental results, and using Black's law to calculate the slope, giving a value of diffusion which was the same as the activation energy of lattice diffusion in pure copper (2.03 eV).

These techniques, however, are all centered on the microscopic scale, giving no importance whatsoever to the macroscopic scale. At the microscale, several properties such as the size of grain in comparison to the line diameter, or the total conducting path length, can cause drastic changes in the ampacity values. In a way of speaking, the articles that have been named above have found the optimal parameters for their composite material to show outstanding ampacity values. However, this optimization had to be done at macroscopic levels too, where grain size would cause a much smaller effect on the overall electromigration values when compared to the much bigger diameter of the conducting path.

Table 1: Comparative table of the different kinds of carbon nanotubes in literature, and the ampacity values exhibited by each of them, as compared to pure metals [20].

Type of CNT	Metal	Form of material	Ampacity A/cm2	Synthesis method	Reference number
Non	Copper	Polycrystalline	$8 - 18 \times 10^6$	Various methods	[25]
Non	Aluminum	Polycrystalline	$5 \cdot 10^4$	Vacuum deposition	[27]
SWCNT	Non	Individual tube	$1 \cdot 10^9$	Suspension deposition	[112]
CNT	Non	Fiber	$1 \cdot 10^5$	Wet spinning method	[88]
MWCNT	Non	Individual tube	$1 \cdot 10^6$	Catalytic process	[113]
MWCNT	Non	Individual tube	$1 \cdot 10^7$	CVD deposition	[114]
MWCNT	Non	Individual tube	$1 \cdot 10^9$	Arc discharge method	[115]

Type of CNT	Metal	Form of material	Ampacity A/cm2	Synthesis method	Reference number
MWCNT	Non	Single tube	$3 \cdot 10^6$	CVD deposition	[116]
CNT	Nickel	Test solder joint	$1 \cdot 10^4$	Ni coating on CNT	[117]
MWCNT	Nickel	Ni filled tube	$1 \cdot 10^7$	MPCVD method	[116]
MWCNT	Copper	Microscopic line	$1 \cdot 10^8$	Electroplating	[118]
SWCNT	Copper	Test line	$6 \cdot 10^8$	Electroplating	[8], [119]
CNT	Copper	Fiber	$1 \cdot 10^7$	CNT aerogel + electroplating	[120]

Several techniques have appeared recently, which allows for bigger productions of carbon nanotubes than the typical methods which have been named in table 1 above [121]–[124]. These carbon nanotube films, can be condensed by using any alcohol to create a densified CNT fiber, cut to create short strips, or can even be used as flat wires directly from synthesis. This has opened a new door for improving the macroscopic composites, which could prove just as important as their microscopic equivalent.

These flat wires, were used during this thesis and have proven the best option for upscaling the technology that Subramaniam et al [8] developed with such success, as it will be developed during the next sections of this thesis. However, at the time when this thesis begun, this method for synthesizing carbon nanotube films was just beginning. The techniques that were more readily available for synthesizing carbon nanotubes were the ones that have been mentioned, CVD, arch discharge and laser ablation. None of these techniques could be used at the time to produce an upscaling as the one that was required for their use as lightning strike protection. Alternatives for this lack of scaling, had to be searched for, and the answer

came as a different allotrope of carbon: graphene, or to be more exact, graphene oxide.

Graphene is a bidimensional layer of carbon atoms, arranged into a honeycomb kind of structure [125] and is the building block of many graphitic materials such as the ones that have been mentioned above. The first time graphene was studied, was in 1947 years ago [126], [127] being this, however, a theoretical study and not a real study of the material as such. However, in 2004, Novoselov et al managed to produce a free standing graphene layer for the first time [128], [129], action which granted him the chance of being Nobel laureated in 2010. Graphene can be considered a 2D material up until approximately 10 layers [130], moment when graphene starts behaving as pure graphite. Single graphene layers can be considered as zero-gap semiconductors, which means that graphene can conduct effectively as a pure metal.

Graphene, just as it happened to carbon nanotubes, can also present different arrangements of the carbon atoms, resulting in different properties. Arrangements such as the previously mentioned zig-zag or armchair can be found in graphene too [131]. Graphene has many outstanding properties, which have made it one of the most researched materials in the recent decade. With a Young modulus of approximately 1 $\pm$ 0.1 TPa and an intrinsic strength of 130 $\pm$ 10 GPa [132], high thermal conductivity of 5000 $W(mK)^{-1}$ [133] and an electrical conductivity which can excel those shown by some metals, such as silver for instance, [134], [135], makes graphene a material to take into account when talking about high conductivity/ampacity composites. Graphene has been used in many different fields, such as for solar cells [136], sensing devices for small molecules [137], batteries [138] and even biomedical uses [139]. However, there is one main drawback to this material, and that is its synthesis methods. Novoselov et al, as mentioned before, managed to obtain the free-standing graphene sheet by using a scotch tape method. By probability, if one exfoliates graphite mechanically, one would be able to at least obtain one graphene sheet. However, it is a completely randomized method, and one which cannot be used to produce larger films of graphene, as the mean size of these flakes were in the order of microns [140]. Synthesis methods for obtaining graphene are diverse nowadays, however, the resulting graphene sheets have also completely different properties from one another. In the 1970's carbon was synthesized on top of transition metal surfaces [141]. However, it was very difficult to measure the electrical properties, as it was challenging to isolate these layers and transferring them

onto insulating substrates. In recent years, various synthesis techniques have been improved on, however, the techniques which are mostly used for the synthesis of this material are mechanical cleavage [142], chemical exfoliation [143], [144], chemical synthesis [145] and chemical vapor deposition [146]. From all of these techniques, the only one which is able to produce larger than centimeter films, is chemical vapor deposition [147]. By this method, graphene has been deposited on many transition metals, but mainly on copper substrates. The main drawbacks for this technique, involves the very limited scalability (a furnace is required for this reaction to occur) and the very high temperatures required for graphene to be produced, usually in the range of 950 °C (on Ni for instance [148]) up to 1000 °C (for Copper [149]).

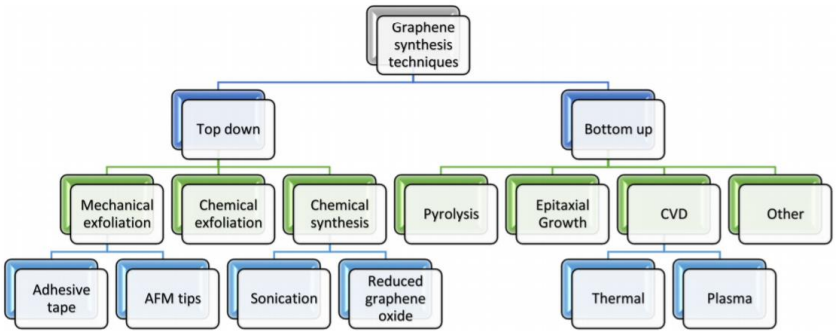

Figure 11: The different routes for graphene synthesis. There are two main ways, the top down approach and the bottom up approach, both of which offer their own advantages and their own disadvantages for the production of high-quality graphene [141].

This limitation for producing graphene has caused very few advances to be made in the field of graphene as high ampacity material. Very few articles have appeared up until this day, that focus on the ampacity properties of graphene, or graphene-based composites. The few that have appeared [150]–[152] have just been published during the last year and claim, that graphene-copper composites increases the ampacity of copper by 39%.

However, and as it has been mentioned in the motivation section, it is necessary to search for a synthesis method which can be upscaled, to meet industrial needs. As it can be observed in Figure 11 there is a top down approach which consists of the chemical synthesis of a carbonaceous material, known as reduced graphene oxide. Graphene oxide is a mixture of carbon, oxygen and hydrogen in varying proportions, and is obtained after treating pure graphite with strong oxidizing agents. This material, can be produced in big volumes and with very low costs, making graphene

oxide a possible successor for pure graphene. The main methods used are Brodie's [153], Staudenmaier [154] and probably the one which is most often used; Hummer's [155]. Variations of these three methods are also often used. Brodie and Staudenmaier use a combination of potassium chlorate and nitric acid, whilst Hummer's method involves the use of potassium permanganate and sulfuric acid. Depending which of the methods are used, the resulting graphene oxide behaves differently, and exhibits completely different properties [156]. However, no matter the method used, a structure similar to the one shown in Figure 12 would be obtained. Graphite oxide is strongly oxygenated and highly hydrophilic material, and it can be easily exfoliated and dispersed in many solvents, specially water, to form single layer sheets known as graphene oxide [157]. This dispersion, can then be used for many applications such as creating graphene oxide fibers [158], films [159]–[161] or scaffolds [162], [163].

There are four types of functionalization which may occur between the oxygens and the carbon atoms in graphene oxide. The main structures formed are epoxides, hydroxyls, carbonyls and carboxyls. Epoxide and hydroxyl are major components and are found in the basal graphene structure. On the other hand, carbonyls and carboxyls are minor components, and are usually found on the edges of graphene oxide. It is however important to mention, that many models have been proposed to present a plausible structure for graphene oxide [164] and even in recent days the structure of this carbonaceous material remains elusive. Hofmann and Holst's structure (Figure 13) consisted of epoxy groups that were spread across the basal planes of the graphene. Accounting for the hydrogen that had been detected on graphene oxide, Ruess proposed a different model, by which hydroxyl groups were incorporated into the basal plane. However, as it has been mentioned before, it is the Lerf-Klinowski model, the one which is most widely accepted.

Even though the exact structure is unknown, it is 100% accurate to assume that oxygen is present in the graphene oxide structure, and therefore this grants the graphene oxide layer with an overall negative charge as it has been widely documented [165], [166].

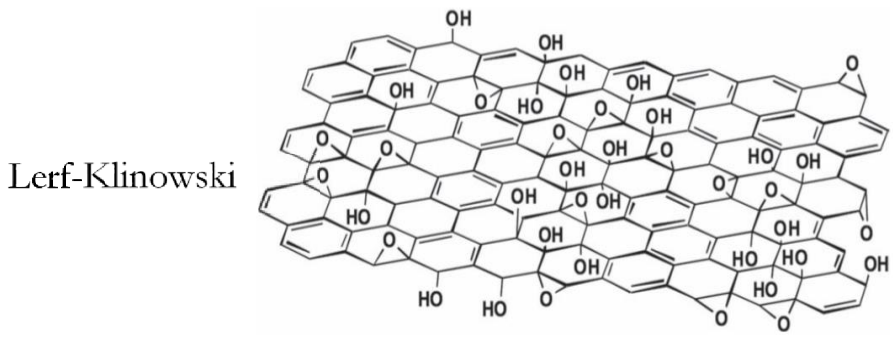

Figure 12: [167] *Lerf-Klinowski model, the most widely accepted model for graphene oxide nowadays. It consists of hydroxyl, carbonyl, epoxy and carboxyl groups.*

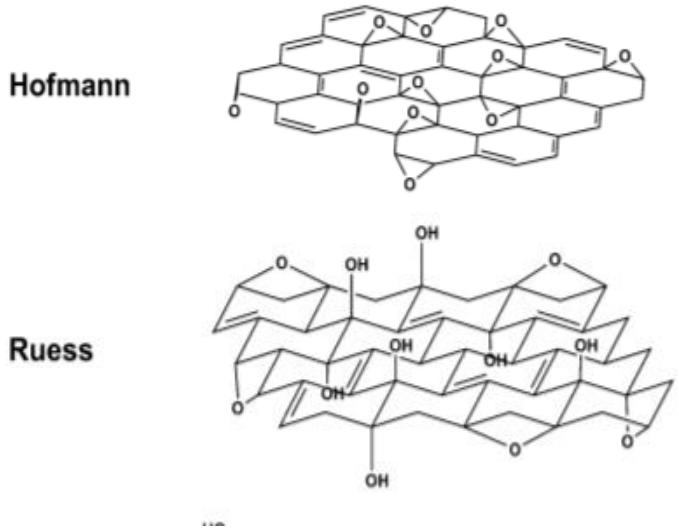

Figure 13: Left, Hofmann and Holst's structure consisted of epoxy groups that were spread across the basal planes of the graphene. Right, Ruess proposed a different model, by which hydroxyl groups were incorporated into the basal plane of graphene [164].

Due to the large amount of defects that are formed during the synthesis of graphene oxide layers and the many oxygenated groups present, properties such as conductivity in these graphene oxide layers is heavily resented, showing extremely low resistivities in the order of 276–2024 Ωsq^{-1} [168]. Recently, there has been an increase in the number of articles which try to revert this oxygenated state, towards a more pristine graphene like structure, by removing many of the oxygenated groups present. This partially reduced form of graphene has been named in many different ways, such as chemically modified graphene, chemically converted graphene or

reduced graphene oxide (which is the name that will be used during this thesis) [169]. However, the complete removal of oxygen groups in graphene oxide is still a dream, and the properties exhibited by these reduced graphene oxides is still far from pristine graphene [170]. Still, this reduced form of graphene oxide improves greatly on the graphene oxide properties, improving conductivity [171] and mechanical properties [172].

It was this reduced graphene oxide form, the one that was used during several stages of this thesis. Being such an unexplored material for electrical purposes meant that any research done, had to be carried out blindly with no literature to be used as guidance. It was believed that the ampacity, being so high in carbon materials, would also be observed in this kind of synthesized material. This, was the beginning of the present project...

Bibliography

[1] S. G. M. Bozzetti, L. Pisu, M.S. Sarto, "Shielding performance of an expanded copper foil over a wide frequency range," in *10th International Symposium on Electromagnetic Compatibility*, 2011, pp. 46–51.

[2] A. Katunin, K. Krukiewicz, A. Herega, and G. Catalanotti, "Concept of a Conducting Composite Material for Lightning Strike Protection," *Adv. Mater. Sci.*, vol. 16, no. 2, pp. 32–46, Aug. 2016.

[3] J. R. (Joseph R. . Davis, *Corrosion of aluminum and aluminum alloys*. ASM International, 1999.

[4] A. V. A. Joh T. Connor, *Copper wire tables*, no. 100. 1966.

[5] L. Chemartin, P. Lalande, B. Peyrou, A. Chazottes, and P. Q. Elias, "Direct Effects of Lightning on Aircraft Structure : Analysis of the Thermal , Electrical and Mechanical Constraints," *J. Aerosp. Lab*, vol. AL05-09, no. 5, pp. 1–15, 2012.

[6] and M. S. R. P. Feynman, R. B. Leighton, "Electricity in the Atmosphere," in *The Feynman Lectures on Physics Vol II*, Pearson India, Ed. 2012.

[7] Y. Wang, "Multiphysics analysis of lightning strike damage in laminated carbon/glass fiber reinforced polymer matrix composite materials: A review of problem formulation and computational modeling," *Compos. Part A Appl. Sci. Manuf.*, vol. 101, pp. 543–553, 2017.

[8] C. Subramaniam *et al.*, "One hundred fold increase in current carrying capacity in a carbon nanotube-copper composite.," *Nat. Commun.*, vol. 4, p. 2202, Jan. 2013.

[9] E. P. Honig and J. A. A. Ketelaar, "Electromigration and self-diffusion in ionic melts," *Trans. Faraday Soc.*, vol. 62, no. l, pp. 190–197, 1966.

[10] D. W. Malone and R. E. Hummel, *Electromigration in integrated circuits*, vol. 22, no. 3. 1997.

[11] K. Sasagawa and M. Saka, *Basis of atomic diffusion*. 2011.

[12] R. Landauer, "Geometry and boundary conditions in the Das-Peierls electromigration theorem," *Phys. Rev. B*, vol. 16, no. 10, pp. 4698–4702, 1977.

[13] R. W. Siegel, "Atomic Defects and Diffusion in Metals," *Point Defects Defect Interact. Met.*, p. 783, 1982.

[14] M. R. P. A. M. J. R. Lloyd, "Observation of electromigration in heavily doped polycrystalline silicon thin films," *Notes Queries*, vol. 30, no. 2, p. 148, 1983.

[15] A. G. (Allan G. . Seabridge and I. (Ian) Moir, *Design and development of aircraft systems*. .

[16] M. Moore, "International Roadmap for devices and systems," 2017.

[17] K. N. Tu, "Electromigration in stressed thin films," *Phys. Rev. B*, vol. 45, no. 3, pp. 1409–1413, 1992.

[18] H. B. Huntington and A. R. Grone, "Current induced marker motion in gold wires," *J, Phys. Chem. Solids*, vol. 20, pp. 76–87, 1961.

[19] J. R.Black, "Electromigration-A brief survey and some recent results," *IEEE Trans. Electron Devices*, vol. ED-16, no. 4, pp. 338–347, 1968.

[20] G. Mokry, J. Pozuelo, J. J. Vilatela, J. Sanz, and J. Baselga, "High ampacity carbon nanotube materials," *Nanomaterials*, vol. 9, no. 3. MDPI AG, 01-Mar-2019.

[21] P. Shewmon, *Diffusion in Solids, second edition*. 1983.

[22] J. J. Clement, "Electromigration modeling for integrated circuit interconnect reliability analysis," *IEEE Trans. Device Mater. Reliab.*, vol. 1, no. 1, pp. 33–42, 2001.

[23] Singapore Press Holdings Ltd. Co., "Electromigration Reliability Issues in Dual-Damascene Cu Interconnections," *The Straits Times*, vol. 51, no. 4, pp. 403–419, 2018.

[24] O. Guise, H. Marbach, J. T. Yates, M. C. Jung, J. Levy, and J. Ahner, "Development and performance of the nanoworkbench: A four tip STM for conductivity measurements down to submicrometer scales," *Rev. Sci. Instrum.*, vol. 76, no. 4, 2005.

[25] J. J. Clement, "Electromigration in Copper Conductors," *Thin Solid Films*, vol. 262, pp. 135–141, 1995.

[26] I. A. Blech and E. S. Meieran, "Electromigration in thin Al films," *J. Appl. Phys.*, vol. 40, no. 2, pp. 485–491, 1969.

[27] J. R. Black, "Electromigration Failure Modes in Aluminum Metallization for Semiconductor Devices," *Proc. IEEE*, vol. 57, no.

9, pp. 1587–1594, 1969.

[28] M. J. Attardo and R. Rosenberg, "Electromigration damage in aluminum film conductors," *J. Appl. Phys.*, vol. 41, no. 6, pp. 2381–2386, 1970.

[29] J. Lienig, M. Thiele, and I. C. Design, *Fundamentals of Electromigration*. .

[30] M. Uekubo *et al.*, "WNx diffusion barriers between Si and Cu," *Thin Solid Films*, vol. 286, no. 1–2, pp. 170–175, 1996.

[31] V. Popov, "Carbon nanotubes: properties and application," *Mater. Sci. Eng. R Reports*, vol. 43, no. 3, pp. 61–102, 2004.

[32] Y. Lin, J. W. Kim, J. W. Connell, M. Lebrõn-Colõn, and E. J. Siochi, "Purification of carbon nanotube sheets," *Adv. Eng. Mater.*, vol. 17, no. 5, pp. 674–688, 2015.

[33] R. F. C. and R. E. S. H.W.Kroto, J.R. Heath, S.C.O'Brien, "C60: Buckminsterfullerene," *Nature*, vol. 318, pp. 162–163, 1985.

[34] A. K. Geim and K. S. Novoselov, "The rise of graphene.," *Nat. Mater.*, vol. 6, no. 3, pp. 183–191, 2007.

[35] S. Iijima, "Helical microtubules of graphitic carbon," *Nature*, vol. 354, no. 56, 1991.

[36] C. Gao, Z. Guo, J. H. Liu, and X. J. Huang, "The new age of carbon nanotubes: An updated review of functionalized carbon nanotubes in electrochemical sensors," *Nanoscale*, vol. 4, no. 6, pp. 1948–1963, 2012.

[37] A. R. Saifuddin and N. Juniazah, "Carbon nanotube: A review on structure and their interaction.," *J. Chem.*, vol. 2013, pp. 1–18, 2013.

[38] Sumio Ijima & Toshinari Ichihashi, "Single-shell carbon nanotubes of 1-nm diameter," *Nature*, vol. 363, pp. 603–605, 1993.

[39] J. V. & R. B. D.S.Bthune, C.H.Klang, M.S. de Vries, G.Gorman, R.Savoy, "Cobalt-catalysed growth of carbon nanotubes with single-atomic-layer walls," *Nature*, vol. 363, pp. 605–607, 1993.

[40] G. Alonso-Nuñez, A. M. Valenzuela-Muñiz, F. Paraguay-Delgado, A. Aguilar, and Y. Verde, "New organometallic precursor catalysts applied to MWCNT synthesis by spray-pirolysis," *Opt. Mater. (Amst).*, vol. 29, no. 1, pp. 134–139, 2006.

[41] J. A. Trapani and P. K. Darcy, "Immunotherapy of cancer," *Aust.*

Fam. Physician, vol. 46, no. 4, pp. 194–198, 2017.

[42] H. K. Youn, J. Kim, and W. S. Ahn, "MWCNT synthesis over Fe-BTC as a catalyst/carbon source via CVD," *Mater. Lett.*, vol. 65, no. 19–20, pp. 3055–3057, 2011.

[43] Á. Kukovecz, D. Méhn, E. Nemes-Nagy, R. Szabó, and I. Kiricsi, "Optimization of CCVD synthesis conditions for single-wall carbon nanotubes by statistical design of experiments (DoE)," *Carbon N. Y.*, vol. 43, no. 14, pp. 2842–2849, 2005.

[44] A. Mansour, M. Razafinimanana, M. Monthioux, M. Pacheco, and A. Gleizes, "A significant improvement of both yield and purity during SWCNT synthesis via the electric arc process," *Carbon N. Y.*, vol. 45, no. 8, pp. 1651–1661, 2007.

[45] M. R. Maschmann, P. B. Amama, A. Goyal, Z. Iqbal, R. Gat, and T. S. Fisher, "Parametric study of synthesis conditions in plasma-enhanced CVD of high-quality single-walled carbon nanotubes," *Carbon N. Y.*, vol. 44, no. 1, pp. 10–18, 2006.

[46] J. K., L. Q., and F. S., "Spinning continuous carbon nanotube yarns," *Nature*, vol. 49, no. 1999, pp. 5246–5252, 2002.

[47] K. Liu *et al.*, "Carbon nanotube yarns with high tensile strength made by a twisting and shrinking method," *Nanotechnology*, vol. 21, no. 4, 2010.

[48] M. Zhang, K. R. Atkinson, and R. H. Baughman, "Multifunctional carbon nanotube yarns by downsizing an ancient technology," *Science (80-.).*, vol. 306, no. 5700, pp. 1358–1361, 2004.

[49] J. Hone *et al.*, "Electrical and thermal transport properties of magnetically aligned single wall carbon nanotube films," *Appl. Phys. Lett.*, vol. 77, no. 5, pp. 666–668, 2000.

[50] S. Muhl, R. Aguilar Osorio, and U. A. Martínez Huitle, "Transparent conductive carbon nanotube films," *Rev. Mex. Fis.*, vol. 63, no. 5, pp. 439–447, 2014.

[51] F. Chastel, E. Flahaut, A. Peigney, and A. Rousset, "Carbon Nanotube – Metal – Oxide Nanocomposites : Microstructure , Electrical Conductivity and," vol. 48, pp. 3803–3812, 2000.

[52] X. Chen, J. Xia, J. Peng, W. Li, and S. Xie, "Carbon-nanotube metal-matrix composites prepared by electroless plating," *Compos. Sci. Technol.*, vol. 60, no. 2, pp. 301–306, 2000.

[53] A. M. K. Esawi, K. Morsi, A. Sayed, A. A. Gawad, and P. Borah, "Fabrication and properties of dispersed carbon nanotube-aluminum composites," *Mater. Sci. Eng. A*, vol. 508, no. 1–2, pp. 167–173, 2009.

[54] J. P. Tu, Y. Z. Yang, L. Y. Wang, X. C. Ma, and X. B. Zhang, "Tribological properties of carbon-nanotube-reinforced copper composites," *Tribol. Lett.*, vol. 10, no. 4, pp. 225–228, 2001.

[55] J. Wang *et al.*, "Carbon nanotube reinforced metal matrix composites – a review," *InterCeram Int. Ceram. Rev.*, vol. 63, no. 6, pp. 286–289, 2014.

[56] J. Wang, G. Chen, M. Wang, and M. P. Chatrathi, "Carbon-nanotube/copper composite electrodes for capillary electrophoresis microchip detection of carbohydrates," *Analyst*, vol. 129, no. 6, pp. 512–515, 2004.

[57] J.-P. Salvetat *et al.*, "Mechanical properties of carbon nanotubes," *Appl. Phys. A Mater. Sci. Process.*, vol. 69, no. 3, pp. 255–260, Sep. 1999.

[58] P. Calvert, "A recipe for strength," *Nature*, vol. 399, no. 6733, pp. 210–211, 1999.

[59] R. E. A.G. Rinzler, J.H. Hafner, P.Nikolaev, Smalley, "Unraveling Nanotubes: Field Emission from an Atomic Wire," *Science (80-.).*, vol. 269, no. September, pp. 1550–1553, 1995.

[60] C. R. Martin, G. Che, B. B. Lakshmi, and E. R. Fisher, "Carbon nanotubule membranes for electrochemical energy storage and production," *Nature*, vol. 393, no. 6683, pp. 346–349, 1998.

[61] O. Z. B.Gao, A.Kleinhammes, X.P.Tang, "Electrochemical intercalation of single-walled carbon nanotubes with lithium," *Chem. Phys. Lett.*, vol. 307, pp. 153–157, 2004.

[62] M. J. H. A.C. Dillion, K.M. Jones, T.A.Bekkedahl, "Storage of hydrogen in single-walled carbon nanotubes," *Nature*, vol. 386, pp. 377–379, 1997.

[63] A. Bachtold, P. Hadley, T. Nakanishi, and C. Dekker, "Logic circuits with carbon nanotube transistors," *Science (80-.).*, vol. 294, no. 5545, pp. 1317–1320, 2001.

[64] P. G. Collins, M. S. Arnold, and P. Avouris, "Engineering carbon nanotubes and nanotube circuits using electrical breakdown," *Science*

(80-.)., vol. 292, no. 5517, pp. 706–709, 2001.

[65] M. Terrones, "Science and Technology of the Twenty-First Century: Synthesis, Properties, and Applications of Carbon Nanotubes," *Annu. Rev. Mater. Res.*, vol. 33, no. 1, pp. 419–501, 2003.

[66] P. J. F. (Peter J. F. Harris, *Carbon nanotubes and related structures : new materials for the twenty-first century*. Cambridge University Press, 2001.

[67] T. W. Ebbesen and P. M. Ajayan, "Large-scale synthesis of carbon nanotubes," *Nature*, vol. 358, no. 6383, pp. 220–222, Jul. 1992.

[68] C. Journet *et al.*, "Large-scale production of single-walled carbon nanotubes by the electric-arc technique," *Nature*, vol. 388, no. 6644, pp. 756–758, Aug. 1997.

[69] A. G. Rinzler *et al.*, "Large-scale purification of single-wall carbon nanotubes: process, product, and characterization," *Appl. Phys. A Mater. Sci. Process.*, vol. 67, no. 1, pp. 29–37, Jul. 1998.

[70] A. Thess *et al.*, "Crystalline Ropes of Metallic Carbon Nanotubes," *Science*, vol. 273, no. 5274, pp. 483–7, Jul. 1996.

[71] M. Endo, K. Takeuchi, K. Kobori, K. Takahashi, H. W. Kroto, and A. Sarkar, "Pyrolytic carbon nanotubes from vapor-grown carbon fibers," *Carbon N. Y.*, vol. 33, no. 7, pp. 873–881, Jan. 1995.

[72] J. Kong, A. M. Cassell, and H. Dai, "Chemical vapor deposition of methane for single-walled carbon nanotubes," *Chem. Phys. Lett.*, vol. 292, no. 4–6, pp. 567–574, Aug. 1998.

[73] B. J. Salvetat *et al.*, "Elastic Modulus of Ordered and Disordered Multiwalled Carbon Nanotubes **," no. 2, pp. 161–165, 1999.

[74] G. Yamamoto, K. Shirasu, Y. Nozaka, Y. Sato, and T. Takagi, "Structure – property relationships in thermally-annealed multi-walled carbon nanotubes," *Carbon N. Y.*, vol. 66, pp. 219–226, 2013.

[75] L. Pauling, *The nature of the chemical bond*, Third edit. Ithaca, New York: Cornell university press, 1960.

[76] P. G. Collins, M. Hersam, M. Arnold, R. Martel, and P. Avouris, "Current saturation and electrical breakdown in multiwalled carbon nanotubes," *Phys. Rev. Lett.*, vol. 86, no. 14, pp. 3128–3131, 2001.

[77] M. H. Van Der Veen *et al.*, "Electrical characterization of CNT contacts with Cu Damascene top contact," *Microelectron. Eng.*, vol. 106, pp. 106–111, 2013.

[78] T. T. T.W.Ebbesen, H.J.Lezec, H.Hiura, J.W.Bennet, H.F. Ghaemi, "Electrical conductivity of individual carbon nanotubes," *Nature*, vol. 382, pp. 54–56, 1996.

[79] H. J. Li, W. G. Lu, J. J. Li, X. D. Bai, and C. Z. Gu, "Multichannel ballistic transport in multiwall carbon nanotubes," *Phys. Rev. Lett.*, vol. 95, no. 8, pp. 1–4, 2005.

[80] P. Poncharal, C. Berger, Y. Yi, Z. L. Wang, and W. A. De Heer, "Feature article Room temperature ballistic conduction in carbon nanotubes," *J. Phys. Chem. B*, vol. 12104, pp. 1–25, 2002.

[81] L. Langer *et al.*, "Quantum Transport in a Multiwalled Carbon Nanotube," *Phys. Rev. Lett.*, vol. 76, no. 3, pp. 479–482, 1996.

[82] S. Sanvito, Y. K. Kwon, D. Tománek, and C. J. Lambert, "Fractional Quantum Conductance in Carbon Nanotubes," *Phys. Rev. Lett.*, vol. 84, no. 9, pp. 1974–1977, 2000.

[83] A. A. Vyas, C. Zhou, P. Wilhite, P. Wang, and C. Y. Yang, "Electrical properties of carbon nanotube via interconnects for 30 nm linewidth and beyond," *MR*, 2015.

[84] F. Kreupl *et al.*, "Carbon nanotubes in interconnect applications," *Microelectron. Eng.*, vol. 64, no. 1–4, pp. 399–408, 2002.

[85] S. Vollebregt, F. D. Tichelaar, H. Schellevis, C. I. M. Beenakker, and R. Ishihara, "Carbon nanotube vertical interconnects fabricated at temperatures as low as 350 °c," *Carbon N. Y.*, vol. 71, pp. 249–256, 2014.

[86] P. Wilhite *et al.*, "Metal-nanocarbon contacts," *Semicond. Sci. Technol.*, vol. 29, no. 5, 2014.

[87] K. Banerjee and N. Srivastava, "Are carbon nanotubes the future of VLSI interconnections?," *2006 43rd ACM/IEEE Des. Autom. Conf.*, pp. 809–814, 2006.

[88] X. Wang, N. Behabtu, C. C. Young, D. E. Tsentalovich, M. Pasquali, and J. Kono, "High-ampacity power cables of tightly-packed and aligned carbon nanotubes," *Adv. Funct. Mater.*, vol. 24, no. 21, pp. 3241–3249, 2014.

[89] C. D. Cress *et al.*, "Carbon nanotube wires with continuous current rating exceeding 20 Amperes," *J. Appl. Phys.*, vol. 122, no. 2, 2017.

[90] L. Ladani, "The Potential for Metal–Carbon Nanotubes Composites as Interconnects," *J. Electron. Mater.*, 2018.

[91] E. Dujardin, T. W. Ebbesen, H. Hiura, and K. Tanigaki, "Capillarity and wetting of carbon nanotubes," *Science (80-.).*, vol. 265, no. 5180, pp. 1850–1852, 1994.

[92] X. U. Wei, H. U. Rui, L. I. Jin-shan, and F. U. Heng-zhi, "Effect of electrical current on tribological property of Cu matrix composite reinforced by carbon nanotubes," *Trans. Nonferrous Met. Soc. China*, vol. 21, no. 10, pp. 2237–2241, 2011.

[93] N. Saikrishna, G. P. K. Reddy, B. Munirathinam, R. Dumpala, M. Jagannatham, and B. R. Sunil, "An investigation on the hardness and corrosion behavior of MWCNT/Mg composites and grain refined Mg," *J. Magnes. Alloy.*, vol. 6, no. 1, pp. 83–89, 2018.

[94] C. He *et al.*, "An approach to obtaining homogeneously dispersed carbon nanotubes in Al powders for preparing reinforced Al-matrix composites," *Adv. Mater.*, vol. 19, no. 8, pp. 1128–1132, 2007.

[95] L. Shi, C. F. Sun, P. Gao, F. Zhou, and W. M. Liu, "Electrodeposition and characterization of Ni-Co-carbon nanotubes composite coatings," *Surf. Coatings Technol.*, vol. 200, no. 16–17, pp. 4870–4875, 2006.

[96] Y. S. Jeon, J. Y. Byun, and T. S. Oh, "Electrodeposition and mechanical properties of Ni-carbon nanotube nanocomposite coatings," *J. Phys. Chem. Solids*, vol. 69, no. 5–6, pp. 1391–1394, 2008.

[97] B. M. Praveen and T. V. Venkatesha, "Electrodeposition and properties of Zn-Ni-CNT composite coatings," *J. Alloys Compd.*, vol. 482, no. 1–2, pp. 53–57, 2009.

[98] C. Guo, Y. Zuo, X. Zhao, J. Zhao, and J. Xiong, "The effects of electrodeposition current density on properties of Ni-CNTs composite coatings," *Surf. Coatings Technol.*, vol. 202, no. 14, pp. 3246–3250, 2008.

[99] P. M. Hannula *et al.*, "Carbon nanotube-copper composites by electrodeposition on carbon nanotube fibers," *Carbon N. Y.*, vol. 107, pp. 281–287, 2016.

[100] G. Xu, J. Zhao, S. Li, X. Zhang, Z. Yong, and Q. Li, "Continuous electrodeposition for lightweight, highly conducting and strong carbon nanotube-copper composite fibers," *Nanoscale*, vol. 3, no. 10, pp. 4215–4219, 2011.

[101] S. Arai, T. Saito, and M. Endo, "Cu–MWCNT Composite Films Fabricated by Electrodeposition," *J. Electrochem. Soc.*, vol. 157, no. 3,

p. D147, 2010.

[102] X. H. Chen, F. Q. Cheng, S. L. Li, L. P. Zhou, and D. Y. Li, "Electrodeposited nickel composites containing carbon nanotubes," *Surf. Coatings Technol.*, vol. 155, no. 2–3, pp. 274–278, 2002.

[103] Q. Li, C. A. Rottmair, and R. F. Singer, "CNT reinforced light metal composites produced by melt stirring and by high pressure die casting," *Compos. Sci. Technol.*, vol. 70, no. 16, pp. 2242–2247, 2010.

[104] H. L. Shi *et al.*, "A Novel Melt Processing for Mg Matrix Composites Reinforced by Multiwalled Carbon Nanotubes," *J. Mater. Sci. Technol.*, vol. 32, no. 12, pp. 1303–1308, 2016.

[105] H. Shi *et al.*, "A novel method to fabricate CNT/Mg-6Zn composites with high strengthening efficiency," *Acta Metall. Sin. (English Lett.*, vol. 27, no. 5, pp. 909–917, 2014.

[106] Q. Ngo, B. A. Cruden, A. M. Cassell, G. Sims, and M. Meyyappan, "Thermal Interface Properties of Cu-filled Vertically Aligned Carbon Nanofiber Arrays," 2004.

[107] S. Bok, K. Matsunaga, Y. Ikuhara, and S. Lee, "Effect of alloying elements on the interfacial bonding strength and electric conductivity of carbon nano-fiber reinforced Cu matrix composites," vol. 451, pp. 778–781, 2007.

[108] Y. Z. Wan, Y. L. Wang, H. L. Luo, X. H. Dong, and G. X. Cheng, "Effects of fiber volume fraction , hot pressing parameters and alloying elements on tensile strength of carbon fiber reinforced copper matrix composite prepared by continuous three-step electrodeposition," vol. 288, pp. 26–33, 2000.

[109] S. Arai, Y. Suwa, and M. Endo, "Cu/Multiwalled Carbon Nanotube Composite Films Fabricated by Pulse-Reverse Electrodeposition," *J. Electrochem. Soc.*, vol. 158, no. 2, p. D49, 2011.

[110] A. Chinnappan, C. Baskar, H. Kim, and S. Ramakrishna, "Carbon nanotube hybrid nanostructures: Future generation conducting materials," *J. Mater. Chem. A*, vol. 4, no. 24, pp. 9347–9361, 2016.

[111] Y. Chai, P. C. H. Chan, Y. Fu, Y. C. Chuang, and C. Y. Liu, "Electromigration studies of Cu/carbon nanotube composite interconnects using Blech structure," *IEEE Electron Device Lett.*, vol. 29, no. 9, pp. 1001–1003, 2008.

[112] Z. Yao, C. L. Kane, and C. Dekker, "High-field electrical transport

in single-wall carbon nanotubes," *Phys. Rev. Lett.*, vol. 84, no. 13, pp. 2941–2944, 2000.

[113] H. Dai, E. W. Wong, and C. M. Liebert, "Probing Electrical Transport in Nanomaterials : Conductivity of Individual Carbon Nanotubes," vol. 272, no. April, pp. 1–4, 1996.

[114] S. Frank, P. Poncharal, Z. L. Wang, and W. A. De Heer, "Carbon nanotube quantum resistors," *Science (80-.).*, vol. 280, no. 5370, pp. 1744–1746, 1998.

[115] B. Q. Wei, R. Vajtai, and P. M. Ajayan, "Reliability and current carrying capacity of carbon nanotubes," *Appl. Phys. Lett.*, vol. 79, no. 8, pp. 1172–1174, 2001.

[116] N. Kulshrestha, A. Misra, and D. S. Misra, "Electrical transport and electromigration studies on nickel encapsulated carbon nanotubes: Possible future interconnects," *Nanotechnology*, vol. 24, no. 18, 2013.

[117] Z. Yang, W. Zhou, and P. Wu, "Effects of Ni-coated Carbon Nanotubes addition on the electromigration of Sn-Ag-Cu solder joints," *J. Alloys Compd.*, vol. 581, pp. 202–205, 2013.

[118] R. Sundaram, T. Yamada, K. Hata, and A. Sekiguchi, "Electrical performance of lightweight CNT-Cu composite wires impacted by surface and internal Cu spatial distribution," *Sci. Rep.*, vol. 7, no. 1, pp. 1–11, 2017.

[119] C. Subramaniam, A. Sekiguchi, T. Yamada, D. N. Futaba, and K. Hata, "Nano-scale, planar and multi-tiered current pathways from a carbon nanotube-copper composite with high conductivity, ampacity and stability," *Nanoscale*, vol. 8, no. 7, pp. 3888–3894, 2016.

[120] H. Rho *et al.*, "Metal nanofibrils embedded in long free-standing carbon nanotube fibers with a high critical current density," *NPG Asia Mater.*, vol. 10, no. 4, pp. 146–155, 2018.

[121] R. J. Mora, J. J. Vilatela, and A. H. Windle, "Properties of composites of carbon nanotube fibres," *Compos. Sci. Technol.*, vol. 69, no. 10, pp. 1558–1563, 2009.

[122] X. H. Zhong *et al.*, "Continuous multilayered carbon nanotube yarns," *Adv. Mater.*, vol. 22, no. 6, pp. 692–696, 2010.

[123] J. J. Vilatela and A. H. Windle, "Yarn-like carbon nanotube fibers," *Adv. Mater.*, vol. 22, no. 44, pp. 4959–4963, 2010.

[124] S. Boncel, R. Sundaram, and A. Windle, "Enhancement of the

Mechanical Properties of Directly Spun CNT Fibres by Chemical Treatment," *ACS Nano*, vol. 5, no. 12, pp. 9339–9344, 2011.

[125] A. K. Geim and K. S. Novoselov, "The rise of graphene," *Nat. Mater.*, vol. 6, no. 3, pp. 183–191, Mar. 2007.

[126] P. R. Wallace, "The Band Theory of Graphite," *Phys. Rev.*, vol. 71, no. 9, pp. 622–634, May 1947.

[127] J. W. McClure, "Diamagnetism of Graphite," *Phys. Rev.*, vol. 104, no. 3, pp. 666–671, Nov. 1956.

[128] K. S. Novoselov *et al.*, "Two-dimensional atomic crystals.," *Proc. Natl. Acad. Sci. U. S. A.*, vol. 102, no. 30, pp. 10451–3, Jul. 2005.

[129] K. S. Novoselov *et al.*, "Electric Field Effect in Atomically Thin Carbon Films," *Science (80-.).*, vol. 306, no. 5696, pp. 666–669, Oct. 2004.

[130] B. Partoens and F. M. Peeters, "From graphene to graphite: Electronic structure around the K point," *Phys. Rev. B*, vol. 74, no. 7, p. 075404, Aug. 2006.

[131] T. Enoki, S. Fujii, and K. Takai, "Zigzag and armchair edges in graphene," *Carbon N. Y.*, vol. 50, no. 9, pp. 3141–3145, Aug. 2012.

[132] C. Lee, X. Wei, J. W. Kysar, and J. Hone, "Measurement of the Elastic Properties and Intrinsic Strength of Monolayer Graphene," *Science (80-.).*, vol. 321, no. 5887, pp. 385–388, Jul. 2008.

[133] R. Murali, Y. Yang, K. Brenner, T. Beck, and J. D. Meindl, "Breakdown current density of graphene nanoribbons," *Appl. Phys. Lett.*, vol. 94, no. 24, p. 243114, Jun. 2009.

[134] L. Pietronero, S. Strässler, H. R. Zeller, and M. J. Rice, "Electrical conductivity of a graphite layer," *Phys. Rev. B*, vol. 22, no. 2, pp. 904–910, Jul. 1980.

[135] S. Das Sarma, S. Adam, E. H. Hwang, and E. Rossi, "Electronic transport in two-dimensional graphene," *Rev. Mod. Phys.*, vol. 83, no. 2, pp. 407–470, May 2011.

[136] Xuan Wang, * and Linjie Zhi, and K. Müllen*, "Transparent, Conductive Graphene Electrodes for Dye-Sensitized Solar Cells," 2007.

[137] F. Schedin *et al.*, "Detection of individual gas molecules adsorbed on graphene," *Nat. Mater.*, vol. 6, no. 9, pp. 652–655, Sep. 2007.

[138] H. Kim, K.-Y. Park, J. Hong, and K. Kang, "All-graphene-battery: bridging the gap between supercapacitors and lithium ion batteries," *Sci. Rep.*, vol. 4, no. 1, p. 5278, May 2015.

[139] R. Kurapati, K. Kostarelos, M. Prato, and A. Bianco, "Biomedical Uses for 2D Materials Beyond Graphene: Current Advances and Challenges Ahead," *Adv. Mater.*, vol. 28, no. 29, pp. 6052–6074, Aug. 2016.

[140] A. A. Balandin *et al.*, "Superior Thermal Conductivity of Single-Layer Graphene," *Nano Lett.*, vol. 8, no. 3, pp. 902–907, Mar. 2008.

[141] M. S. A. Bhuyan, M. N. Uddin, M. M. Islam, F. A. Bipasha, and S. S. Hossain, "Synthesis of graphene," *Int. Nano Lett.*, vol. 6, no. 2, pp. 65–83, Jun. 2016.

[142] K. S. Novoselov *et al.*, "Electric field effect in atomically thin carbon films.," *Science*, vol. 306, no. 5696, pp. 666–9, Oct. 2004.

[143] L. M. Viculis, J. J. Mack, and R. B. Kaner, "A chemical route to carbon nanoscrolls.," *Science*, vol. 299, no. 5611, p. 1361, Feb. 2003.

[144] M. J. Allen, V. C. Tung, and R. B. Kaner, "Honeycomb Carbon: A Review of Graphene," *Chem. Rev.*, vol. 110, no. 1, pp. 132–145, Jan. 2010.

[145] S. Park and R. S. Ruoff, "Chemical methods for the production of graphenes," *Nat. Nanotechnol.*, vol. 4, no. 4, pp. 217–224, Apr. 2009.

[146] A. Reina *et al.*, "Large Area, Few-Layer Graphene Films on Arbitrary Substrates by Chemical Vapor Deposition," *Nano Lett.*, vol. 9, no. 1, pp. 30–35, Jan. 2009.

[147] X. Wang *et al.*, "Large-Scale Synthesis of Few-Layered Graphene using CVD," *Chem. Vap. Depos.*, vol. 15, no. 1–3, pp. 53–56, Mar. 2009.

[148] A. N. Obraztsov, E. A. Obraztsova, A. V. Tyurnina, and A. A. Zolotukhin, "Chemical vapor deposition of thin graphite films of nanometer thickness," *Carbon N. Y.*, vol. 45, no. 10, pp. 2017–2021, Sep. 2007.

[149] X. Li *et al.*, "Large-area synthesis of high-quality and uniform graphene films on copper foils.," *Science*, vol. 324, no. 5932, pp. 1312–4, Jun. 2009.

[150] S. J. Kim *et al.*, "Ultrastrong Graphene–Copper Core–Shell Wires for High-Performance Electrical Cables," *ACS Nano*, vol. 12, no. 3,

pp. 2803–2808, Mar. 2018.

[151] W. Zhang *et al.*, "High current carrying and thermal conductive copper-carbon conductors," *Nanotechnology*, vol. 30, no. 18, p. 185701, May 2019.

[152] K. Zhao *et al.*, "High ampacity of superhelix graphene/copper nanocomposite wires by a synergistic growth-twisting-drawing strategy," *Carbon N. Y.*, vol. 141, pp. 198–208, Jan. 2019.

[153] B.C.Brodie, "XIII. On the atomic weight of graphite," *Philos. Trans. R. Soc. London*, vol. 149, pp. 249–259, Jan. 1859.

[154] L. Staudenmaier, "Verfahren zur Darstellung der Graphitsäure," *Berichte der Dtsch. Chem. Gesellschaft*, vol. 31, no. 2, pp. 1481–1487, May 1898.

[155] W. S. Hummers and R. E. Offeman, "Preparation of Graphitic Oxide," *J. Am. Chem. Soc.*, vol. 80, no. 6, pp. 1339–1339, Mar. 1958.

[156] H. L. Poh, F. Šaněk, A. Ambrosi, G. Zhao, Z. Sofer, and M. Pumera, "Graphenes prepared by Staudenmaier, Hofmann and Hummers methods with consequent thermal exfoliation exhibit very different electrochemical properties," *Nanoscale*, vol. 4, no. 11, p. 3515, Jun. 2012.

[157] J. I. Paredes, S. Villar-Rodil, A. Martínez-Alonso, and J. M. D. Tascón, "Graphene Oxide Dispersions in Organic Solvents," *Langmuir*, vol. 24, no. 19, pp. 10560–10564, Oct. 2008.

[158] Z. Xu, H. Sun, X. Zhao, and C. Gao, "Ultrastrong Fibers Assembled from Giant Graphene Oxide Sheets," *Adv. Mater.*, vol. 25, no. 2, pp. 188–193, Jan. 2013.

[159] S. Pei, J. Zhao, J. Du, W. Ren, and H.-M. Cheng, "Direct reduction of graphene oxide films into highly conductive and flexible graphene films by hydrohalic acids," *Carbon N. Y.*, vol. 48, no. 15, pp. 4466–4474, Dec. 2010.

[160] H. A. Becerril, J. Mao, Z. Liu, R. M. Stoltenberg, Z. Bao, and Y. Chen, "Evaluation of Solution-Processed Reduced Graphene Oxide Films as Transparent Conductors," *ACS Nano*, vol. 2, no. 3, pp. 463–470, Mar. 2008.

[161] D. A. Dikin *et al.*, "Preparation and characterization of graphene oxide paper," *Nature*, vol. 448, no. 7152, pp. 457–460, Jul. 2007.

[162] M. González, J. Baselga, and J. Pozuelo, "High porosity scaffold

composites of graphene and carbon nanotubes as microwave absorbing materials," *J. Mater. Chem. C*, vol. 4, no. 36, pp. 8575–8582, 2016.

[163] M. González, J. Baselga, and J. Pozuelo, "Modulating the electromagnetic shielding mechanisms by thermal treatment of high porosity graphene aerogels," *Carbon N. Y.*, vol. 147, pp. 27–34, Jun. 2019.

[164] D. R. Dreyer, S. Park, C. W. Bielawski, and R. S. Ruoff, "The chemistry of graphene oxide," *Chem. Soc. Rev.*, vol. 39, no. 1, pp. 228–240, 2010.

[165] D. Li, M. B. Müller, S. Gilje, R. B. Kaner, and G. G. Wallace, "Processable aqueous dispersions of graphene nanosheets," *Nat. Nanotechnol.*, vol. 3, no. 2, pp. 101–105, Feb. 2008.

[166] C. Vallés *et al.*, "Solutions of Negatively Charged Graphene Sheets and Ribbons," *J. Am. Chem. Soc.*, vol. 130, no. 47, pp. 15802–15804, Nov. 2008.

[167] Y. Zhu *et al.*, "Graphene and Graphene Oxide: Synthesis, Properties, and Applications," *Adv. Mater.*, vol. 22, no. 35, pp. 3906–3924, Sep. 2010.

[168] S.-H. Kang, T.-H. Fang, and Z.-H. Hong, "Electrical and mechanical properties of graphene oxide on flexible substrate," *J. Phys. Chem. Solids*, vol. 74, no. 12, pp. 1783–1793, Dec. 2013.

[169] G. Eda and M. Chhowalla, "Chemically Derived Graphene Oxide: Towards Large-Area Thin-Film Electronics and Optoelectronics," *Adv. Mater.*, vol. 22, no. 22, pp. 2392–2415, Jun. 2010.

[170] S. Pei and H.-M. Cheng, "The reduction of graphene oxide," *Carbon N. Y.*, vol. 50, no. 9, pp. 3210–3228, Aug. 2012.

[171] S. Pei, J. Zhao, J. Du, W. Ren, and H.-M. Cheng, "Direct reduction of graphene oxide films into highly conductive and flexible graphene films by hydrohalic acids," *Carbon N. Y.*, vol. 48, no. 15, pp. 4466–4474, Dec. 2010.

[172] J. T. Robinson *et al.*, "Wafer-scale Reduced Graphene Oxide Films for Nanomechanical Devices," *Nano Lett.*, vol. 8, no. 10, pp. 3441–3445, Oct. 2008.

Chapter 2: Materials and methods

This section will contain a brief summary of all the materials and methods that were used during this thesis in order of appearance.

Materials

Chemicals used for graphene oxide synthesis: Graphite (200 mesh, 99.9995 %, Alfa Aesar); sulfuric acid (98% v/v, Panreac); sodium nitrate (Sigma-Aldrich); Potassium permanganate (Panreac); hydrogen peroxide (30% w/v. Panreac).

Silicon dioxide wafer: For doing AFM characterization of the graphene oxide produced, silicon dioxide wafer was bought from University Wafer type N/Ph with oxide thickness 280 nm

Copper microwires: The copper microwires that were used during chapter 3, were bought in Goodfellow, with references CU005110 (diameter 0.01 mm, purity 99.9% and hard tempered), CU005170 (diameter 0.02 mm, purity 99.99+% and hard tempered) and CU005195 (diameter 0.025 mm, purity 99.99+% and hard tempered). Resistivity 1.69 μOhm cm as stated by provider.

Commercial copper films: Used during chapter 5. Provided by onlinemetals.com; Copper 110 annealed foil 0.0007" and copper 110 annealed sheet 0.00135". 100% IAS. Resistivity 1.68 μOhm cm as stated by provider.

Carbon nanotube yarns: Carbon nanotube yarns were provided by the Penn State University and IMDEA Materiales labs. Penn State University carbon nanotubes yarns were obtained by vertical CNT forest pulling. The multiwalled nanotube forest was synthesized by catalytic chemical vapor deposition, and acetylene gas was used as the carbon source. The forests had heights between 100 and 800 μm. The nanotubes had an outer diameter of ~12 nm and contained ~9 walls. Yarns provided by IMDEA Materiales lab were obtained by oven drawn carbon nanotubes. The nanotubes used, were synthesized at 1250 °C by chemical vapor deposition from a mixture which contained thiophene, ferrocene and a carbon source. Hydrogen was used as the carrier gas and the nanotubes produced were in the order of 4-10 nm diameter, and 1mm of length.

Chemicals used for electrodeposition: Sulfuric acid (98% v/v, Panreac), copper (II) sulfate pentahydrate 99.99%.

Techniques

Atomic force microscopy: The model of the AFM used is a Nanoscope IV Multimode AFM from Veeco and the probes used for obtaining the images were the NCHV probes made of antimony doped silicon. Measures were done in tapping mode.

Power source unit: The power unit used was an Agilent B2911A precision Source/Measure Unit, 1 channel, minimum source resolution of 10 fA/100nV, maximum output 210 V, 3 A DC / 10.5 A when pulsed. Software used to measure conductivity/ampacity is the Quick I/V measurement software, and this software was also used to create the wave functions that were used for electrophoretic deposition and electrodeposition throughout the thesis. When experimental measurements are done, measurement limitations, such as instrument precision, causes errors in the observed variables. These errors propagate when combined into more complicated formulas, and therefore it is necessary to stablish this uncertainty if the obtained measurements are to be valid. With the B2911A precision source/measure unit, ampacity and resistivity values in 1-D samples were calculated. It is known that the relative error of the product is the sum of the relative errors of the individual numbers, therefore this error is calculated by taking into account the measurement limitations of each product; these errors are the sum of the power unit error (0.2%), the cross section of the sample measurement accuracy (5%) and the distance between the electrodes accuracy (1%). Therefore, the total relative error of the measurements was stablished to be of 6.2% for the resistivity values and 5.2% for the ampacity values.

Power source unit (600A): DC AMREL SPS10-600 source used for the ampacity measurements in the composite and copper films. 10 Volts, 600 Amps and 6.6 KW. Ideally, four-point probe measurements should be used when doing current-voltage measurements. However, this power unit did not have the option of using four-point probe, therefore thick, 1 cm diameter, copper wires were used to prevent contact resistivity issues. With the DC AMREL SPS10-600 source, ampacity and resistivity values of 2-D samples were calculated. The relative error that were stablished for this

power unit were the sum of the current measurement accuracy (0.75%), voltage measurement accuracy (0.5%), sample's thickness measurement accuracy (10%), sample´s width measurement accuracy (0.2%) and distance between electrodes accuracy (0.1%). Therefore, the relative error for resistivity measurements was 11.55% whilst the relative error for the ampacity measurements was 10.95%.

SEM characterization: SEM images were obtained using a *Phillips XL30* model. Scanning electron microscopy uses electrons to form a magnified image of the surface of the sample analyzed. It can be used both for organic and inorganic samples, however these must be conductive. The SEM is composed of several detectors, which have been used during this chapter. Secondary electrons mode (SE) and backscattered electrons (BSE) were the two main modes used. The backscattered electrons are detected, after these have reflected back after elastic interactions between the beam and the sample. On the contrary, secondary electrons originate from the atoms of the sample analyzed and are a result of inelastic interactions between sample and beam. BSE can analyze deeper regions of the sample whilst secondary electrons originate at the surface of the sample. BSE mode, therefore, have a higher sensitivity to atomic weight of the sample, and can therefore show as brighter or darker images, regions with higher or lower atomic weight respectively. SE can provide more surface detail on the other hand, which was usually used for determining morphological properties of the samples analyzed.

FESEM: The Field Emission Scanning Electron Microscope (FESEM) is an instrument which provides information about the sample surface, but with higher resolution and a much greater energy range than the usual SEM microscopes. The biggest difference between a FESEM and a SEM is the electron generation system. FESEM usually uses extremely focused electron beams, obtained using field emission guns. This, improves greatly the spatial resolution and allows the user to reduce the working potentials which are usually required, which in turn reduce the charging effect on non/conducting (or low/conducting) samples and avoids damage that the electron beam might cause to the sample. The FESEM used during this thesis is a Zeiss Gemini 500 Field Emission Scanning Microscope.

TEM characterization: Transmission electron microscope 200 kV Tecnai 20-F with X-ray analysis and STEM.

Measuring cell: The electrical properties measuring cell can be observed in Figure 1. The cell consists of two copper electrodes with a variable gap

in between Figure 1B. The copper electrodes used are around 2cm in diameter, a thickness that was specially selected so that high current densities would not cause Joule heating. The copper electrodes could not be the cause of unwanted resistances as it would be results in incorrect measurements of the actual material resistances. At both ends of the electrodes, two flat surfaces tightened by screws would act as the contact area between the electrodes and the material. It was believed that two flat surfaces causing a "sandwich" effect with the material to be measured, would possess less contact resistance areas than any other geometry. This is of utmost importance, as any unwanted resistances would result in the incorrect measurement of the conductivity and the ampacity. As the distance between the electrodes can be altered, it is possible to change the length of the conducting path measured, making this measuring cell suitable for longer or shorter materials as required. A circular methacrylate piece (Figure 1C) was added to the whole setup, which was sealed around the copper electrodes by means of two o-rings. With this addition, the whole measuring setup could be inserted into a chamber connected to a turbo-molecular vacuum pump. This allowed the measuring of electrical conditions at vacuum values close to $1 \cdot 10^{-5}$ mBar. It is important to mention that conductivity measurements in microscopic materials might suffer from uncontrollable errors in the measuring setup. For instance, synthesis of materials is subjected to small morphological changes, which, due to the scales at which measurements are done, could account for big changes in electrical values. Resistivity can be explained by means of several variables; resistance and distance between electrodes should not be affected by morphological changes in the synthesized material. However, measuring the diameter of the synthesized fibers was a source of debate during this work, as variations of several micrometers could be observed at different sections of the synthesized fibers. To try and minimize these errors, SEM microscopy was used to measure cross sections. However, the method for obtaining these cross sections was probably "altering" the morphology of the fiber. This, together with small diameter changes along the fiber, caused small errors during the conductivity measurements, something which was tried to avoid by repeating measurements in several sections along the fiber, trying to minimize the morphological effect in the measurements. The calculated error when measuring with the B2911A was calculated to be 6.2% due to the errors in the equipment used and the morphological changes in the samples.

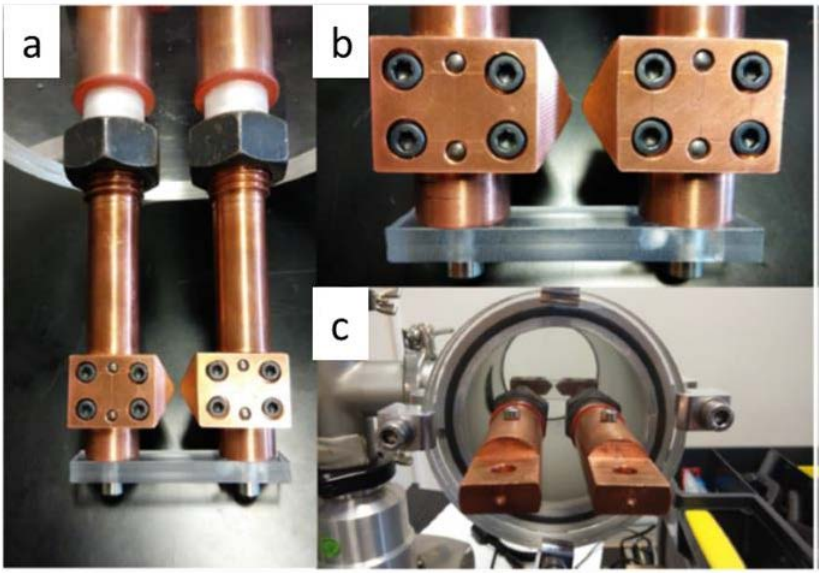

Figure 1: Ampacity cell designed especially for this thesis. It consisted on two copper electrodes, 1cm in diameter, connected to a methacrylate piece which is then connected to the vacuum chamber. Both electrodes were sealed against the methacrylate by means of o-rings. At the edges of both electrodes, there were two copper plates with screws, where the sample was placed. The distance between electrodes could be modified from few microns up to 2 cm.

Ampacity measurements: Ampacity was measured through several methods depending on the morphology of the sample. With all the thin wires and fibers, ampacity was measured by using the measuring cell described above and applying a stepped continuous current ramp with the B2911A power unit, from 0A to 2.5A. The step time was 0.01 seconds and each step were 0.0025 Amps. Four-point probe measurements were used in order to reduce the contact resistivity that could have an impact on the data obtention. For film ampacity measurements the DC AMREL SPS10-600 was used which did not allow for automatization of the measures, therefore manual measurements were done. 1 Amp steps were used (due to resolution limit), and each step was left for 1 second before noting down the current-voltage values. This was done in order to allow for the measurement to stabilize. These differences in the measuring techniques and apparatus used, were a source of errors, but could not be avoided due to the nature of the samples measured. As it will be explained in chapter 3, the reason why small diameters of copper and PTFE capillaries were used to synthesize the samples for the first half of the thesis, is mainly due to the lack of options for measuring ampacity. Bigger dimeters of copper would have required, even if the ampacity was not to be improved, power units

which could supply currents in the order of hundreds of amps. It is therefore important to keep in mind, that samples measured using the B2911A and the DC Amrel SPS10-600 power units should not be compared due to the difference in the measuring errors of each type of power unit. More importantly the DC Amrel SPS10-600 power unit didn't allow for 4-point probe measurements, something which was accounted for by increasing the diameter of the measuring cables to reduce any cable resistance which could "alter" the measurements.

Chapter 3: Copper-graphene oxide materials

Synthesis and characterization of graphene oxide

The first material that was synthesized during this thesis, was composed of copper and graphene oxide. As it has been stated in the state-of-the-art section, graphene oxide has an overall negative charge, due to the oxygenated state of the exfoliated graphene layers that were synthesized by modified Hummer's method. This method consists of several steps which are as follows:

The first step consists of a pre-oxidation step of the graphite powder. A three necked flask in a cold-water bath is used. 180 ml of sulfuric acid followed by 2 grams of sodium nitrate and 4 grams of graphite powder are added in that order and magnetically stirred for two hours. This creates graphite oxide.

The second step involves the slow addition of 11 grams of potassium permanganate, always making sure the temperature of the mixture remains below 20 C°. After the totality of the potassium permanganate is added, the dispersion is slowly heated until a temperature close to 35 C° is reached. The whole dispersion is left for two more hours in agitation. The third step is the end of the oxidation reaction, and for this, 180 ml of water is added drop by drop so that the temperature rises slowly. The mixture is left for another 15 minutes in agitation by magnetic stirring and the cleanse of the graphene oxide begins. The fourth step is the cleaning of the graphene oxide. For this, 30 ml of hydrogen peroxide is added in order to remove any remaining potassium permanganate [1]. The mixture is then left 40 minutes with no stirring. The whole mixture is centrifuged at 4000 rpm for 30 minutes until the supernatant is completely clear. This supernatant is removed, and clean water is added to the mixture. The cleaning cycles must be repeated until a pH close to 6 is reached. The last step, which is an optional step, was the lyophilization of the mixture after freezing it in liquid nitrogen. This lyophilization step allows the graphene oxide to be stored as a powder without losing its properties.

However, a special mention must be done on this behalf, as graphene oxide which is left for long periods in air, tend to hydrate and this changes the

properties. For this reason, graphene oxide had to be done every two months, making sure it was always at its optimal conditions.

Figure 1: Left, Graphene oxide after lyophilization. It forms a powder which can then be dispersed in water (right), to form a graphene oxide aqueous dispersion. It is important to use ultrasonication as means for the correct dispersion of the graphene oxide, as otherwise powder deposits could be found in the liquid medium.

Characterization of the graphene oxide powder was done by atomic force microscopy in tapping mode. A dispersion of graphene oxide in water (1mg/ml) was obtained, and a drop of this dispersion place on top of silicon dioxide, usually used in atomic microscopies due to its atomically flat surface, for the characterization. Atomic force microscopy allows for the visualization of atomic sized features, and this makes it a technique of great interest for material engineering.

The images were taken in random places of the dried drop, and no specific area was looked for. Tapping mode consist of making the cantilever oscillate at the natural frequency of oscillation and looking at the amplitude changes in this oscillation whenever there are interactions between the atomic point of the cantilever, and the atoms in the sample. The results of these atomic microscopies can be observed in Figure 2.

Graphene oxide layers have been found to have thicknesses around 0.7 nm as stated in the literature [2] therefore the layer shown in Figure 2 is one or maximum two layers of graphene oxide. The average size distribution shows that the layers are around 2 to 5 micrometers in length.

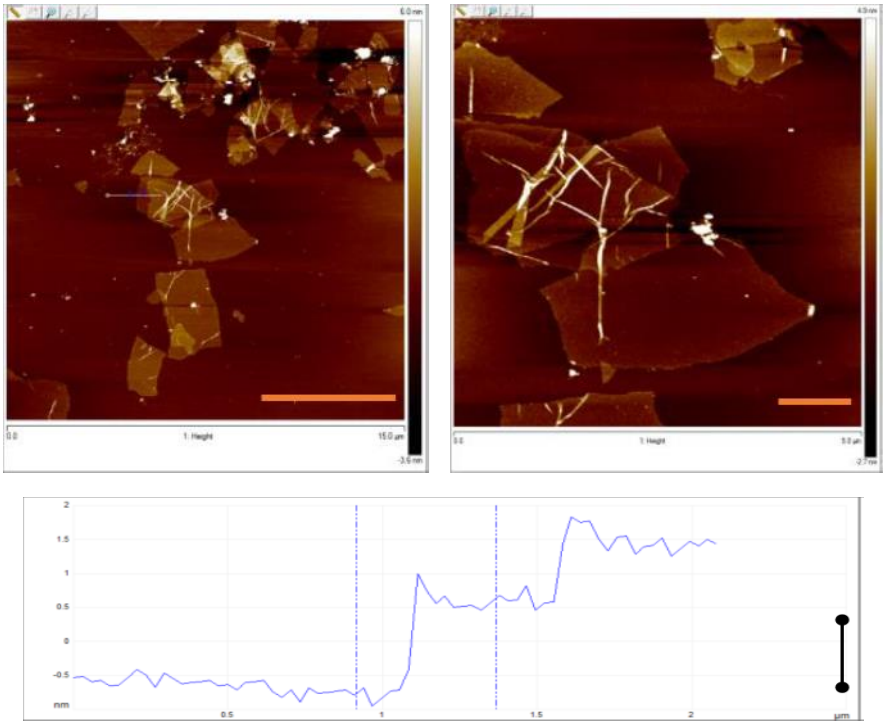

Figure 2: Top, atomic force microscopy (AFM) of graphene oxide platelets deposited on the surface of atomically flat silicon oxide substrate, left a 15um x 15 um area is scanned (scale bar 3 um) whilst right is the same area on a 5.5um x 5.5um scan size (scale bar 1 um) . When the thickness was measured (bottom) it is possible to see that most of the platelets found where in the order of 1nm, which corresponds to approximately one layer of graphene oxide as stated in literature (vertical scale=1nm).

Due to the oxygenated functional groups that are formed during the synthesis of graphene oxide, GO can form stable aqueous colloids due to electrostatic stabilization at pH values above pH 4, and can be considered to have an overall negative charge [3]. This has been proven by zeta potential measurements where it was possible to observe that GO (as well as r-GO), had zeta potentials around -30 mV from pH 4 to 12. Usually, colloids which possess zeta potentials higher than +30 mV or lower than -30 mV are considered to form stable suspensions due to interparticle electrostatic repulsions [4].

Electrophoretic deposition of GO

The idea was, therefore, to use this negative charge, to produce a homogeneous layer of graphene oxide, on the surface of a conducting electrode, in this case a conducting wire of copper. Electrophoretic deposition consists in a two-step process, by which the charged particle

suspension is able to move towards an electrode of the opposite charge, due to the influence of an electric field (Figure 3). The second step is the deposition of these charged particles to form a compact film on the surface of such electrode [5], [6]. Thanks to the overall negative charge of the graphene oxide layers, it is possible to this technique, often abbreviated as EPD, to deposit a suspension of graphene oxide in water, on the surface of a conducting electrode with the opposite charge. Electrophoretic deposition is a technique which offers very short processing times and requires very simple equipment. At the same time, it is a technique that with such simplicity, is able to produce uniform deposits with high microstructural homogeneity, making it one of the most interesting techniques for coatings [7], [8].

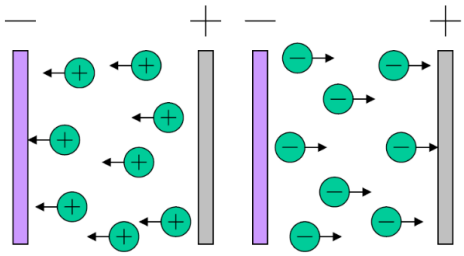

Figure 3: (Left) Cathodic electrophoretic deposition. Positively charged particles are attracted and deposited on the negative electrode. (Right) Anodic electrophoretic deposition. Negatively charged particles are deposited on the positive electrode.

Sometimes, the term electrophoretic deposition and electrodeposition are ambiguously used, although they are two different techniques; the main difference shortly, lies in EPD being based in a suspension of particles (charged particles) and electrodeposition (EDP) is based on solutions of salts, and therefore on ionic species [9]. There are two types of electrophoretic deposition depending on the electrode at which the deposition occurs. When the particles are positively charged, the deposition happens on the cathode, and therefore is known as cathodic electrophoretic deposition. When the opposite happens and the particles are negatively charged, the deposition occurs at the anode, therefore the process is known as anodic electrophoretic deposition. Usual electrophoretic deposition is done by applying a constant current or voltage for a certain time period. This kind of electrophoretic deposition is known as DC-EPD and an illustrative example can be observed in Figure 4. The first experimental results that were achieved during this thesis, were obtained by this method as it will be explained below.

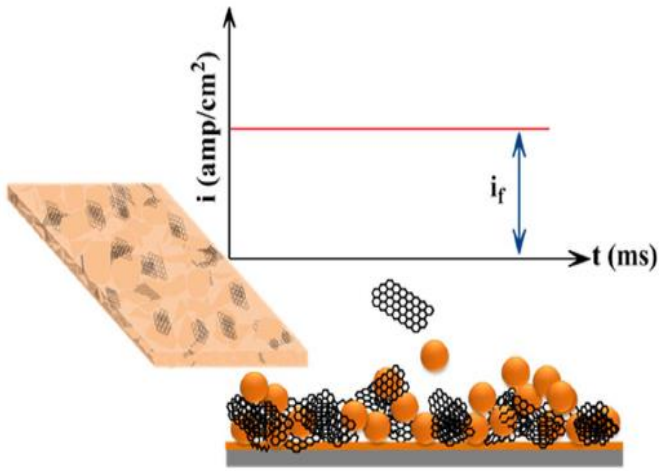

Figure 4: Unipolar wave in a usual cycle of DC-EPD. In this type of electrophoretic deposition, a constant current is applied for a time t. During a cycle, the sign of this wave is always the same, which attracts the oppositely charged colloids in the dispersion [10]

As it has been explained in the sections above, literature about the ampacity of graphene or graphene oxide was very limited at the time this thesis begun. It was believed that graphene oxide could be a very interesting material for the synthesis of high ampacity materials, as, the same that happens with carbon nanotubes, the carbon-carbon atoms present in graphene oxide should provide this material with outstanding ampacity properties. This property together with the conductivity values of copper, could prove to be a very good alternative for the carbon nanotube-copper composite that was presented by Subramaniam et al [11].

The idea was to use a copper microwire to use as the positive electrode during the electrophoretic deposition. Graphene oxide, attracted by the opposite charge of the electrode, would move towards that electrode, forming a compact film of graphene oxide on the surface of the microwire. This film would be left to dry, and the material synthesized would be tested for conductivity and ampacity. The diagram of the designed experiment can be seen in Figure 5. It is important to note, that a microwire was used, instead of a macroscopic copper wire, due to technical limitations when testing ampacity. According to Subramaniam et al [11], the ampacity of the composite material they synthesized was in the order of 600 x 10^6 A/cm^2, which meant that very thin conducting lines were to be used in order to reach the maximum current density during the tests. For instance, a conducting line of 400 micrometers in diameter would require 750000

Amps to reach that failure point. This is completely impossible to reach in normal laboratories, as most power units which are available commercially are not able to obtain these values. Therefore microwires, with sizes of 10, 20 and 25 micrometers were used instead, making sure that ampacity could be measured, no matter the current density the synthesized material could withstand.

To begin the process, graphene oxide was dispersed in distilled water at a concentration of 1mg/ml. because it is one of the best solvents for maintaining the dispersion for longer periods of time [12]. The graphene oxide powder that was obtained by means of lyophilization, was dispersed in water by means of an ultrasonic finger using times no longer than 30 seconds each time. Such small times were used, as bibliography states that longer times of ultrasonication exfoliation could produce smaller sized graphene oxide layers [13] which usually results in deteriorated properties of the carbon material.

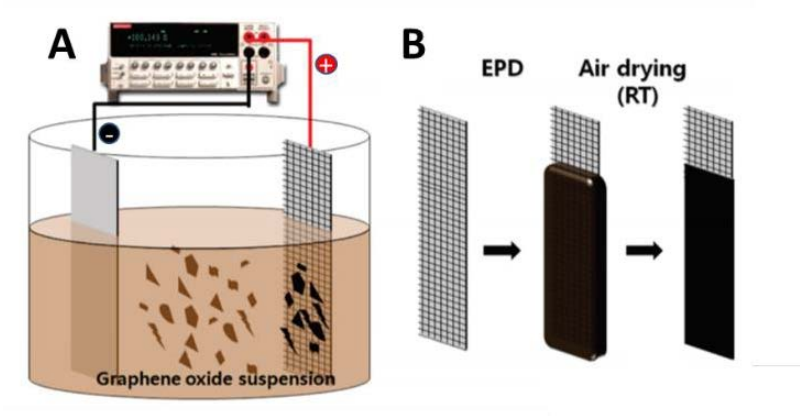

Figure 5: EPD diagram. Image obtained from reference [14]. *Graphene oxide deposited on copper electrode. The process of electrophoretic depositions consists on using the negative charge of the graphene oxide platelets in the suspension, to be able to attract them towards the surface of the positively charged electrode surface. After the process of EPD, a wet film of graphene oxide is deposited on the surface of the electrode, which is then left to dry in air.*

Designing the experiment was not as trivial as expected; due to the small size of the microwires, a support had to be made, as surface tensions present in the dispersion caused the bending of the wires when they came into contact with the liquid medium. The support had to be able to clamp the wire with ease without breaking it and had to do good electric contact with the microwire. The design that was done for this support can be seen in Figure 6.

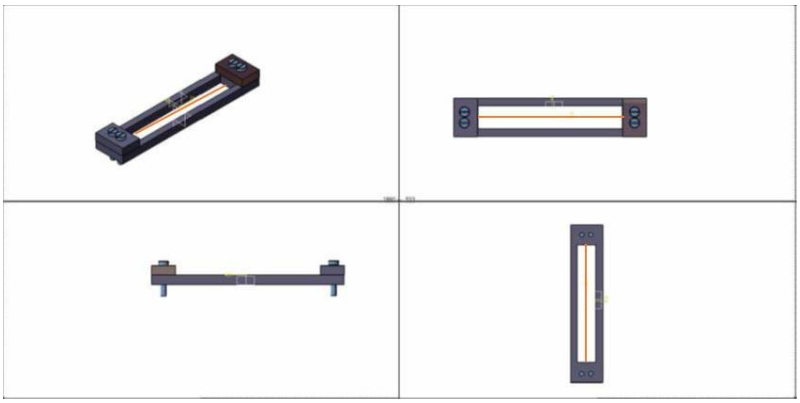

Figure 6: Design of the support for the copper microwire, which was designed to allow for the correct introduction of these wires into a liquid medium. One edge of the support has a copper contact, place where the power unit would be connected to.

Unfortunately, this was not the only drawback that was found in the preparatory stages. As it is well known for electrodeposition [15], electrode geometry can affect the overall deposition and film size, as edges, curves, holes or even a misalignment can produce different charge density which would result in heterogeneous deposition of the material, in this case the graphene oxide layers. As the microwire could be considered a cylinder like object, it was believed that a counter electrode with the same shape would provide the most homogeneous deposition as shown in Figure 7 schematically, and with the tests that were done to prove this. Being the copper wire surrounded by the negative electrode would provide a constant electric field throughout the dispersion, allowing the homogeneous deposition around the wire of graphene oxide platelets.

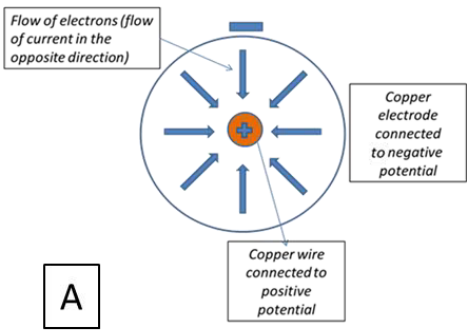

Figure 7A: schematic diagram of experimental setup, where the counter electrode would be a circular cylinder surrounding the microwire to be coated. This type of shape would allow for a more homogeneous distribution of charges during the process of electrophoretic deposition.

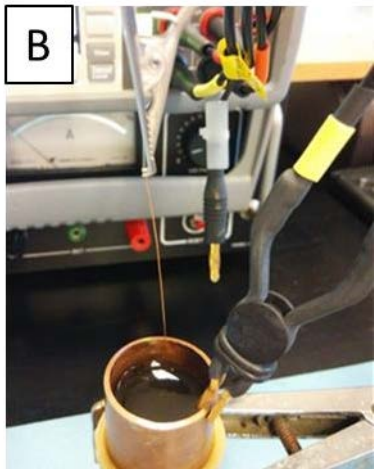

Figure 7B: Copper wire (400um in diameter) before and after electrophoretic deposition. It is possible to observe how after deposition, there is a black deposit on the edge of the electrode.

With these preliminary tests, it was possible to determine that the setup was working efficiently, and that the graphene oxide was indeed depositing on the copper wire being inserted into the dispersion. The next step was to determine electrochemical parameters for depositing on the 10, 20 and 25 micrometers microwires efficiently.

The first tests were carried out using the Agilent power supply unit at a voltage of 5 Volts and a duration of 10 seconds. Copper wires were introduced connected to the positive electrode, whilst the negative electrode was the rounded cylinder filled with the graphene oxide dispersion in water, at a concentration of 1 mg/ml.

Control of the power supply is done through a program available for PC which allows the user to create current/voltage profiles as well as stablish the duration of the deposition. As soon as the electrophoretic deposition was finished, the wire was removed from the dispersion and left to dry in ambient conditions.

The obtained electrophoretically deposited GO – copper wires were characterized by means of scanning electron microscopy (SEM). Results are shown in Figure 8 below. As it is possible to observe at higher magnifications, high porosity seems to be achieved by this method. Homogeneous deposition is achieved although high rugosity can be observed throughout the coating. This roughness is most likely caused by the quick drying process to which the wet graphene oxide coating is subjected to. Bibliography has observed similar results in graphene oxide

when subjected to a fast drying process in air [16]. Also noticeable in the SEM characterization, is the fact the graphene oxide on the surface of the wire does seem to follow a direction along the axial direction of the copper wire. Again, this is most likely caused by the drying process which "wraps" the graphene oxide against the wire, causing wrinkle-like structures.

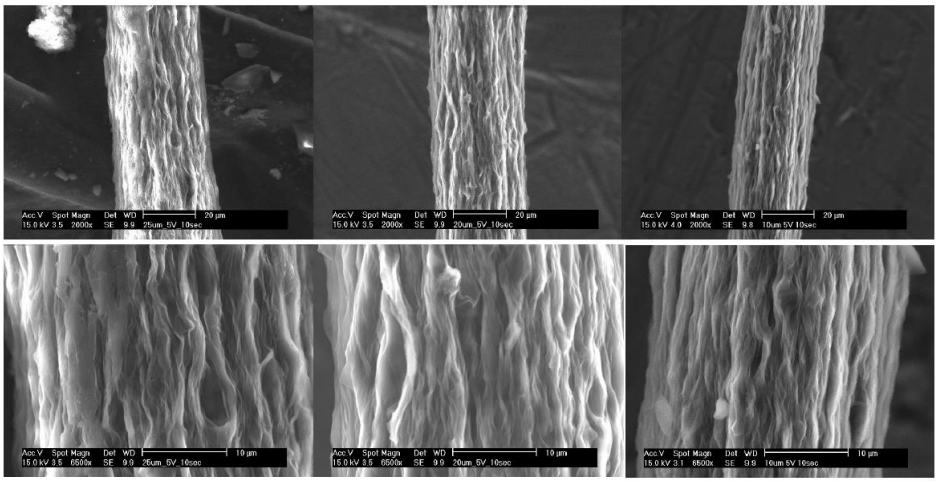

Figure 8: Scanning electron microscopy characterization of three different wires (25, 20 and 10 um) after having been electrophoretically deposited with graphene oxide. The surface shows a wrinkle like structure, due to the drying process in air, which contracts the graphene oxide layer that has been deposited, in the same axial direction as the microwire.

Having observed the surface morphology by SEM characterization, the next step was to determine the electrical properties of the new wires that had been created, namely conductivity and ampacity. Due to the small diameter of the coated wires, handling of these to make electrical measurements of any type showed great difficulty. Trying to connect both ends of the wire to normal crocodile clip connections deemed impossible at first. For this reason, a new kind of equipment was designed and implemented, and this equipment has been used during the thesis for testing out the conductivity and ampacity of the several materials that were synthesized. The equipment used is described in the materials and methods section.

The first measurements done to these GO-Cu wires were conductivity measurements by using a four-point probe setup, to avoid incorrect measurements due to the measuring cable resistances. To this end, the same B2911A power unit as the one used for the electrophoretic deposition phase was used. Using the Easy-EXPERT software, a current ramp from -0.001A to 0.001A was applied to the electrodes, and an I-V curve was

obtained. Small currents were used as it was necessary to maintain the structure of the line intact, and as soon as higher current are used, electromigration might begin to occur altering the results of the following ampacity measurements. The GO-Cu wire showed the behavior of a perfect conductor, so a straight line was obtained when the voltage-current was represented. From the slope of the I-V curve, it is possible to calculate the resistance of the wire by using Ohm's law, and using Pouillet's law, resistivity of the material could be obtained. The resistivity of these first three wires, was found to be around 2.5 x 10^{-8} Ω*m, double of the usual values found in bibliography. However, this higher resistivity, in comparison to bulk resistivity, has been documented before for ultra-thin and microscopic sized materials [17]–[19], so this higher resistivities (even in the bare copper reference wire) could be due to the microscopic sized diameters. One of the reasons CVD graphene is so conducting [20], is due to the large areas it possess, without any interruption to the carbon lattice, no defects, and therefore very few points for electron scattering during conduction. The size of the graphene oxide layers that were produced are far too small, probably due to the synthesis method together with the dispersion technique used, as ultrasonic fingers have been seen to produce smaller sized films than other dispersion methods [21](although these are usually less effective).

Ampacity had to be measured next. To measure ampacity, as it has been explained in the state-of-the-art section above, the resistivity and the current density had to be calculated. As a reminder, the ampacity point was the maximum current density, at which the resistivity remained constant. Above that point, there would be an increase in the resistivity due to the electromigration of the metal atoms in the conducting line. It is therefore easy to see, that the ampacity set-up would have to be the same as the one that was used for the conductivity measurements, with the only difference being, that instead of using a ramp with small currents as the ones used for conductivity, a series of steps with increasing current values were used. The limit of the ramp would be the limit of the power unit, which in this mode was 2 Amps. For calculating ampacity, a second set of synthesized wires were used for comparative reasons, and the 20 um sized copper wire was used this time: one was deposited for a smaller time (2 seconds) and a higher voltage (20 V), the second was deposited as the initial ones at 5 Volts for 10 seconds, and the third was deposited using 2.5 Volts and a time of 10 seconds too. Longer times produced thicker coating of GO as it was possible to observe visually, so longer periods of time were avoided as the

overall thickness of the composite material above those values reached values close to 60 μm in thickness. A bare wire with no EPD was used as reference. Values for resistivity and for ampacity were plotted on a graph and the results are shown below (Figure 9)

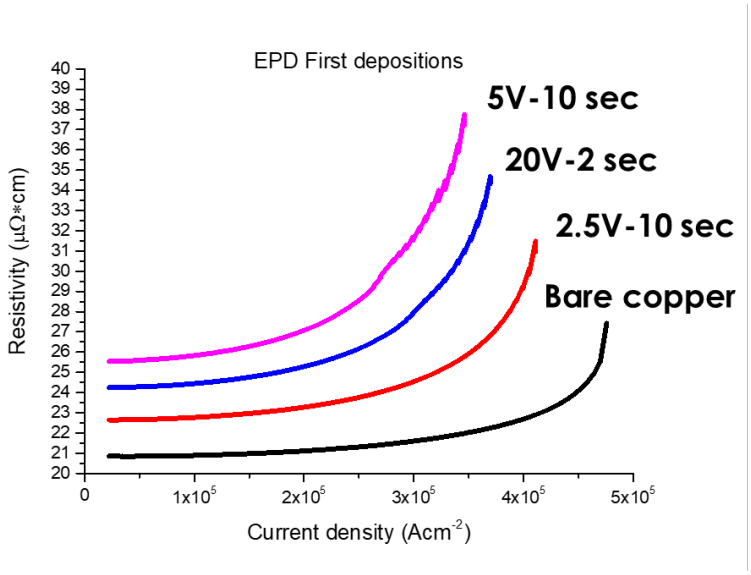

Figure 9: Ampacity comparison between different GO-Cu wires with different synthesis conditions. Compared to the bare copper reference, the three conditions that were used meant higher resistivities for the synthesized microwires, and smaller ampacity values.

From these first results, several conclusions were obtained. The first, the resistivity didn't remain constant as it was theoretically predicted, and instead behaved as a normal metal would, increasing the resistivity with the increase in current density. As it was very difficult from these graphs to determine the exact point at which failure mechanisms begun (take for instance 5V for 10 seconds in the graph above which is a curve from beginning to end), we decided that ampacity would be considered as the point of failure instead of the point at which the process of electromigration begun. Secondly, from this graph it was also possible to observe, that no matter the times or voltages used, there was a decrease in the maximum current density the synthesized materials could withstand, and an increase overall to the resistivities exhibited by these materials when compared to copper. There were some mechanisms occurring during EPD which was deteriorating the material and it had to be resolved. This was completely unexpected, and therefore a reason for this anomalous behavior was searched for. The answer came when the wires were characterized for a second time by SEM technique as seen in Figure 10.

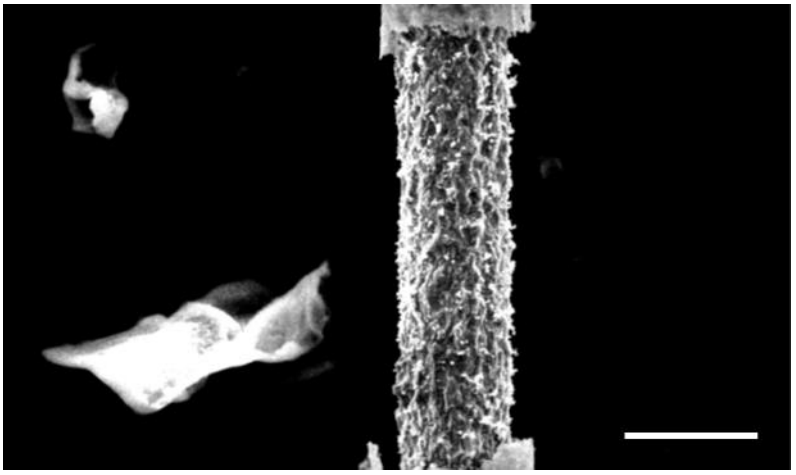

Figure 10: Pitting occurring in copper subjected to EPD. The micrograph shows a section of the microwire where the graphene oxide coating had been removed. The copper underneath shows a wrinkled structure, which was later demonstrated to be caused by oxidation processes occurring during EPD. Copper wire CU005170. Scale 20 um

The SEM image shows a section of the copper wire coated with graphene oxide at two of the edges, and a section which has no graphene oxide coating (reasons for this delamination are unknown but could have been due to manipulation of the wire). In the micrograph it is possible to observe a pitting of the copper core of the material. This kind of structure was observed several times with different electrophoretic deposition voltages and times, proving that there was some unknown mechanism occurring during EPD.

The best guess was that corrosion was occurring on the surface as the graphene was being deposited, as when a voltage is applied to the electrodes, our working electrode turns into an anode. Therefore, we can safely assume that the following half reaction is occurring at the same time as GO is being deposited on the surface:

$$\boxed{Anode}\ Cu \xrightarrow[Oxidation]{} Cu^{2+} + 2e^{-}$$

The SEM image supports this idea of the copper being oxidized and hence the pitted like structure. Many possibilities to try and avoid this damage were studied, and finally a different approach was used. An alternative although similar method, was used by Pavithra et al [22] to deposit graphene oxide on a conducting substrate. Instead of using direct current electrophoretic deposition, a method known as pulse reverse electrophoretic deposition (PREPD) was used. The main difference as explained by [10] between DC-EPD and Pulse Reverse Electrophoretic

deposition, is that in DC-EPD a voltage value is chosen and applied for a certain time with no variations. These waves are called unipolar, where all pulses are in one direction. On the other hand, PREPD consists on applying cathodic and anodic pulses instead of just unipolar waves, with small pauses in between during which no current passes through (Figure 11). This kind of wave form is known as bipolar.

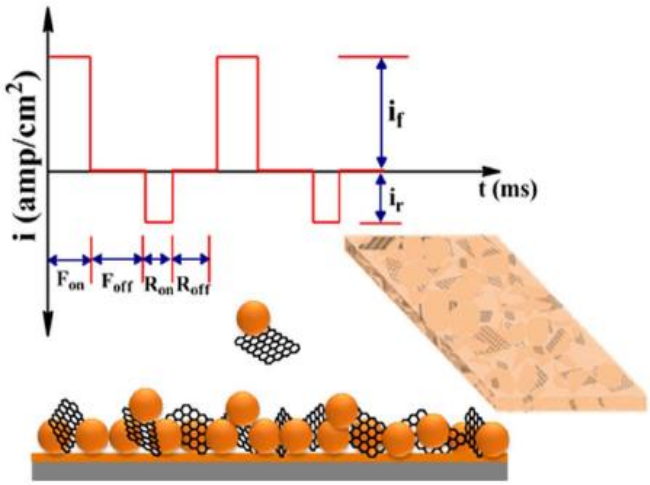

Figure 11: Pulse reverse electrophoretic deposition wave. This is known as bipolar, as during a cycle of duration t, there are both positive and negative pulses, as compared to unipolar waved in DC-EPD, where the wave sign remained constant throughout the deposition process [10]

However, the most interesting fact of PREPD is that there can be simultaneous deposition and reduction of the graphene oxide. On the anodic pulses of the cycle, the GO nanosheets are attracted towards the working electrode and deposited on the surface of the conducting substrate. When the wave then changes to the cathodic pulse, the film that has been deposited on the anodic pulse begins to reduce [23] as seen in Figure 12.

As it was explained above, during DC-EPD, a positive voltage causes an oxidation reaction on the surface of the electrode. It is important to notice, that there are other reactions occurring at the same time as well, such as the adsorption of negative GO onto the surface of the copper wire. However, for the sake of simplifications only the reaction occurring at the copper electrode surface will be mentioned for explanatory purposes. During PREPD, as the polarity changes, as well as oxidation of the copper wire, a reduction step also occurs caused by the anode and cathode alternating during the same cycle. Therefore, the copper electrode that was an anode,

becomes, during the same cycle, into a cathode with the following reaction occurring:

$$\boxed{Cathode}\ Cu^{2+} + 2e^{-} \xrightarrow[Reduction]{} Cu$$

The copper ions, therefore, that were in the electrolyte after the positive voltage that had been applied, would be attracted back towards the copper wire, reducing back on the electrode and "repairing" the surface pits and any other defects that the positive pulse might have caused. At the same time, and one of the main benefits of this technique, is that applying a reversed pulse causes the reduction of the graphene oxide on the surface of the wire without having to do any further thermal or chemical reduction steps.

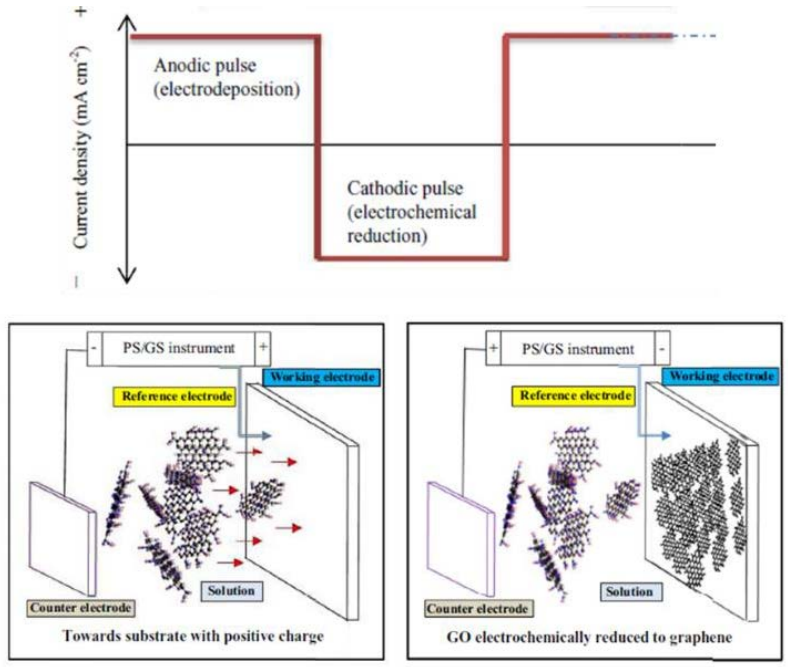

Figure 12: Anodic and cathodic pulses and the effect on the deposition of graphene oxide on a substrate. During the anodic pulse, the graphene oxide with negative charge, is attracted towards the positively charged electrode surface. When the sign of the wave is changed, and the cathodic pulse begins, a reduction process of the graphene oxide occurs, producing like this reduced graphene oxide (r-GO) [23]

Pulse reverse electrophoretic deposition

It is necessary to consider, that unlike DC-EPD, PREPD requires a much more complicated optimization. Unlike DC-EPD, which only has the current/voltage parameter, and the total time of deposition, PREPD has positive and negative current/voltage value which must be determined, times of cathodic and anodic pulses, times for ions replenishment in between pulses as well as total cycle time. This makes PREPD much more complicated to optimize and this was the first step that had to be done if an improvement in conductivity and ampacity was to be obtained.

The following table (Table 1), shows some of the parameters that were changed; where T_{for} accounts for the time of the forward pulse, T_{off} the time between pulses to allow for ion replenishment in the neighboring areas of the electrode, T_{rev} being the time of reverse pulse, I_{for} being the current density used for the forward pulse and I_{rev} the same but for the reverse pulse condition.

Table 1: Different parameters used for depositing 7 copper wires. The conditions are changed varying the time of the positive and negative pulses, the time between pulses, and the current density of these pulses. The number of cycles is constant for all the wires. As a reference, bare copper was used, and it exhibited a resistivity of 1.7 ($\mu\Omega \times cm$)

Wire number	Nº Cycles	Tfor (ms)	Toff (ms)	Trev (ms)	Ifor (Acm^{-2})	Irev (Acm^{-2})	Resistivity values ($\mu\Omega$*cm)
0	0	0	0	0	0	0	1.7
1	5	50	100	10	0.2	0.005	2.76
2	5	50	100	10	0.4	0.01	4.10
3	5	50	100	10	0.6	0.015	4.02
4	5	50	100	10	0.8	0.02	6.32
5	5	100	200	20	0.4	0.01	12.32
6	5	200	400	40	0.4	0.01	4.50
7	5	300	600	60	0.4	0.01	7.82

However, resistivities of each one of these pulse parameters resulted in a higher resistivity overall when compared to bare copper. There were some of the wires which exhibited values close to those of copper (such as wires 2, 3 and 6) but these were not conducting enough to be used as effective substitutes for copper. SEM characterization (Figure 13A) also showed a very heterogeneous coating when these parameters were used.

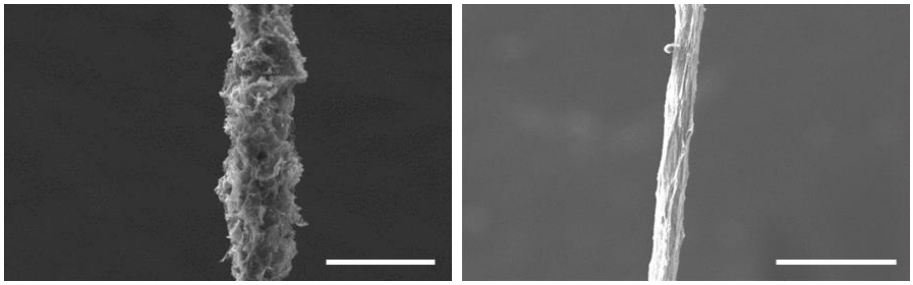

Figure 13: Left (A), copper wire after PREPD, with the conditions showed in table 1 for wire 2, scale 10 um. Right (B), copper wire after PREPD with low current densities of 237 mA cm being used for the deposition. Micrographs clearly show that with lower current densities, homogeneity of the coating produced is much better. Scale 100 um

Later, this heterogeneity was accounted for due to the oxygen production due to high voltage used (above hydrolysis voltages of water), and due to incorrect pulse times. In the article by Yaghoubinezhad et al [23], a wide variety of parameters for the deposition of graphene oxide by pulse reverse electrophoretic deposition had been studied and documented. The relation between the parameters according to this article could be summarized by the following equation:

$$Q(C) = -5058.32 + 40.35 * (i) - 3667.27 * (T_a) + 3374.03 * (T_c) + 33.50 * (T_t)$$

In this equation, Q refers to electrical charge, i the current density, T_a the anodic pulse duration, T_c the cathodic pulse durantion and T_t the total pulse reverse electrodeposition time. According to this article, the CCD algorithm they had used stated that T_a and T_c are more critical than the total time or the current used. According to this article also, the optimum parameters are those, in which the cathodic duration time (required time for reducing the graphene nanosheets upon the surface) is in the high levels

and anodic time is in the low levels. In other words, at the selected range of applied current densities, the movement of GO nanosheets from the bulk of the suspension to near the surface is very high (very short anodic times) whilst the times required to thoroughly remove the functional groups (reduction) are much longer in comparison, and hence the cathodic pulses are required to be longer.

Mainly, at each cathodic pulse, potential in front of the cathode interface must be raised up to a specific value for the reduction of nanosheets at the cathode surface, due to the capacitor rule of electrical double layers. If charge and discharge times of the double layer becomes more than the cathodic and anodic periods in pulses, damping will happen and cause unsuccessful deposition and reduction in the process. In principle, after deposition, an electrochemical driving force must be supplying the adequate negative charge towards overcoming the energy barriers of GO and the reduction of oxygen functionalities brings about modifications of the electronic states of the Fermi energy levels of the electrode surface. As far as the applied current densities is referred, the increment of the current density leads to an increase in the deposition.

It is important to mention though, that the hydrolysis of water occurs at -1.22 V meaning that at long cathodic times, and/or high current densities, the portion of hydrogen evolution will increase due to water decomposition, which causes bubbles an in turn severe damage to the deposited layer as it has been explained in bibliography before [24]. With these facts in mind, the optimum parameters that were found, were at a current density equal to 237 mA cm^{-2}, T_a equal to 3.25 ms, T_c of about 7.75 ms and a total time (T_t) of approximately 474.64 seconds. With these parameters in mind, new synthesized wires (20um diameter) were subjected to the conductivity and ampacity tests, and the results are shown in Figure 14. It is important to mention, that all the synthesized wires from this point onwards, were done with the 20 um diameter wires, as, in terms of conductivity, they were the same as the 10 and 15 um wires, with the benefit that the handling was easier than for the two thinner versions.

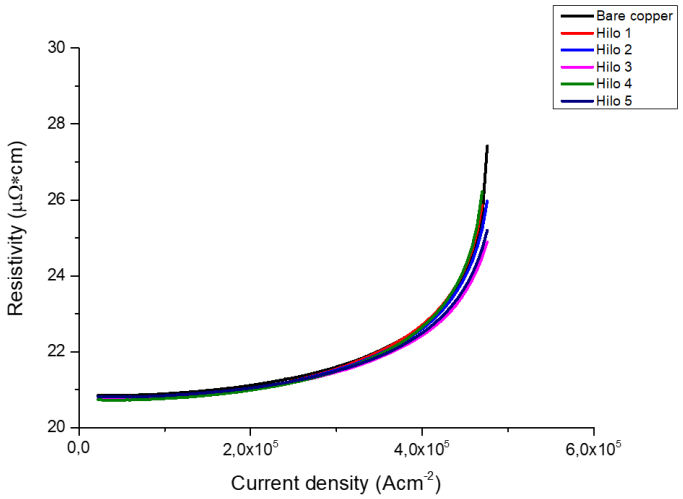

Figure 14: PREPD repeated on 5 different copper wires, 20 um in diameter, and synthesized using the low current density conditions (237 mA cm^{-2}). Reference bare copper was also measured for comparative reasons.

As it is clearly visible in the graph, there was a significant improvement of the obtained material when compared to the wires that were being obtained by DC-EPD. Resistivity as well as ampacity of the reduced graphene – copper wires is equally good as those shown by bare copper. As an additional control step, SEM characterization was required, as it had to be proven that the pitting of the copper core was being caused by the DC-EPD as it had been hypothesized. SEM characterization is shown in Figure 15, where it is possible to see that the pitting of the wires was no longer occurring when using PREPD. Bare areas in the copper wire (Figure 15C and D) shows a flat uniform surface, exactly the same as for the bare copper with no electrochemical treatment. This proved the point, that the ampacity and conductivity were being diminished by the oxidation of the copper electrode whilst undergoing DC-EPD, and this effect was being avoided completely when using PREPD. Figure 13 shows that from the initial parameters used (Figure 13A) to the optimized parameters (Figure 13B) there is a clear morphological change on the coating produced, as well as for the values of the conductivity and ampacity values as it has been shown in Figure 14.

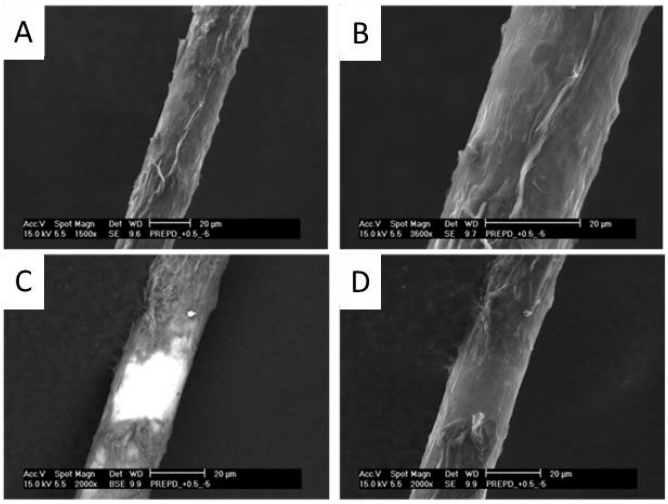

Figure 15: SEM characterization of a copper wire after undergoing pulse reverse electrophoretic deposition. Images A and B exhibit a uniform coating on the surface of the copper wire. Bare areas of the coated copper wire (C and D) exhibit no pitting, therefore oxidation is avoided with this kind of process.

Aiming for an even greater conductivity improvement, and extra step was implemented, were thermal anneal at 700 °C in Argon atmosphere for 1 hour was used. This step has been widely documented in literature [25], [26], where a thermal anneal step is usually used to reduce the graphene oxide further, and at the same time, it can benefit the conductivity of the copper by increasing the size of its crystal grains . Increasing crystal grains results in less grain boundaries in the crystal structure which improves the overall conductivity of any metal.

However, the results that were obtained, as seen in Figure 16, indicated that the thermal anneal was having no effect on the conductivity/ampacity of the synthesized wires, and neither on the bare copper reference wire which had been subjected to the same conditions for comparative reasons.

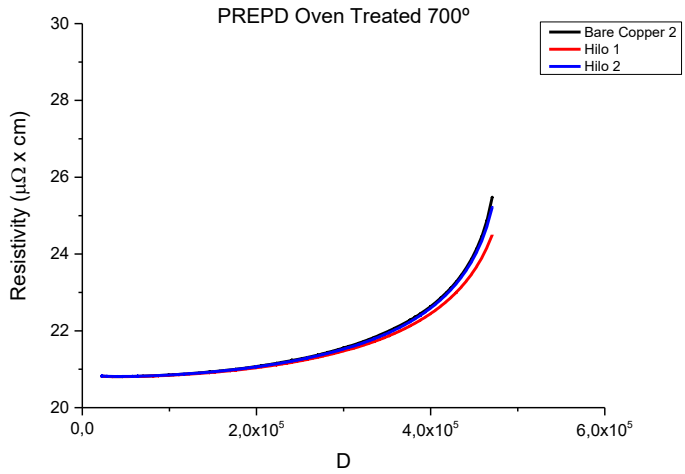

Figure 16: Graph of resistivity vs current density for the pulse reverse electrophoretic deposited copper wires. It is possible to observe no decrease of either the conductivity or the ampacity of the copper-graphene oxide wire, as compared to the bare copper wire that was used for reference purposes, and thermal anneal did not show any improvements on these properties.

Chapter 3 conclusions

There are several conclusions which can be obtained from this first chapter. First, and most important, pulse reverse electrophoretic deposition must be used whenever there is graphene oxide involved in the deposition process as opposed to normal electrophoretic deposition by constant current. Having during the same cycle anodic and cathodic pulses allows for a homogeneous deposition of the graphene oxide platelets and helps the reduction of the coating produced. This reduction has been proven by the fact that when undergoing a thermal anneal, as it was presented in Figure 16, there is no improvement on the overall conductivity. If the graphene oxide was still oxidized after its deposition on the surface of the copper wire, this would have produced an increase in the overall resistivity when compared to bare copper.

On the other hand, after having determined the optimal parameters, the ampacity and conductivity of the synthesized wires were constant and comparable to bare copper. There is no improvement in any of the properties when compared to the pure metal, which shows that the effect of coating copper wires with graphene oxide (DC-EPD), or reduced graphene oxide (PR-EPD), causes no interaction between the copper atoms

and the carbon atoms in the synthesized material. As it has been explained in the state-of-the-art section, an interaction between both materials must be achieved in order to improve ampacity. As it was stated by Subramaniam et al [11], the carbon nanotubes in their synthesized material, were caging the copper atoms and preventing them from electromigrating when under high current densities. On the wires that were synthesized during this first chapter, there seems to be no interaction between the two different materials, which causes the "normal" electromigration process along the copper core, causing the failure of the whole wire as it would occur in bare copper wires, and this has been repeatedly observed in the resistivity-current density graphs that have been presented.

Lastly, using a "coating" of any type increases, no matter how little the density of the coating material, the overall weight of the synthesized material when compared to the bare material prior to coating. If ampacity would have been improved even slightly, this would have opened the opportunity for reducing the cross-section area of the copper core. However, as it has been observed, ampacity remains the same with no relation to the coating being used, which means that there has been an increase in the overall weight due to the addition of the graphene oxide, with no improvement on the ampacity or conductivity, meaning that this technique is not effective for obtaining a material which could substitute the copper wires in any case.

With all these factors in mind, it is safe to assume that electrophoretic deposition is not a technique which can improve conductivity or ampacity when compared to pure copper. It might provide other benefits to the coated wire, such as improved mechanical properties or improved conductivity at higher temperatures. However, these properties were out of the scope for the project.

Bibliography

[1] M. J. Yoo and H. B. Park, "Effect of hydrogen peroxide on properties of graphene oxide in Hummers method," *Carbon N. Y.*, vol. 141, pp. 515–522, Jan. 2019.

[2] J. W. Suk, R. D. Piner, J. An, and R. S. Ruoff, "Mechanical Properties of Monolayer Graphene Oxide," *ACS Nano*, vol. 4, no. 11, pp. 6557–6564, Nov. 2010.

[3] B. Konkena and S. Vasudevan, "Understanding Aqueous Dispersibility of Graphene Oxide and Reduced Graphene Oxide through pKi Measurements," *J. Phys. Chem. Lett.*, vol. 3, no. 7, pp. 867–872, Apr. 2012.

[4] R. J. Hunter, *Zeta potential in colloid science : principles and applications*. .

[5] P. Sarkar and P. S. Nicholson, "Electrophoretic Deposition (EPD): Mechanisms, Kinetics, and Application to Ceramics," *J. Am. Ceram. Soc.*, vol. 79, no. 8, pp. 1987–2002, Aug. 1996.

[6] O. O. Van der Biest and L. J. Vandeperre, "Electrophoretic deposition of materials," *Annu. Rev. Mater. Sci.*, vol. 29, no. 1, pp. 327–352, Aug. 1999.

[7] A. Chavez-Valdez, M. S. P. Shaffer, and A. R. Boccaccini, "Applications of Graphene Electrophoretic Deposition. A Review," *J. Phys. Chem. B*, vol. 117, no. 6, pp. 1502–1515, Feb. 2013.

[8] O. O. Van der Biest and L. J. Vandeperre, "Electrophoretic deposition of materials," *Annu. Rev. Mater. Sci.*, vol. 29, no. 1, pp. 327–352, Aug. 1999.

[9] L. Besra and M. Liu, "A review on fundamentals and applications of electrophoretic deposition (EPD)," *Prog. Mater. Sci.*, vol. 52, no. 1, pp. 1–61, 2007.

[10] M. S. Chandrasekar and M. Pushpavanam, "Pulse and pulse reverse plating-Conceptual, advantages and applications," *Electrochim. Acta*, vol. 53, no. 8, pp. 3313–3322, Mar. 2008.

[11] C. Subramaniam *et al.*, "One hundred fold increase in current carrying capacity in a carbon nanotube-copper composite.," *Nat. Commun.*, vol. 4, p. 2202, Jan. 2013.

[12] J. Taha-Tijerina *et al.*, "Quantification of the Particle Size and Stability of Graphene Oxide in a Variety of Solvents," *Part. Part. Syst.*

Charact., vol. 32, no. 3, pp. 334–339, Mar. 2015.

[13] X. Qi, T. Zhou, S. Deng, G. Zong, X. Yao, and Q. Fu, "Size-specified graphene oxide sheets: ultrasonication assisted preparation and characterization," *J. Mater. Sci.*, vol. 49, no. 4, pp. 1785–1793, Feb. 2014.

[14] S. J. An *et al.*, "Thin Film Fabrication and Simultaneous Anodic Reduction of Deposited Graphene Oxide Platelets by Electrophoretic Deposition," *J. Phys. Chem. Lett*, vol. 1, pp. 1259–1263, 2010.

[15] Y. D. Gamburg and G. Zangari, *Theory and practice of metal electrodeposition*. Springer, 2011.

[16] X. Ma, M. R. Zachariah, and C. D. Zangmeister, "Crumpled Nanopaper from Graphene Oxide," *Nano Lett.*, vol. 12, no. 1, pp. 486–489, Jan. 2012.

[17] S. Dutta *et al.*, "Thickness dependence of the resistivity of Platinum group metal thin films," Jan. 2017.

[18] E. Schmiedl, P. Wissmann, and H.-U. Finzel, "The Electrical Resistivity of Ultra-Thin Copper Films," 2008.

[19] F. Lacy, "Developing a theoretical relationship between electrical resistivity, temperature, and film thickness for conductors.," *Nanoscale Res. Lett.*, vol. 6, no. 1, p. 636, Dec. 2011.

[20] A. Reina *et al.*, "Large Area, Few-Layer Graphene Films on Arbitrary Substrates by Chemical Vapor Deposition," *Nano Lett.*, vol. 9, no. 1, pp. 30–35, Jan. 2009.

[21] S. Pan and I. A. Aksay, "Factors Controlling the Size of Graphene Oxide Sheets Produced via the Graphite Oxide Route," *ACS Nano*, vol. 5, no. 5, pp. 4073–4083, May 2011.

[22] C. L. P. Pavithra, B. V Sarada, K. V Rajulapati, T. N. Rao, and G. Sundararajan, "A new electrochemical approach for the synthesis of copper-graphene nanocomposite foils with high hardness.," *Sci. Rep.*, vol. 4, p. 4049, Jan. 2014.

[23] Y. Yaghoubinezhad and a. Afshar, "Design of Experiments for Pulse Reverse Electrodeposition of Graphene Oxide toward Hydrogen Evolution Reaction," *ECS J. Solid State Sci. Technol.*, vol. 4, no. 3, pp. M7–M17, 2015.

[24] S. Cherevko, N. Kulyk, and C.-H. Chung, "Pulse-reverse

electrodeposition for mesoporous metal films: combination of hydrogen evolution assisted deposition and electrochemical dealloying.," *Nanoscale*, vol. 4, no. 2, pp. 568–75, Jan. 2012.

[25] A. Bagri, C. Mattevi, M. Acik, Y. J. Chabal, M. Chhowalla, and V. B. Shenoy, "Structural evolution during the reduction of chemically derived graphene oxide," *Nat. Chem.*, vol. 2, no. 7, pp. 581–587, Jul. 2010.

[26] S. Pei and H.-M. Cheng, "The reduction of graphene oxide," *Carbon N. Y.*, vol. 50, no. 9, pp. 3210–3228, Aug. 2012.

Chapter 4: Graphene oxide microwires

As it has been presented in the second chapter of the thesis, coating a copper wire didn't seem to improve the ampacity and clearly would not help in decreasing the density of the final material. An alternative method had to be searched for, one which would allow to synthesize a real hybrid material, and not just a coating on the surface. The answer came by an article presented by Yu. et al [1] and which was corroborated by other research groups at the time [2]. The idea was to produce microfibers of carbonaceous materials, with techniques that could be upgraded to the macroscopic scale. The materials these groups produced had great flexibility and most importantly, they were found to be weavable. Being weavable opened many different opportunities for the use in the aircraft industry. As it has been explained in the state-of-the-art section, light strike protection is usually a mesh produced from a copper foil that is simultaneously slit and stretched, expanded, into a single uniform, precision, non-woven structure as seen in Figure 1A.

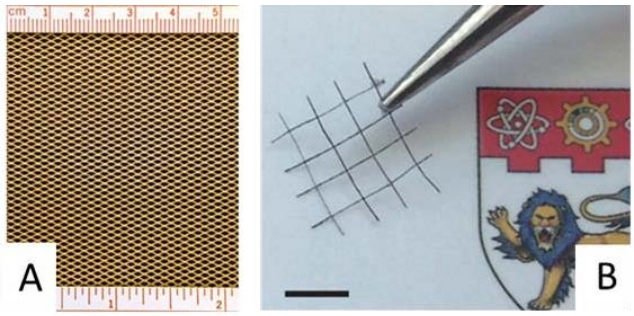

Figure 1: A) shows the expanded copper foil structure (Dexmet) used for lightning strike protection in aircraft industry. B) Weaved mesh of reduced graphene and CNT fibers showing the potential of this kind of structure [1].

With this in mind, it was believed that searching for a material so flexible that it could be woven into different structures (Figure 1B), could be a good starting point in searching for an alternative to pure copper structures. The idea, that was being used by the group of Yu et al, was to create an aqueous feeding solution which was composed of graphene oxide, single walled carbon nanotubes and ethylene diamine (EDA), which would act as a nitrogen dopant. As EDA possessed two $-NH_2$ end anchors, it was used to bind the oxidized carbon nanotubes to the graphene oxide platelets. This allowed for the creation of three-dimensional architectures. By means of a peristaltic pump, and a flow of nitrogen, the solution was passed through a

capillary tube. Both ends of the capillary tube would then be sealed, to maintain a high pressure of nitrogen in the inside of the tube, and the capillary would remain inside an oven for 6 hours at 220 °C. After that time, both ends would be opened and the synthesized fiber would be expelled out of the capillary, by the effect of nitrogen pressure on one of the ends. This process, although with small modifications, is known as hydrothermal synthesis. Hydrothermal processes are used to synthesize materials from aqueous solutions at high pressures, in confined vessels which are known as autoclaves [3]–[7]. The hydrothermal technique appeared in the mid-19th century, where the term was used to describe the formation of minerals by hot water solutions rising from cooling magma. Usually, hydrothermal (and solvothermal for organic solvents) synthesis, requires high temperatures ranging from 100-1000 °C, and high pressures, usually from 1-100 MPa [8]. According to reaction temperatures, hydrothermal synthesis can be classified into subcritical and supercritical synthesis reactions. Usually, the temperatures used in laboratory experiments which range in the 100-250 °C are considered to be subcritical.

However, Yu et al [1] were aiming to achieve a highly porous material, for their use as micro-supercapacitors and hence some of the parameters that were used in their article, had to be changed to suit the requirements of this project. For instance, their search for high specific surface area, so necessary for capacitors, was the reason why EDA and nitrogen doped carbon nanotubes were used. Although these three components together, formed very stable structures, as it has been mentioned, it also caused an indirect reduction in the conductivity of the material produced since the introduction of nitrogen atoms in the material distorts the graphitic-like lattice by increasing the number of defects present in the carbon lattice [9]. As it has been explained in the state-of-the-art section, these points of defect concentration are "failure points" for electromigration mechanisms as well as areas where electron movement is opposed causing an increase in the overall resistivity of the material. These negative effects on the electrical properties of the material motivated the search for a different alternative.

Graphene oxide in aqueous dispersion, together with hydrothermal and solvothermal synthesis, has been used for the synthesis of aerogels for some time [10]–[13]. When an aqueous dispersion of graphene oxide is inserted into an autoclave at high temperature and pressure, the reduction of such layers occurs, causing the self-assembly of the individual platelets into a 3-D materials [14], [15]. According to some studies, during the hydrothermal process the oxygenated groups present in the graphene oxide are gradually

removed in the form of CO_2, causing a change in the graphene oxide structure. Hydrophobicity and the π- π interactions between the layers of graphene oxide are increased, causing the attraction between layers to form a three dimensional structure, with aleatorily assembled reduced graphene oxide platelets, and a micro-porosity in the range of a few microns. [16].

Although Yu et al [1], had proposed an automatized method for producing graphene oxide fibers (Figure 2), several modifications had to be done, due to some limitations that were encountered. The capillary that was used to replicate the experiment by Yu et al, were made out of stainless steel. In particular, this tubing had been initially acquired for HPLC chromatography, so it was believed that these tubing would withstand the high pressures required. However, it was soon discovered, that stainless steel was not a good option, as graphene oxide fibers got "stuck" in the inside of the capillary, and it was impossible to withdraw a complete fiber from their interior. Pushing high pressure gases through the capillary was not effective, and neither was flowing liquids through the capillary. Other problems also appeared during the automatization in our laboratory, the motorized syringe that was being used to push the dispersion into the capillary tube exerted too much pressure for the capillary joints causing the liquid to leak. With these problems, it was decided that a different approach had to be searched for.

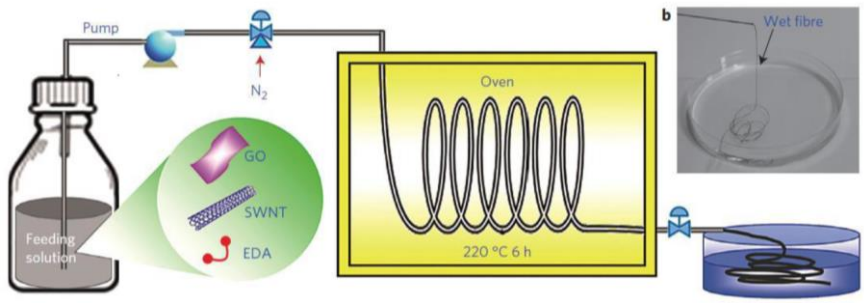

Figure 2: Image obtained from reference [1]. Yu et al method for producing GO, SWNT and EDA fibers in continuous form. This is a variation of the actual technique that was used during the thesis, as the feeding solution used was graphene oxide and water only, and instead of having a continuous line, the capillary was sealed inside an autoclave so no optimization of gas flows, or solution feed rates had to be done. This way, the number of variables needed to be controlled were highly reduced, producing the same results for testing purposes.

An autoclave was designed, following other bibliographical references which had also synthesized graphene oxide fibers [17]. The autoclave in its interior, consisted on a PTFE container which was filled up with water, and this is where the capillary tubes were placed. A PTFE capillary 50 μm in diameter was used, and a dispersion of graphene oxide (1mg/ml) in water

was flown into the capillary until the whole interior was filled up. Sealing of the capillary occurred naturally by the surface tension of the liquids inside the capillary, so no extra sealing was required. The capillaries filled up with the dispersion were submerged underneath the water, and the autoclave closed. By leaving the autoclave overnight (10 hours) at a temperature of 180 °C, results similar to the ones observed through thermal reductions at temperatures close to 300 °C in reducing atmospheres can be observed [18]. Through this method, reduction of the graphene oxide was achieved, and in the interior of the PTFE tubing the reduced graphene oxide fiber was produced. In order to understand more in depth, the morphology that was being formed, SEM characterization of these fibers was done as seen in Figure 3.

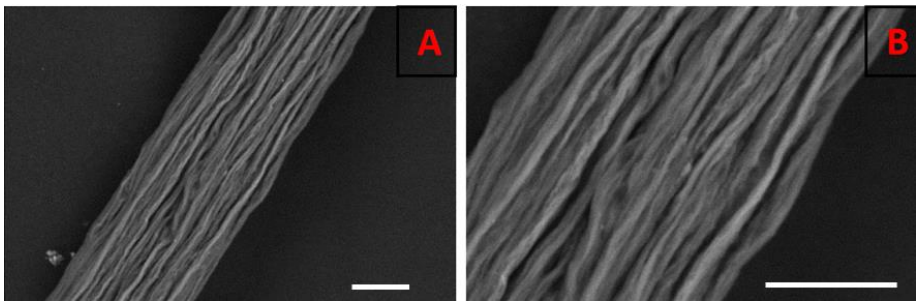

Figure 3: A and B shows SEM microscopies of the same r-GO fibers once dried in air. They have a diameter of about 35 micrometers, proving that they shrink in size when dried as compared to the initial capillary diameter which was 4 times the size. They exhibit an orientation longitudinal to the fiber, showing that the flow of the solution through a capillary must orient the present GO platelets. Scale bar 20um

As it is possible to observe from these images, the fiber looks similar to the coating that were produced by electrophoretic deposition in the previous chapter. However, this time, the fibers were produced in its totality by reduced graphene oxide, which means that the density of these fibers was much smaller than the one that a copper wire of the same diameter could present. From the images it is also possible to see the wrinkle like structure of the surface, which again, is probably caused by the quick shrinkage of the fiber when drying. To characterize the density of these fibers, helium densitometry and Archimedes method were employed. However, due to the very small features of these fibers, these methods resulted in erratic results. Trying to calculate the density through volume and mass was also impossible, as the mass could not be measured by any means available. For this kind of measurement to be done, meters of the material had to be synthesized. However, before producing such quantities of material, other experimental properties such as the electrical properties had to be determined.

The extent of this hydrothermal reduction had been widely researched by our group [19]. With the XPS it is possible to observe an increase in the aromatic (C=C) and aliphatic (C-C) structures, at the same time a severe decrease in the C-O band occurs. This decrease corresponds to the hydroxyl and epoxy groups which have been reduced, and to the stacking of the layers of carbon between them. Thanks to XPS results, it was also possible to observe a decrease in the oxygen content by more than 50% with respect to the unreduced graphene oxide. Again, as it has been mentioned above, these results confirm bibliographical facts, that state that hydrothermal reduction at these temperatures is equivalent to thermal reductions at much higher temperatures [20].

Conductivity measurements were done to these fibers, and these values were in the order of 300-400 Sm^{-1}, well below the values for any metal, and 5 orders of magnitude below those values of copper. As it has been reported in literature, reduced graphene oxide structures exhibit these orders of conductivity by other reduction routes, such as by hydrazine (270 Sm^{-1}) or by acid reduction (298 Sm^{-1}) [21]. This means, that no matter how well the graphene oxide is reduced, an improvement step must be added if the conductivity is to be increased such as in our case, where electrical properties are needed. As it has been stated in the introduction section of this thesis, at least a conductivity close to the one shown by copper is required. Therefore, the addition of copper to the graphene oxide fibers, seemed as the most logical approach, and this was exactly what was tried. The following sections will synthesize the most important findings in the r-GO – Copper fiber approaches.

r-GO – Copper fiber functionalization

There are several possible ways, to functionalize graphene oxide (reduced graphene oxide in our case) with copper. However, every technique has its own advantages and drawbacks. Functionalization of graphene with several metals, such as Au, Ag, Pt, Pd, Co and Rh have been done in bibliography by different chemical methods [22], [23]. However, and due to the difficulty of scaling these methods, a different approach was searched for, one which could be easily scaled and at the same time cost-effective.

Microwave functionalization

A technique known as microwave-induced fabrication, was the first of these techniques to be used. This technique had been used to decorate with metallic nanoparticles the surface of carbon nanotubes [24] but the same principles could be applied to graphene oxide [25]. In the article by Leelaviwat et al, it was reported that functionalization was done to the oxidized carbon nanotubes by mixing them with a copper sulfate solution in water and applying microwave radiation in a normal household microwave. Oxidation had to be done prior to the reaction, so that the carbon nanotubes had anchoring points in the surface, such as the carbonyl, carboxyl and hydroxyl groups which are also present in the graphene oxide which is used to create the fibers. It is important to remind the reader, that although reduction is achieved via hydrothermal reduction, more than 50% of oxygenated groups in the reduced graphene oxide fibers still remain , meaning that the functional groups which have been mentioned can still be found in the surface of the fibers. As it has been stated in bibliography, the main mechanism behind the microwave assisted method, is the Joule heating that occurs in the carbonaceous materials, causing a local "thermal" reduction mechanism [26].

Anchoring of the copper nanoparticles prior to the fiber formation was discarded, as the formation of the fibers is subjected to the interaction between the graphene oxide sheets once they are reduced, and any addition of particles prior to the hydrothermal synthesis resulted in the non-formation of the R-GO fibers. Reduced graphene oxide fibers were therefore submerged into a solution of copper nitrate (0.1 M) in ethanol, as this would be our reducing medium, and microwave pulses for a total duration of 2 minutes was used to decorate the surface of the fiber. The addition of copper nanoparticles on the surface of carbon nanotubes, which can be extrapolated to the reduced graphene oxide fibers, usually occurs in several steps; an electrostatic adsorption step between the copper ions in the solution and the oxygenated groups on the surface of the CNTs occurs first, anchoring copper ions to the surface of the CNTs; then, a secondary microwave irradiation step by which reduction and nucleation of the copper occurs on the surface of the CNTs due to the high temperatures which are locally caused around the CNTs; lastly a third step by which crystal growth occurs as more copper ions reduce on the surface of the deposited copper. The detailed mechanism of Cu or copper oxides deposition is under study,

but the experimental fact is that copper containing particles were formed on the surface of r-GO microfibers.

However, instead of the typical round copper containing particles, ringed like structures had deposited on the surface of the fiber as revealed by the SEM images shown in Figure 4. These rings correspond to the copper oxide whilst the darker areas of the image correspond to the reduced graphene oxide. The images observed in Figure 4, correspond to the two minutes functionalization that has been mentioned.

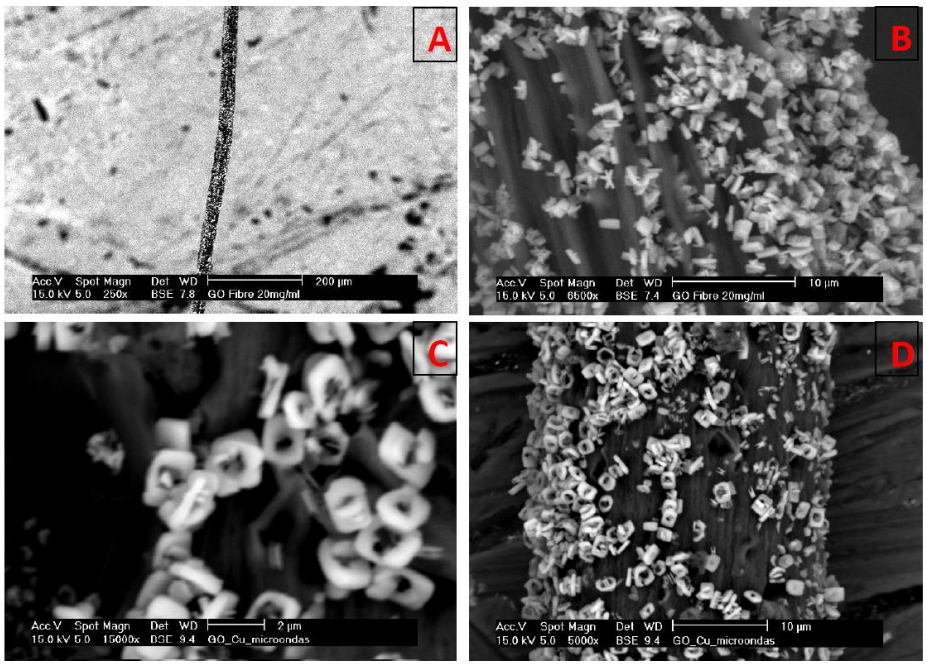

Figure 4: Microwave assisted copper deposition: A-D show SEM images of the copper deposited on the surface of the r-GO fibers by microwave radiation, by the insertion of the fibers into a microwave, in a solution of ethanol and copper nitrate. The fibers were left for 2 minutes in the microwave, obtaining like this a surface covered with ring shaped copper crystals.

Longer times under microwave radiation caused an increased coverage throughout the fibers. However, as it could be clearly seen in the SEM micrographs, the copper oxide rings seemed to be depositing in the outside of the reduced graphene oxide fiber. Conductivity of the reduced graphene oxide fiber as it has been mentioned above, was in the order of 300 Sm^{-1} at room temperature, and after functionalization this conductivity raised to 400 Sm^{-1} approximately. It is difficult to state, whether this increased conductivity is due to the copper (copper oxide) on the surface of the reduced graphene oxide fiber, or due to a more extensive reduction of the fiber due to the microwave radiation as already reported. [27], [28]. This

could account for the small increase in conductivity which was observed after the copper functionalization. The oxygenated groups that remain in the fiber are severely reduced after the hydrothermal process, therefore further reduction by any means (in this case due to microwave radiation), can only reduce the fiber in the areas which have not been previously reduced. Some further tests were carried out to check how the copper oxide had deposited within the fiber or just in the outside. For this end, transmission electron microscopy was used. Sample areas from different parts of the fiber were obtained and the results can be seen in Figure 5.

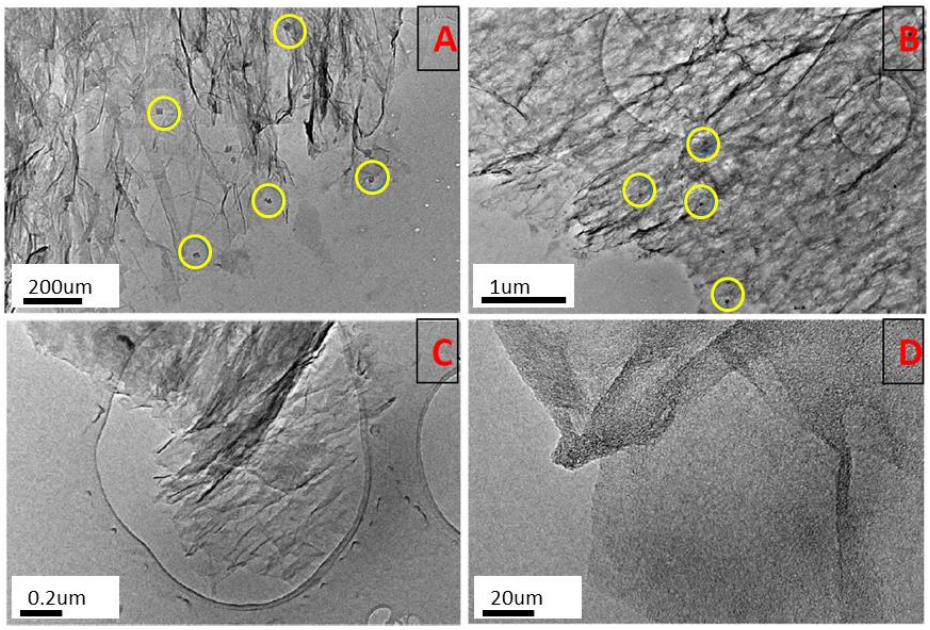

Figure 5: TEM microscopy of the reduced graphene oxide fiber after microwave assisted functionalization. On A and B, it is possible to observe (surrounded by circles) copper particles. However, most of the areas were similar to C-D which shows no copper deposited at all. This clearly indicates that although copper had been deposited on the fiber, it was not homogeneously distributed throughout the fiber.

It was possible to see that the flakes corresponding to the outer regions of the fibers, showed traces of copper and copper oxide (Figure 5A and B), whilst the interior of the fiber had no copper whatsoever. This was further proof that this method would not be useful for the ends intended in the project, as a hybrid would have to show a homogeneous distribution of copper throughout the whole material. These fibers were discarded immediately, as neither conductivity nor the homogeneity of the material were found to be enough. However, other options for introducing copper within the reduced graphene oxide fiber were done. The following section explains the second method that was tried for this; electrodeposition.

Copper electrodeposition in fibers

The main problem during the microwave functionalization, was that copper oxide was depositing on the fiber, and it was pure copper what was required if a better conductivity was to be achieved. Electrodeposition is a technique which has been long studied and the deposition mechanisms of copper are widely known [29]. With this technique, it was possible to be sure that pure copper would be obtained in the surface of our reduced graphene oxide electrode, and at the same time it is a technique which can be easily scaled and doesn't require complex apparatus. The same as what happens with electrophoretic deposition (as it has been explained in the second chapter of this thesis), tuning the current densities applied to the deposition process causes changes in the thickness and homogeneity of the deposited copper on the surface. With electrodeposition, the reduced graphene oxide fiber is connected to the negative terminal. When the circuit is closed, electrons flow through the reduced graphene oxide fiber towards the liquid medium. As the negative charge concentration on the fiber is so high, this attracts copper ions from the solution towards the electrode and are in turn reduced on the surface of the fiber forming in this way nucleation points throughout the fiber. As the fiber becomes full of nucleation sites, a new growth mechanism will become dominant, causing the nucleation sites to grow in size. Bigger crystals will therefore be formed and, if left for enough time, will come into contact with each other forming a conducting metal matrix.

Electrodeposition was done to the reduced graphene oxide fiber at a voltage of 1V for 5, 10 and 15 minutes. The solution was made up of an aqueous dispersion of copper sulfate at a concentration of 1M. The fibers were readily washed after electrodeposition with ethanol and dried in air. Optically, as seen in Figure 6, the fibers show copper on the surface. With 5 minutes, the amount of copper that had deposited was very little, which meant that the conducting pathways between the copper nuclei would probably have not been formed. However, for 10 and 15 minutes of electrodeposition, copper could be seen homogeneously distributed throughout the fiber.

Figure 6: Optical photographs of the 5 (A), 10 (B) and 15 (C) minutes electrodeposited r-GO fibers, showing an increasing coverage of the copper coating, being 5 minutes clearly insufficient to coat the fiber, and 15 minutes exhibiting a slight diameter increase.

Conductivity values for the three fibers were obtained, and a fourth "bare" control fiber was also measured. As it was stated before, the bare fiber showed conductivities around 300 Sm^{-1} again as it was expected, whilst the 5-minute electrodeposited fiber presented conductivity values of 800 Sm^{-1}. After 10 minutes of electrodeposition, the value of conductivity raised to $1.25 \cdot 10^4$ Sm^{-1} whilst at 15 minutes of electrodeposition the value of conductivity was $2.75 \cdot 10^4$ Sm^{-1}. These values were much higher than the original conductivities of the bare r-GO fiber, being still however, two orders of magnitude below copper standards.

Further characterization of the fibers by SEM microscopy (Figure 7), showed that even though copper was depositing correctly on the surface of the r-GO fibers, diffusion of the copper ions within the fiber was not taking place. For the cross-section characterization of fibers, they are submerged into liquid nitrogen, and pulled apart by the effect of two tweezers, one at each of its ends. Cryogenic fracture was used throughout the thesis for obtaining cross sections for characterization, without affecting their morphological appearance by using other cutting equipment such as scissors which would collapse the structure, making it uncharacterizable. In

the SEM images it was possible to observe a ring of copper that was being formed around the r-Go fiber. Longer electrodeposition times only caused a thicker outer coating, whilst lower deposition times made an un-connected matrix of copper nuclei. Although the diffusion of copper ions had to be the dominant process during the electrodeposition, it was the nucleation and growth of copper in the outside which was causing the "coating effect".

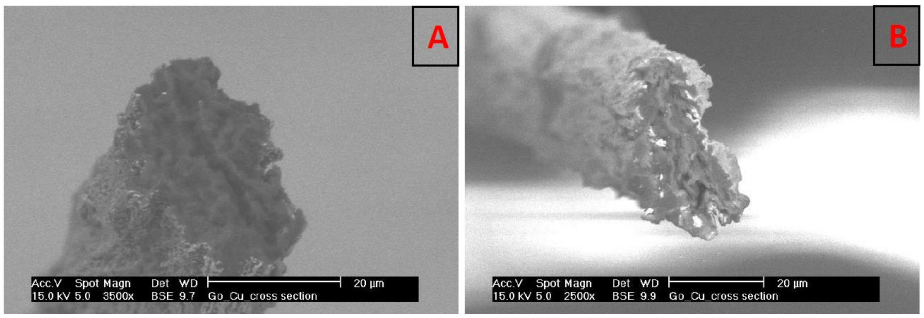

Figure 7: SEM microscopy for the cross-section areas of a r-GO after 10 (A)- and 15 (B)-minutes electrodeposition. Copper can be observed as the lighter regions in the image, whilst the darker regions account for the reduced graphene oxide. It is clearly visible that there is no copper diffusing into the inside of the fibers, and most of the copper remains in the outside of the material.

Further investigation into the possible alternatives to avoid the complete coating of the fibers was searched for. During electrodeposition, the growth of a copper film surrounding the fiber, caused the complete blockage of the microporosity of the fiber. This, in turn, avoided any further diffusion of copper ions in the interior, and therefore, the growth phase in the inside of the fiber. This was clearly observed in the SEM characterizations, as small nuclei could be observed in the core of the fiber, however, never big enough to have caused any significant contribution to the overall conductivity of the fiber. Having read the work by Subramaniam et al [30], and although the structure of their hybrid material was different, we believed that the mechanisms involved in our synthesis and theirs, did not differ so much.

According to their work, the electrodeposition had to be separated into two phases: firstly, they did a wetting phase to the hydrophobic CNTs with copper ions in an organic solution, to nucleate Cu seed on the CNT surface, and secondly, they grew the Cu seeds in an aqueous solution until all the mesopores were filled. In the organic electrodeposition phase, the homogeneous seeding of Cu nuclei required that the rate-limiting step had to be the Cu nucleation on the CNTs rather than the Cu ion diffusion through the CNT structure. As it was stated in their article, slow deposition rates (1-5 mA cm^{-2} versus conventional rates of 50-100 mA cm^{-2}) are

required to electrodeposit Cu through the dense CNT matrix, and not only on the outer surface as was our case. At low current densities, copper homogeneously nucleates throughout the CNT matrix, resulting in high conductivities and a high copper filling ratio, but maintaining low specific surface areas. On the opposite case, at higher current densities, copper nucleated on the outside surface of the CNT fibers, resulting in the opposite effect.

If done right, a low current density would maintain the overall thickness of the material close to a constant value whilst the conductivity increases greatly. When the internal filling is complete, conductivity remains constant whilst the thickness increases, which would account for the outer filling of the material. However, and unlike the referenced article, CNTs are hydrophobic whilst the graphene oxide fiber is hydrophilic. For this reason, the use of an organic solvent, like the one used by Subramaniam et al, was unnecessary, and an aqueous solution with the same copper salt (copper acetate 2.75 mM) was used. The fibers were submerged into the solution for 20 minutes prior electrodeposition. The time required to deposit $3.1 \cdot 10^{-5}$ grams of copper was calculated by using Faraday's law of electrolysis. This mass of copper was estimated by calculating the mass that would be required to form a thin layer of copper in the outside of such thin r-GO fibers, and by estimating the volume and density of such film.

For a current density of 2.5 mA cm^{-2} and a time of 6000 seconds a fiber coated with copper should be obtained. Using secondary electrons (SE) mode in SEM (Figure 8 left), a complete coverage of the fiber is observed. However, as seen in Figure 8 right, which shows the back scattered electrons (BSE) mode of the cross section of the fiber, the copper seemed to have diffused approximately by 5 μm inside the r-GO fiber (lighter regions of the microscopy), and the overall size of the hybrid fiber has also increased, meaning that once the initial copper had diffused those 5 μm, it had blocked further diffusion and changed to the growth phase, which had in turn increased the size without further copper diffusion. However, when the conductivity of these graphene-copper fibers was measured, they showed a huge improvement in comparison to previous fibers reported.

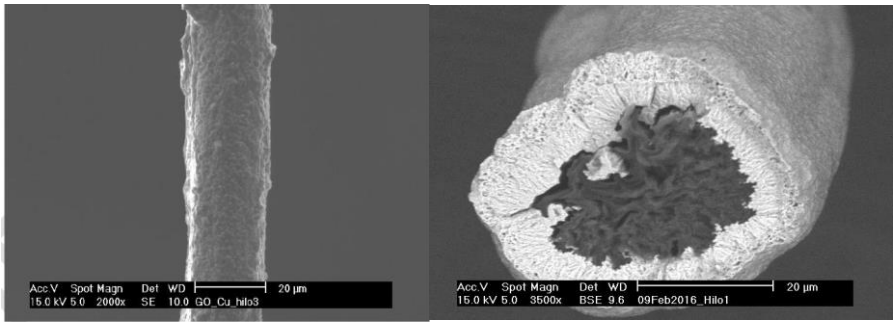

Figure 8: A Low current density electrodeposition for 6000 seconds. Left, homogeneous coverage of copper can be observed throughout the hole fiber. Right, cross section of fibers. It is possible to observe, that copper had penetrated very little into the r-GO fiber (estimation of 5 um according to initial images). Also observed was the fact that the diameter of the fiber had increased, meaning that once the initial copper had diffused those 5 um, it had blocked further diffusion

At this point it is important to mention, that conductivity could be measured by taking into account different sections of the fiber, which could give different information; One of the methods, was to measure the full cross section area, taking into account the r-GO section and the copper section too. The second method was to measure the "hybrid" section of the fiber, or the part where the copper and the graphene oxide were interconnected. We believed that the full cross section area would be more realistic, as the ring section could not be "extracted" or isolated easily, meaning that the full cross section area would be a more realistic scenario. An I-V measurement was carried out and the slope of the obtained measurement was measured to obtain the resistance of the full fiber. The calculated value was 2.4 x 10^6 Sm^{-1} , a value very close to the usual conductivity values found in ultra-thin copper films, and one order below bulk copper [31], [32]. At the same time the ampacity exceeded the ones that had been observed up to that point, as with the maximum current that the source could produce (2.5 Amps) the fiber remained intact, exhibiting ampacities higher than those had been previously measured, reaching, at least, values of $2 \cdot 10^5$ Acm^{-2}.

However, it was believed, that a superior conductivity could be obtained if the copper managed to diffuse even further inside the fiber. The porosity of the fiber seemed far too small in order to let copper ions diffuse easily throughout the fiber. Therefore, a new step was introduced in the synthesis of the fibers, aiming to increase the porosity of such fibers. These created channels, would in theory allow for the easier diffusion of copper into the fiber, allowing for the growth phase to take place throughout the entire fiber.

There were several drawbacks to the idea of producing a porous microfiber. First, if pores were introduced during the hydrothermal step, it was very likely that the microfibers would not form, as the mechanical resistance of the fiber would suffer due to the introduction of such defects into its structure. In macroscopic structures, such as scaffolds [33]–[35], introducing pores has usually negative effects to the mechanical properties, however, the outside structure remains similar to the non-porous version of the same material. However, at micrometer scales, such as the fibers that were being synthesized by hydrothermal synthesis, a pore which could have 5 to 10 μm would correspond to half the size of the diameter, meaning that the fragility of the fiber would turn the material unusable. As a second negative downside for introducing pores into the reduced graphene oxide microfibers was the conductivity. Introducing defects into the fiber would create even more scatter points for the electron movements, causing a decrease in conductivity, and theoretically a reduced ampacity. However, this could be overcome, if copper could diffuse and deposit inside those pores, causing an increase in conductivity and most likely for ampacity.

As soon as the fibers had been obtained by the hydrothermal approach, they were extracted from the capillary PTFE tube, and left in an aqueous media (so that they could not dry) until they were frozen in liquid nitrogen; and as soon as they were completely solid, they were introduced in the lyophilization chamber. Lyophilization, also known as freeze drying, consists on reducing the pressure surrounding the sample (in this case the fiber) and as the temperature begins to gradually rise (from the nitrogen temperature which is -195 ºC up until -50 ºC) the ice crystals sublimate directly to form gas, leaving behind the cavities that were before occupied by these crystals. By this method, porous fibers were created, and such fibers could be observed in the Field Effect Scanning Electron Microscope (FESEM) as shown in Figure 9.

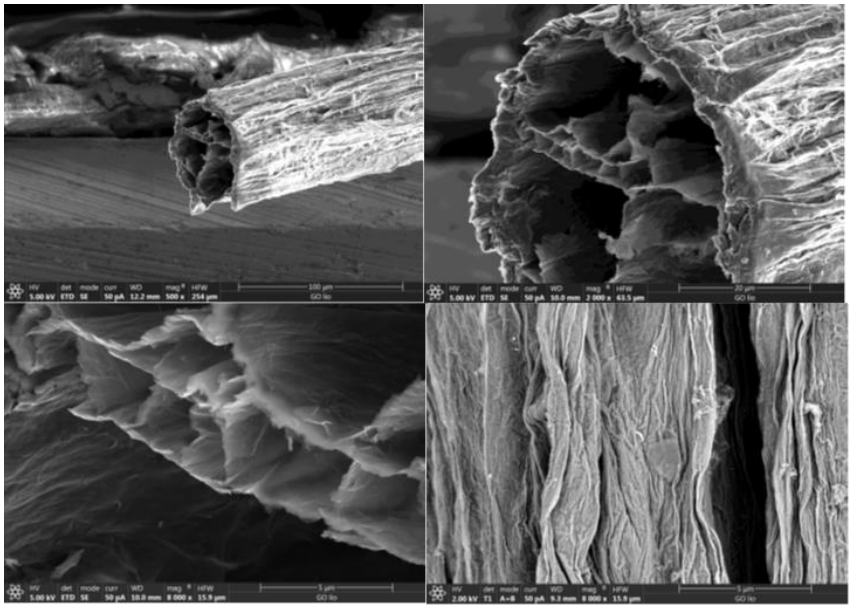

Figure 9: FESEM image of lyophilized porous reduced graphene oxide fibers. The interior of the fibers showed voids and spaces produced by the sublimation of water from ice crystals to gas. These pores should allow easier ion diffusion into the interior of the fibers. The walls of the fiber, although they seem compact, are also porous.

As it can be observed, a heterogeneous porosity could be obtained by this method. Pores ranging from 3 μm to approximately 10 μm were achieved. This porosity opened the possibility for an easier diffusion of copper ions into the fiber. With these new pores, electrodeposition was repeated, low constant current densities again were used (2 $mAcm^{-2}$) together with times in the range of 9000 seconds, and the results can be seen in Figure 10 below.

The copper this time, did diffuse into the core of the fiber, and deposited in the interior filling the walls of all the cavities inside the fiber. The conductivity for these synthesized fibers in DC electrodeposition, were in the order of 1.2 x 10^6 Sm^{-1} when measured (taking into account the whole diameter of the fiber) and an ampacity of $1.2 \cdot 10^5$ Acm^{-2} approximately as it can be observed in Figure 11 below. However, it is also important to notice, that copper mainly deposited on the outer walls of the fiber. This is expected in electrodeposition, as it is this place where the copper ion concentration is higher. In the interior of the fiber, once the copper ions have diffused and an electric current applied, the ions deposit, leaving like this the interior areas depleted of copper ions as time evolves. For this reason, it is of utmost importance, that a constant flow of ions into the fiber is obtained, or otherwise the copper ions inside the fibers cannot be replenished, causing a very thin layer of copper, and not the intended full

pore. As the copper ion concentration is much higher in the surrounding of the fiber, the outside section of the fiber rapidly increases in size during electrodeposition.

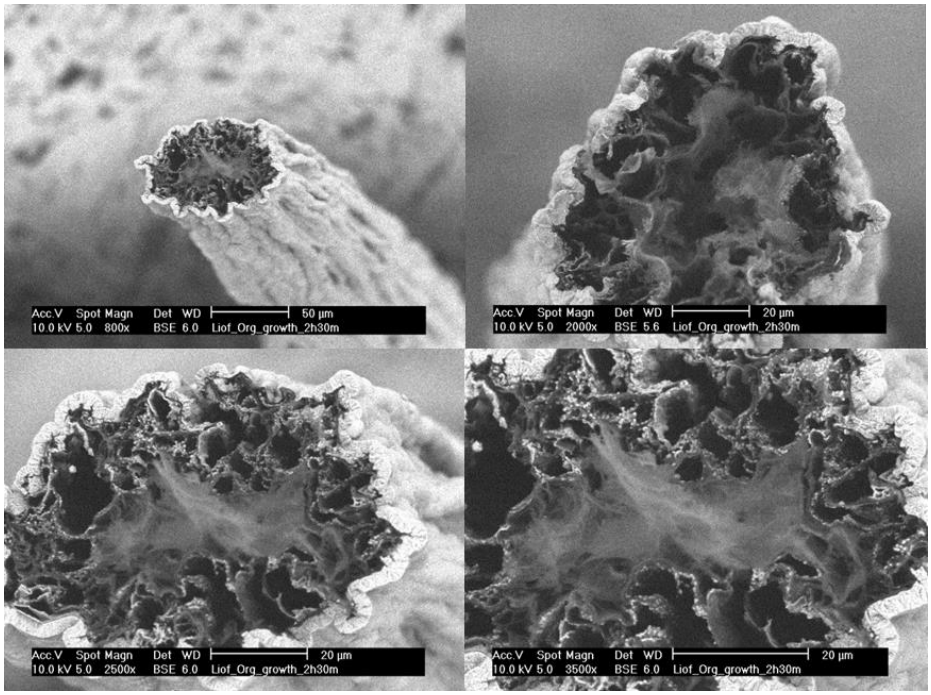

Figure 10: Copper electrodeposition 9000s 2mA/cm2 porous r-go fibers. From the images it is possible to observe that copper ions diffused into the interior of the fibers and had deposited throughout the surfaces of the pores. However, most of the copper remained in the exterior of the fiber, which blocked further passage of ions.

A technique which could help in improving this setback was required, and pulse-reverse electrodeposition could prove useful for this end. As it has been mentioned, there are three times which can be tuned during electrodeposition. Two opposing pulses and a dead time in between these pulses which could help the replenishment of ions during electrodeposition. Stirring of the medium was also introduced, as a mean to keep the ion concentration homogeneous throughout the medium. It is widely known that it helps the replenishment of ions during electroplating techniques and enhances the coatings quality [36], [37].

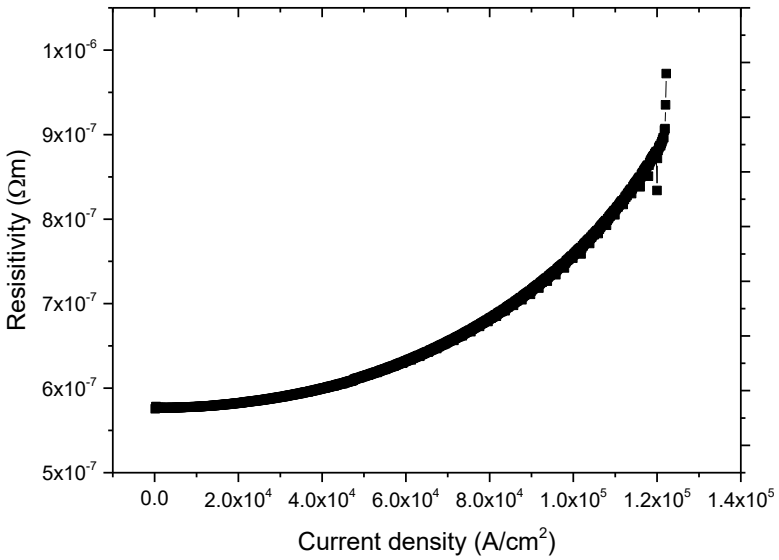

Figure 11: Resistivity/conductivity vs current density graph for DC electrodeposited porous fibers ((2 mA cm-,2 9000 seconds), exhibiting conductivities and ampacities one order below those of bulk copper.

Several of the parameters for pulse reverse electrodeposition were optimized for months, changing anodic and cathodic times, dead times, current densities in both anodic and cathodic pulses, but the best fiber obtained, the one that was synthesized by applying current densities of 1 $mAcm^{-2}$ for both anodic and cathodic pulses, pulse times of 0.5 seconds and a total deposition time of 18000 seconds, achieved a conductivity of 4325 Sm^{-1}, two orders of magnitude below the conductivity that had been achieved by the DC electrodeposition process. Ampacity values were in the range of $6 \cdot 10^3$ Acm^{-2}, again, far below those of copper and of the previously mentioned fibers. SEM characterization (Figure 12) of these fibers showed that the copper that was being deposited, seemed to aggregate together into bigger grains, showing that the dominant phase was the growth phase and not nucleation as it happened with DC electrodeposition. This kind of growth meant that copper grains were not in contact with each other, and therefore no conducting path could form inside the fibers hence the low conductivities that were observed.

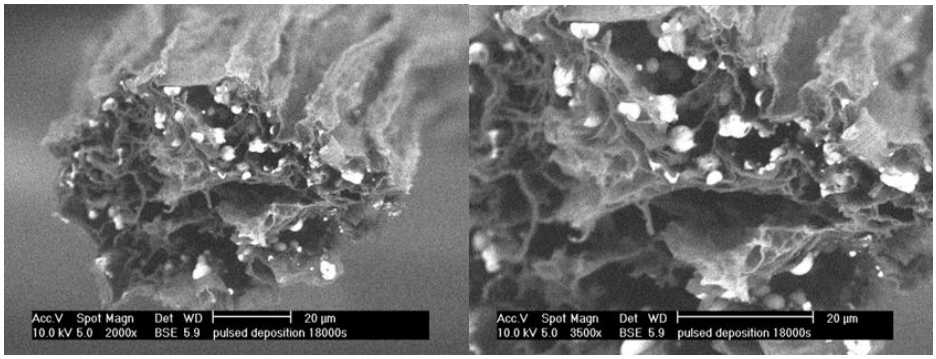

Figure 12: Pulse reverse electrodeposition in porous fibers, with current densities of 1 mAcm-2 for both anodic and cathodic pulses, pulse times of 0.5 seconds and a total deposition time of 18·103 seconds. The conductivity was two orders of magnitude below those of pure copper. This could be explained by SEM characterization, where copper particles could be observed to have grown in the interior of the fiber, having however no electrical connection between them, accounting most likely, for the low conductivity the fiber possesses.

One of the main objectives of this project, as it has already been mentioned above, was to find a reproducible technique which would allow to synthesize the desired material with a high degree of similarity every time. During DC or pulsed electrodeposition, it was observed that the amount of copper deposited could vary a lot between batches, and at the same time, the reduced graphene oxide fibers exhibited very different internal morphologies. Controlling the many parameters that seemed to be affecting the growth of the copper inside and outside the fibers, at the same time as the synthesis and internal porosity of the fibers, seemed far too complex for a technique which would have had to be used effectively in industry. For this reason, this technique had to be abandoned, in pursue of a different technique which could prove easier to scale and to control.

Table 2: Different synthesis conditions with their corresponding observed conductivities.

Description	Conductivity (Sm^{-1})
Bare r-GO fibers	$3 \cdot 10^{2}$
r-GO Fibers + Cu microwave functionalization	$4 \cdot 10^{2}$
r-GO Fibers + Cu electrodeposition	$2.7 \cdot 10^{4}$
r-GO Fibers + Cu electrodeposition (low current density)	$2.4 \cdot 10^{6}$
Porous r-GO fibers + copper electrodeposition (low current density)	$1.2 \cdot 10^{6}$
Porous r-GO fibers + pulse reverse electrodeposition	$4 \cdot 10^{3}$

Chapter 4 conclusions

The work that has been presented in this chapter, tries to summarize the difficulties that were found when trying to introduce copper into a synthesized reduced graphene oxide fiber. The fibers on their own had very low conductivities to start with, which made them unusable by themselves for industrial purposes. Introduction of copper into the interior of these fibers proved very difficult when the fibers were fully compacted as the concentration of copper ions in the aqueous medium was much higher than any copper ion that might have diffused into the interior of the fiber, causing during the electrodeposition stage a complete coating of the fiber, preventing any further ion diffusion towards the interior of the fiber. Introduction of a porous structure, such as the one found in 3D scaffolds seemed the way forwards. This kind of structure was achieved using lyophilization of the fibers after synthesis, which produced microscopic heterogeneous porosity in the interior of the fiber. Using electrodeposition, copper was again deposited, observing however that the majority of copper deposited as a coating of the fiber, and very few copper nucleuses could be observed inside the fiber. Even though this was the case, there was still an increase in the copper introduced when compared to non-porous fibers, which made them better candidates for industrialization. Pulse reverse electrodeposition was also tried, looking for the ion concentration replenishment inside the fiber during the dead times. However, the resulting fibers didn't conduct as well as the DC-electrodeposited ones, which made them unusable by industrial standards. Continuous synthesis of the fibers and further lyophilization did prove complicated, and the reproducibility of such fibers seems far too low to be implemented and upscaled. Due to these reasons, reduced graphene oxide fibers with copper inserted by electrodeposition was discarded for their use in our project.

Bibliography

[1] D. Yu *et al.*, "Scalable synthesis of hierarchically structured carbon nanotube-graphene fibres for capacitive energy storage.," *Nat. Nanotechnol.*, vol. 9, no. May, pp. 1–8, Jul. 2014.

[2] G. Sun, X. Wang, and P. Chen, "Microfiber devices based on carbon materials," *Mater. Today*, vol. 18, no. 4, pp. 215–226, 2015.

[3] † V. Subramanian, † Hongwei Zhu, ‡ Robert Vajtai, ‡ and P. M. Ajayan, and † Bingqing Wei*, "Hydrothermal Synthesis and Pseudocapacitance Properties of MnO2 Nanostructures," 2005.

[4] B. L. and and H. C. Zeng*, "Hydrothermal Synthesis of ZnO Nanorods in the Diameter Regime of 50 nm," 2003.

[5] O. M. Yaghi and H. Li, "Hydrothermal Synthesis of a Metal-Organic Framework Containing Large Rectangular Channels," *J. Am. Chem. Soc.*, vol. 117, no. 41, pp. 10401–10402, Oct. 1995.

[6] S. Yang, P. Y. Zavalij, and M. Stanley Whittingham, "Hydrothermal synthesis of lithium iron phosphate cathodes," *Electrochem. commun.*, vol. 3, no. 9, pp. 505–508, Sep. 2001.

[7] S. F. and and R. Xu*, "New Materials in Hydrothermal Synthesis," 2000.

[8] S.-H. Feng and G.-H. Li, "Hydrothermal and Solvothermal Syntheses," *Mod. Inorg. Synth. Chem.*, pp. 73–104, Jan. 2017.

[9] Z. R. Ismagilov *et al.*, "Structure and electrical conductivity of nitrogen-doped carbon nanofibers," *Carbon N. Y.*, vol. 47, no. 8, pp. 1922–1929, Jul. 2009.

[10] Y. Li, J. Chen, L. Huang, C. Li, J.-D. Hong, and G. Shi, "Highly Compressible Macroporous Graphene Monoliths via an Improved Hydrothermal Process," *Adv. Mater.*, vol. 26, no. 28, pp. 4789–4793, Jul. 2014.

[11] Y. Qian, I. M. Ismail, and A. Stein, "Ultralight, high-surface-area, multifunctional graphene-based aerogels from self-assembly of graphene oxide and resol," *Carbon N. Y.*, vol. 68, pp. 221–231, Mar. 2014.

[12] Y. Liu, D. He, H. Wu, J. Duan, and Y. Zhang, "Hydrothermal Self-assembly of Manganese Dioxide/Manganese Carbonate/Reduced Graphene Oxide Aerogel for Asymmetric Supercapacitors,"

Electrochim. Acta, vol. 164, pp. 154–162, May 2015.

[13] M. Nawaz, W. Miran, J. Jang, and D. S. Lee, "One-step hydrothermal synthesis of porous 3D reduced graphene oxide/TiO2 aerogel for carbamazepine photodegradation in aqueous solution," *Appl. Catal. B Environ.*, vol. 203, pp. 85–95, Apr. 2017.

[14] K. SHENG, Y. XU, C. LI, and G. SHI, "High-performance self-assembled graphene hydrogels prepared by chemical reduction of graphene oxide," *New Carbon Mater.*, vol. 26, no. 1, pp. 9–15, Jan. 2011.

[15] L. Zhang *et al.*, "Porous 3D graphene-based bulk materials with exceptional high surface area and excellent conductivity for supercapacitors," *Sci. Rep.*, vol. 3, no. 1, p. 1408, Dec. 2013.

[16] H. Gao and H. Duan, "2D and 3D graphene materials: Preparation and bioelectrochemical applications," *Biosens. Bioelectron.*, vol. 65, pp. 404–419, Mar. 2015.

[17] Y. Meng *et al.*, "All-Graphene Core-Sheath Microfibers for All-Solid-State, Stretchable Fibriform Supercapacitors and Wearable Electronic Textiles," *Adv. Mater.*, vol. 25, no. 16, pp. 2326–2331, Apr. 2013.

[18] C. Nethravathi and M. Rajamathi, "Chemically modified graphene sheets produced by the solvothermal reduction of colloidal dispersions of graphite oxide," *Carbon N. Y.*, vol. 46, no. 14, pp. 1994–1998, Nov. 2008.

[19] M. González Sánchez, "Aerogeles De Grafeno Y Nanotubos De Carbono. Nuevos Materiales Para El Apantallamiento Electromagnético," 2018.

[20] Y. Zhou, Q. Bao, L. A. L. Tang, Y. Zhong, and K. P. Loh, "Hydrothermal Dehydration for the 'Green' Reduction of Exfoliated Graphene Oxide to Graphene and Demonstration of Tunable Optical Limiting Properties," *Chem. Mater.*, vol. 21, no. 13, pp. 2950–2956, Jul. 2009.

[21] S. Pei, J. Zhao, J. Du, W. Ren, and H.-M. Cheng, "Direct reduction of graphene oxide films into highly conductive and flexible graphene films by hydrohalic acids," *Carbon N. Y.*, vol. 48, no. 15, pp. 4466–4474, Dec. 2010.

[22] P. V. Kamat, "Graphene-Based Nanoarchitectures. Anchoring Semiconductor and Metal Nanoparticles on a Two-Dimensional

Carbon Support," *J. Phys. Chem. Lett.*, vol. 1, no. 2, pp. 520–527, Jan. 2010.

[23] J. Granatier *et al.*, "Interaction of Graphene and Arenes with Noble Metals," *J. Phys. Chem. C*, vol. 116, no. 26, pp. 14151–14162, Jul. 2012.

[24] N. Leelaviwat, S. Monchayapisut, C. Poonjarernsilp, K. Faungnawakij, K.-S. Kim, and T. Charinpanitkul, "Microwave-induced fabrication of copper nanoparticle/carbon nanotubes hybrid material," *Curr. Appl. Phys.*, vol. 12, no. 6, pp. 1575–1579, Nov. 2012.

[25] Y. Lin, D. W. Baggett, J.-W. Kim, E. J. Siochi, and J. W. Connell, "Instantaneous Formation of Metal and Metal Oxide Nanoparticles on Carbon Nanotubes and Graphene via Solvent-Free Microwave Heating," *ACS Appl. Mater. Interfaces*, vol. 3, no. 5, pp. 1652–1664, May 2011.

[26] L. Huang, Z. R. Guo, M. Wang, and N. Gu, "Facile Synthesis of Gold Nanoplates by Citrate Reduction of AuCl 4-at Room Temperature," 2006.

[27] W. Chen, L. Yan, and P. R. Bangal, "Preparation of graphene by the rapid and mild thermal reduction of graphene oxide induced by microwaves," *Carbon N. Y.*, vol. 48, no. 4, pp. 1146–1152, Apr. 2010.

[28] Y. Zhu, S. Murali, M. D. Stoller, A. Velamakanni, R. D. Piner, and R. S. Ruoff, "Microwave assisted exfoliation and reduction of graphite oxide for ultracapacitors," *Carbon N. Y.*, vol. 48, no. 7, pp. 2118–2122, Jun. 2010.

[29] D. Grujicic and B. Pesic, "Electrodeposition of copper: the nucleation mechanisms," *Electrochim. Acta*, vol. 47, no. 18, pp. 2901–2912, Jul. 2002.

[30] C. Subramaniam *et al.*, "One hundred fold increase in current carrying capacity in a carbon nanotube-copper composite.," *Nat. Commun.*, vol. 4, p. 2202, Jan. 2013.

[31] Fen Chen and D. Gardner, "Influence of line dimensions on the resistance of Cu interconnections," *IEEE Electron Device Lett.*, vol. 19, no. 12, pp. 508–510, Dec. 1998.

[32] K.-Y. Chan, T.-Y. Tou, and B.-S. Teo, "Thickness dependence of the structural and electrical properties of copper films deposited by dc magnetron sputtering technique," *Microelectronics J.*, vol. 37, no. 7,

pp. 608–612, Jul. 2006.

[33] W. Nie *et al.*, "Three-dimensional porous scaffold by self-assembly of reduced graphene oxide and nano-hydroxyapatite composites for bone tissue engineering," *Carbon N. Y.*, vol. 116, pp. 325–337, May 2017.

[34] S. H. Kazemi, E. Ghodsi, S. Abdollahi, and S. Nadri, "Porous graphene oxide nanostructure as an excellent scaffold for label-free electrochemical biosensor: Detection of cardiac troponin I," *Mater. Sci. Eng. C*, vol. 69, pp. 447–452, Dec. 2016.

[35] M. González, M. Crespo, J. Baselga, and J. Pozuelo, "Carbon nanotube scaffolds with controlled porosity as electromagnetic absorbing materials in the gigahertz range," *Nanoscale*, vol. 8, no. 20, pp. 10724–10730, 2016.

[36] H. Y. R. Atapattu, D. S. M. De Silva, K. A. S. Pathiratne, and I. M. Dharmadasa, "Effect of stirring rate of electrolyte on properties of electrodeposited CdS layers," *J. Mater. Sci. Mater. Electron.*, vol. 27, no. 5, pp. 5415–5421, May 2016.

[37] K. R. Mamaghani and M. Naghib, "The Effect of Stirring Rate on Electrodeposition of Nanocrystalline Nickel Coatings and their Corrosion Behaviors and Mechanical Characteristics," *Int. J. Electrochem. Sci*, vol. 12, pp. 5023–5035, 2017.

Chapter 5: Carbon nanotube copper hybrids

As it was mentioned at the beginning of this thesis, carbon nanotubes were not considered at the beginning of this project, as only small scale synthesis of this material had been done at the time, and even the methods that claimed to be able to produce large quantities of carbon nanotubes, could not possibly meet the requirements for a large scale synthesis required by industry [1]–[6]. During the years, new techniques have appeared which allow the synthesis of macroscopic carbon nanotube yarns [7]–[9], films [10], [11] and fibers [12]–[15]. These techniques are varied in form and type of the material produced, but also in the scalability of the synthesis methods and they are mostly borrowed from polymer fiber-processing technologies directly. There are three main approaches to produce carbon nanotube fibers; the first, is spinning from a lyotropic liquid crystalline suspension of nanotubes, similarly to the process done to produce aramid fibers [16]; the second directly spinning from carbon nanotubes previously grown on a substrate as a vertically aligned carpet of parallel tubes [17], [18]; and the third spinning directly from a chemical vapor deposition reactor from an aerogel of carbon nanotubes (single and double-walled) [19]. From these methods, two were chosen due to their scalability, and due to the accessibility to the necessary technology.

Spinning from vertically aligned forest of carbon nanotubes

As it has been shortly summarized above, one of the selected methods consisted on creating a continuous webbing of carbon nanotubes, which can be obtained from a vertically aligned forest of tightly packed CNTs. These CNTs when pulled, tend to form these yarns due to the Van der Waal forces acting to stick them together [20]–[29]. These yarns can then be modified and altered in shape to form other morphologies with better mechanical and electrical properties [28] as observed in Figure 1 below.

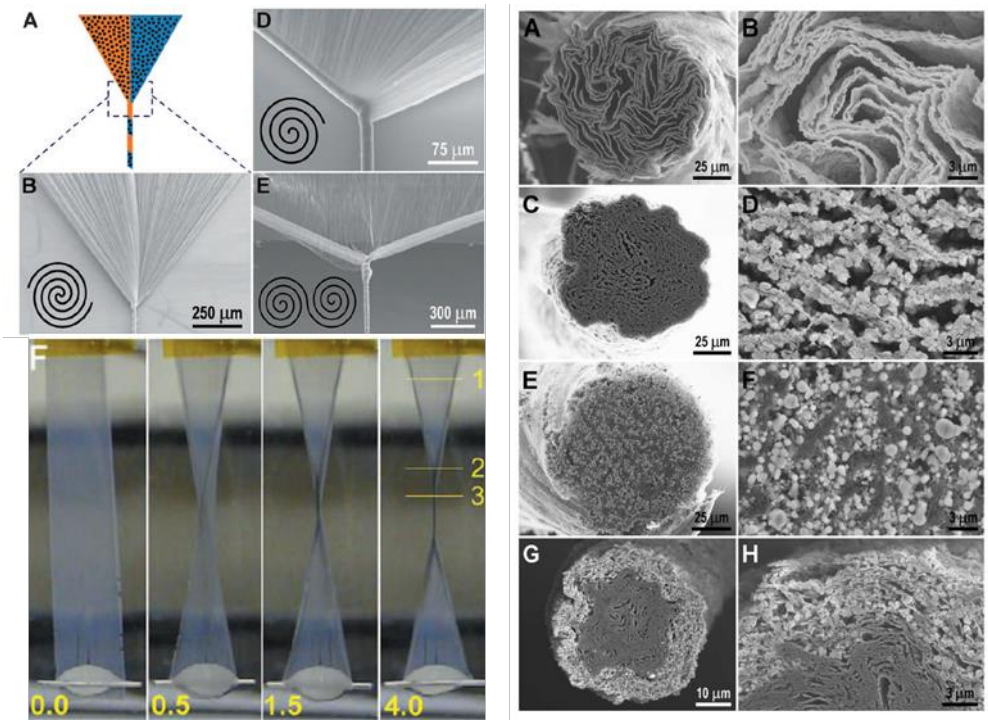

Figure 1: Left (A,B,D,E) shows carbon nanotubes being drawn from a CNT substrate, and twisted into a fiber directly. F) is the extended yarn, which inside an acetone solvent and under mechanical stirring can produce very thin fibers. If the yarns have been deposited with some material in their surface, once they begin to twist and form the fiber, they will confine the deposited material in the inside of the fiber, as seen on the right images A-H. [28]

The initial idea was to deposit copper by using a physical vapor deposition (PVD) process on the surface of one of these yarns, and then to twist them to confine the copper to the inside of the created fiber. By confining copper inside the fiber, it was believed that conducting paths could be formed, which would grant the fiber with an overall metal conductivity. At the same time, in case a second deposition process, such as electrodeposition (EDP), would to be used, copper would act as nucleation points and would therefore help in the deposition process greatly. In contrast with graphene oxide, carbon nanotubes fibers seem to have much higher porosity, which would allow rapid ion diffusion towards the inside of such fibers.

The process of pulling a proper yarn was complicated, and the optimization of such method was long and difficult. As it has been explained, when a single carbon nanotube is pulled away from the densified vertical forest, it attracts by Wan der Vaal forces the next tube closest to it, creating a process of chain reaction by which one tube pulls the next and so forth [30].

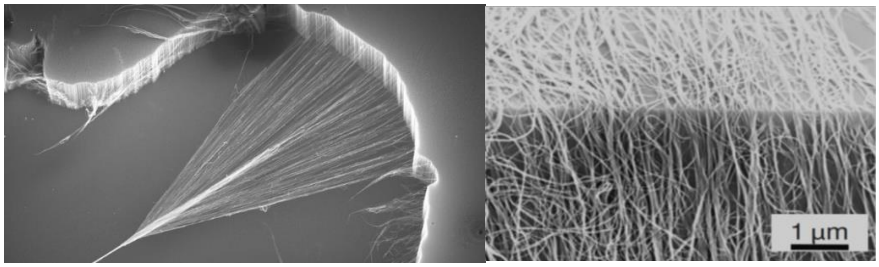

Figure 2: Left, carbon nanotube yarn being pulled from a vertically aligned multi walled carbon nanotube forest [31]. Right cross section of vertically aligned CNTs ,Baughman et al [30]

The work that will be described below was carried out in Penn State University (State College, Pennsylvania, United States of America). The multiwalled nanotube forest was synthesized by catalytic chemical vapor deposition, and acetylene gas was used as the carbon source. The forests had heights between 100 and 800 µm. The nanotubes had an outer diameter of ~12 nm and contained ~9 walls [32].

Multi walled carbon nanotubes were synthesized on top of a silicon wafer and the carbon nanotube sheets had to be drawn directly from this wafer by the drawing method; the draw is initiated using a scotch tape or a blade's edge. By slowly hand-drawing, it is possible to obtain long sheets of aligned carbon nanotubes. Reproducibility of such technique by hand-drawing is very small, producing sheets ranging from a single millimeter to various centimeters, depending on the initial pull. SEM microscopy of the initially obtained sheets can be seen in Figure 3.

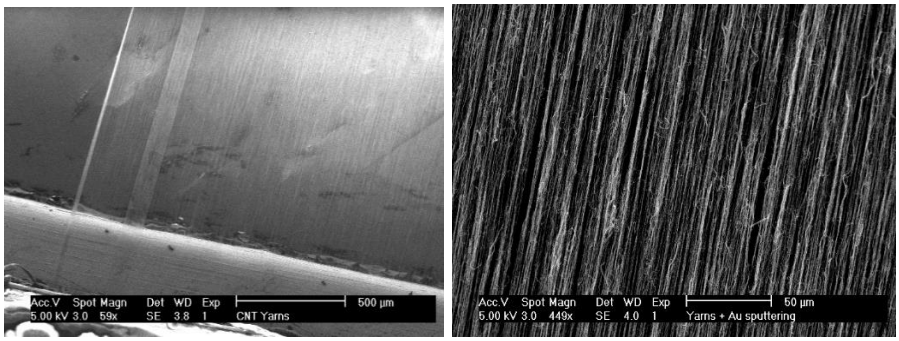

Figure 3: Hand-drawn CNT sheets from vertically aligned CNT forest. It is clearly visible that there is a preferred orientation of the carbon nanotubes (parallel to each other) and all oriented towards the direction of the initial pull.

As it was possible to see from the SEM characterization of such sheets, there is a preferred orientation of the carbon nanotubes, parallel to each other and oriented towards the direction of the initial pull. There is a high homogeneity in the sheets produced, although the areas of these sheets do

seem to vary greatly depending on the initial pull as it has been mentioned above. The fragility of the sheet was very high, and any air current or surface which touched the sheets, made them break. For this reason, a small device was invented, which allowed the twisting of the sheets into fibers, and at the same time could be used as the support for the handling of the carbon nanotube sheets. This support, as seen in Figure 4A, consisted of two glass surfaces opposing each other, where the CNT sheet, once drawn, would be placed. One of the glass surfaces, was connected to a never-ending screw, which allowed the rotation of the glass with the sheet attached to it. This allowed the twisting of the fibers as well as support for the sheets.

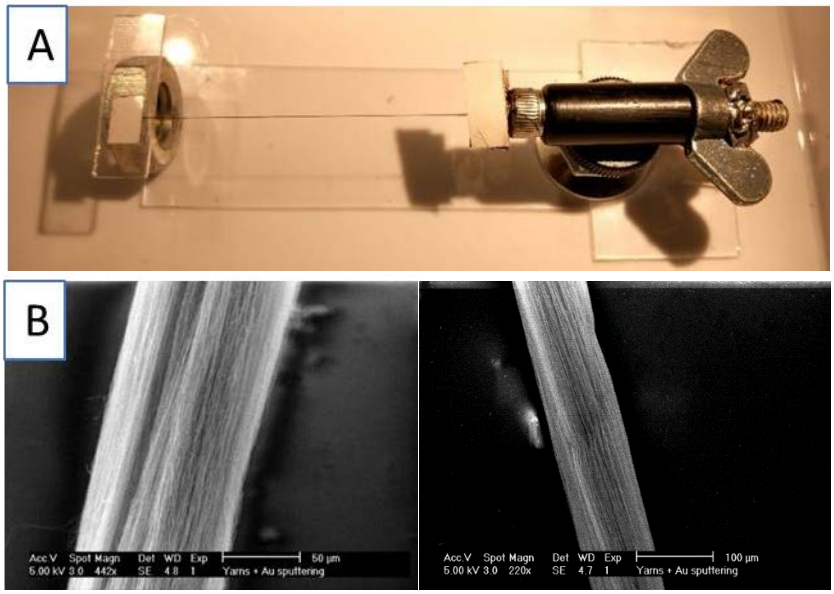

Figure 4: A) Twisting device that was designed during this thesis which allowed for the twisting of the carbon nanotube yarns into fibers. B) SEM microscopies of carbon nanotube twisted fibers (gold sputtered).

Conductivity of the twisted fibers was in the order of 1 Sm^{-1}, very low when compared to the desired conductivities we were aiming for. Sheets of carbon nanotubes were taken to the PVD chamber and they were sputtered with a copper target, searching for an improvement in the overall conductivity of the material. After sputtering the carbon nanotube films and twisting them into fibers, conductivity was measured once again. This time, conductivity was in the order of $2 \cdot 10^3$ Sm^{-1}, higher than the initial conductivities exhibited by the bare fibers, but far from our objective. SEM characterization of such fibers (Figure 5), showed that there seemed to be copper on the surface of the carbon nanotube fibers.

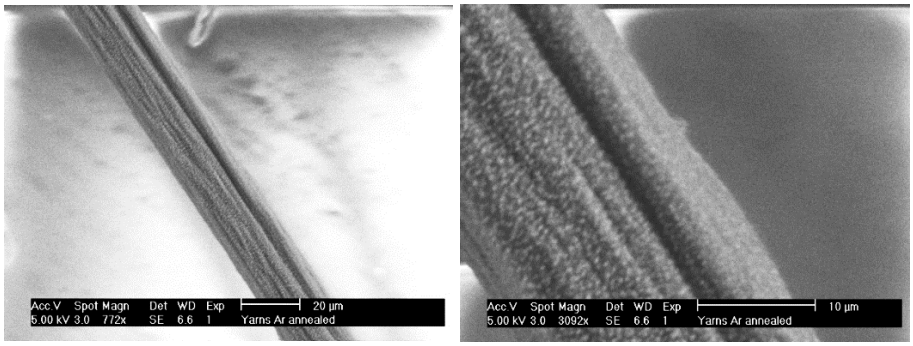

Figure 5: SEM microscopy of carbon nanotube twisted fibers, after having undergone copper deposition by sputtering method.

However, looking at bibliography, it was soon discovered that depositing copper through magnetic sputtering created a layer of copper oxide no matter the argon saturation used as sputtering atmosphere [33]. This was a definitive set-back, as no matter the total time used for the deposition process, there would always be copper oxide on the fibers, which would cause lower conductivities than those required. Once again, electrodeposition seemed as the only way forward to deposit copper on the carbon nanotube fibers. However, having such low conductivities meant that electrodeposition would not occur homogeneously throughout the fiber. This fact is mentioned in several papers; with growing sizes of the CNT lines being used for electrodeposition, comes a decrease in the distribution of charge when undergoing electrodeposition [34]. The area closest to the electrodes, would show a higher copper deposition rate than the areas further from the electrode. As mentioned by Hannula et al [35], the high resistivity of carbon nanotubes could affect the electrodeposition severely. Due to the charge density being highest closest to the electrical contact, the number of nucleation sites would also be higher, decreasing exponentially along the carbon nanotube line. For this reason, a higher initial conductivity was mandatory for an efficient electrodeposition process.

The idea for improving conductivity appeared after the observation of a SEM microscopy, where a CNT twisted fiber had been placed between two electrodes, and the electrical contact done with silver paint. In the places where the silver ink contacted the twisted fiber, a shrinkage of fiber diameter could be observed (Figure 6).

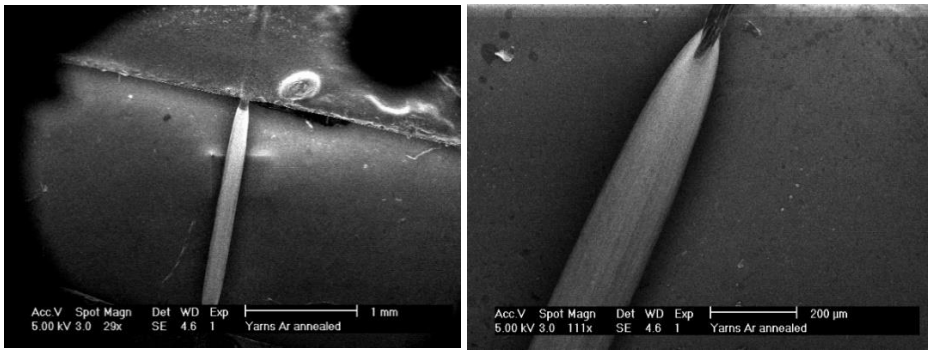

Figure 6: SEM microscopy of a twisted fiber on top of a copper electrode used for conductivity measurements. Shrinkage of the fiber diameter can be observed in the areas where the silver paint was applied which proved that the interior of the fibers had big amounts of free space.

This shrinkage was due, most likely, to the presence of too much air, because of the high porosity that the carbon nanotubes produced inside the fibers, and it was probably this fact which caused the small conductivity values measured. It is important to keep in mind, that the diameter used for these calculations is the total diameter (air + fibers), and therefore it was logical that the conductivity exhibited was so small. Therefore, compacting of the fibers was done in order to increase the overall conductivity. To achieve the close packing of the fibers, 2-propanol 99.5% could be used, as once inserted into any alcohol, the fast-drying process would pack the fibers rapidly without losing the orientation along the fiber, something that with other slow evaporation solvents such as water, would probably cause morphological changes of the fiber orientation or structure. Even though 2-propanol was used, It is also true that any other alcohol could be used, such as ethanol or acetone for example, but 2-propanol is known for being one of the best cleaning solvents, as it leaves nearly no residues when compared to ethanol or methanol, being this one of the main reasons why this solvent is used in semiconductor industry, to remove any residues left by acetone and methanol [36]. These fibers were measured to have a conductivity of $1 \cdot 10^3$ Sm^{-1} as synthesized and compacted. It is important to mention, that electrical measurements in these range of resistances is around 0.2% due to the measuring setup being used, and the diameter of the fibers can also be subjected to morphological changes, such as diameter changes due to the roughness of the synthesized fiber, by more than 5%, being a source of constant errors.

This conductivity was enough to achieve a homogeneous distribution of charge as it was soon discovered. Electrodeposition at 1V for 1 minute was repeated on the compacted fiber, using water, copper sulphate (1 M) and

sulfuric acid (pH=1), and this time, a conductivity of $2 \cdot 10^6$ Sm^{-1} was achieved, a conductivity very close to the one exhibited by pure copper. It is important to mention, that sulfuric acid was used, as it has been observed to improve electrodeposition in many cases. Sulfuric acid tends to improve conductivity of the solution due to the higher number of hydronium ions available for charge transport. At the same time, it was observed that hydrolysis of water causes hydrogen to leave the dispersion in the form of bubbles, whilst OH^- ions continue increasing the pH of the dispersion

This same fiber was examined by SEM imaging, both the cross section and the exterior of the fiber. As it can be observed in Figure 7, the cross section of the fiber seemed to show a brittle intergranular type of fracture inside the fiber, something which would not be possible if only carbon nanotubes were present. This hinted that copper had readily diffused inside the CNT structure.

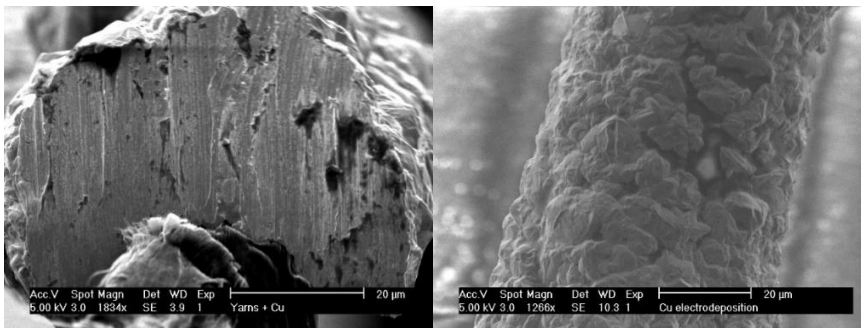

Figure 7: SEM microscopy of the CNT fibers after compacting them with 2-propanol and undergoing the process of electrodeposition for 15 minutes. Left- SEM microscopy showing the cross section of the hybrid fiber, after a fracture in liquid nitrogen. Right- SEM microscopy show the exterior of a different area of the same fiber. A grainy exterior can be seen, and this could probably be improved by means of thermal annealing. The cross section seems to show copper in the interior of the fiber. SEM microscopies were used to determine the diameter of the fibers and to obtain the resistivity values which have been reported. However, as it is possible to observe, roughness of the synthesize fibers can be a source of error, being possible to observe diameter changes by ±5 micrometers in some regions of the sample.

Copper could also be observed along the whole length of the fiber, having homogeneously deposited on its surface. Even though there was enough evidence to believe copper had been properly deposited inside the fiber, this had to be proved by means of EDX mapping. From the EDX mapping shown on Figures 8 and 9, it is easily seen, that copper has efficiently diffused into the inside of the fiber. The outside of the fiber presents a small amount of copper oxide, however in the inside no oxide can be observed. This small oxide layer was expected, as any copper in contact with air will oxidize quickly. There is a high similarity between the work presented by Subramaniam et al [38] and the fibers obtained by the method herein

presented. In the fibers it can also be observed a small amount of Sulphur. This could be explained by the sulfuric acid that is used in the electrodeposition dispersion, which might leave some residues if not properly cleaned after.

With these results, it was safe to assume that copper had been correctly inserted into the carbon nanotube structure, creating in the process a hybrid material of copper and carbon.

Due to confidentiality issues, it was impossible to continue the work with these fibers. An alternative had to be searched for as a way of continuing with the work that was carried out in Penn State University. As it has been stated in the opening of this chapter, there was a second technology available at the time, which was the direct spinning of CNT yarns from a chemical vapor deposition reactor [39].

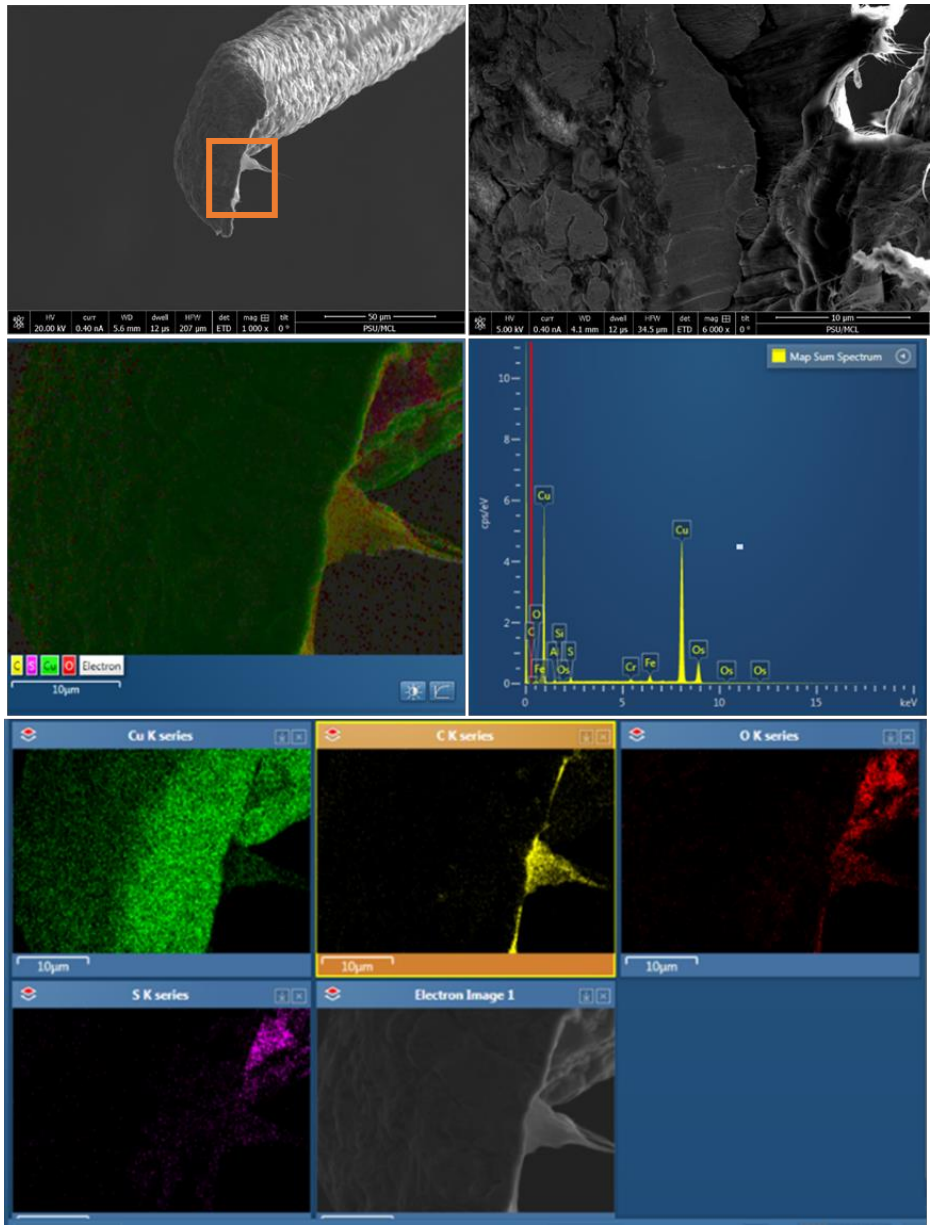

Figure 8: Top, FESEM microscopy of a CNT-Cu fiber. The square shows the area in which the EDX mapping was carried out. Bottom is the EDX mapping, which clearly shows that copper has diffused into the interior of the fiber (green), whilst the CNTs are still present (yellow). There is a thin layer of copper oxide present in the outer region of the fiber (red) and some Sulphur residues in the outside of the fiber too, which is due to the dispersion used for the electrodeposition process. This residue should be cleaned for further tests as it might have some negative effects on the properties

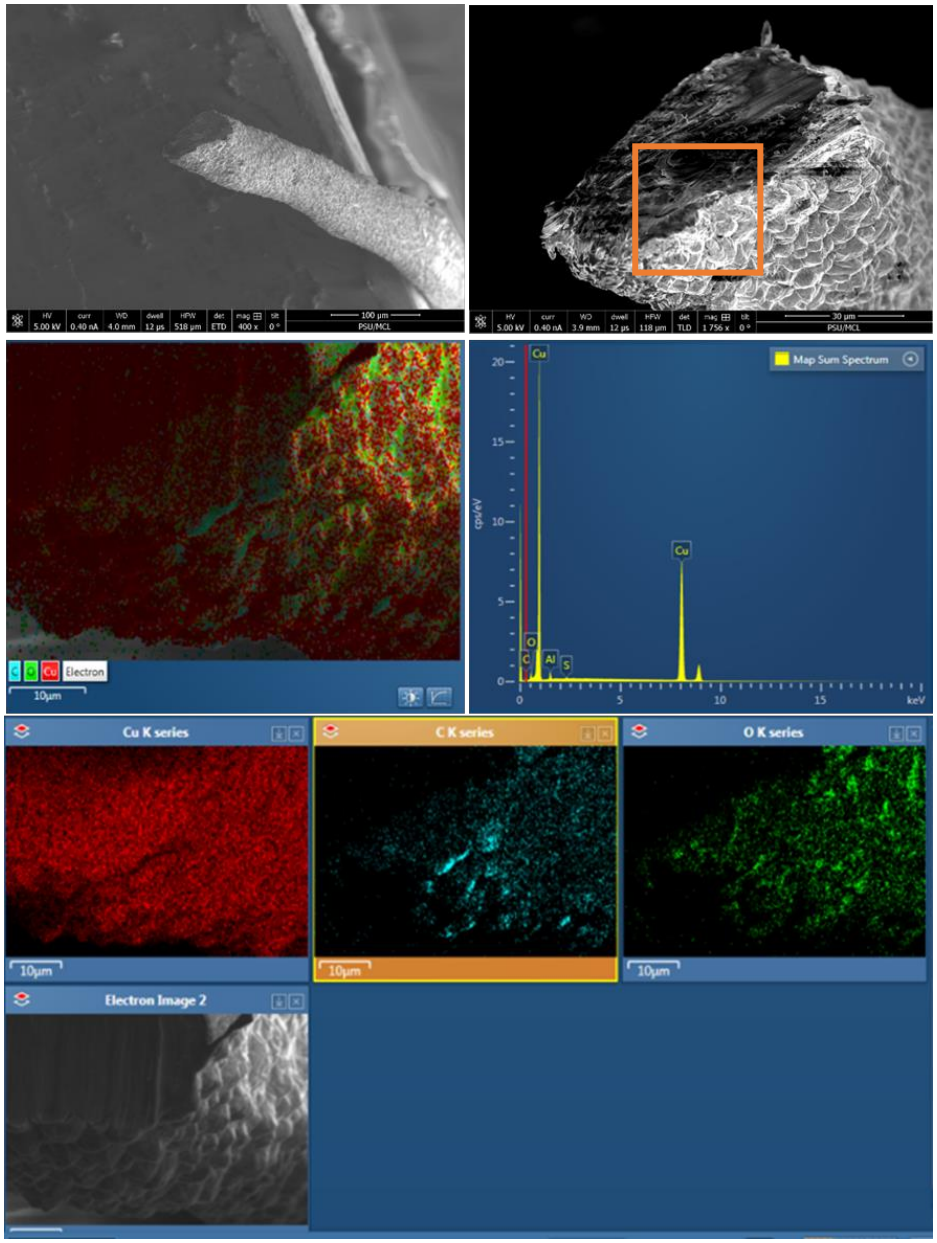

Figure 9: EDX mapping of a second fiber with the same conditions as the one shown in figure 8, shows that both results match, and that copper has correctly diffused into the interior of the fiber. Again, a thin layer of oxide can be seen in the exterior of the fiber and some carbon is detected as expected from the presence of carbon nanotubes.

Direct Spinning of Carbon Nanotubes yarns from a Chemical Vapor Deposition reactor (Oven drawn)

Through a collaboration with IMDEA materials institute, where Prof. Juan José Vilatela had developed a method which could be used to produce very similar carbon nanotube structures to the ones that had been previously used in Penn State University, the work that had been done on previous chapters could be carried on. By mechanically drawing the carbon nanotubes from the gaseous reaction zone (where the CNTs form an aerogel), it is possible to produce continuous and aligned carbon nanotube fibers. The nanotubes that were used, were in the order of 4-10 nm diameter, and in the order of 1mm of length [39]. By this method, there is no need to do any post-processing to the fibers, such as the addition of polymers or fiber twisting [40], [41] in order to increase the mechanical strength they possess. With this method, the act of pulling the aerogel out of the reaction chamber orients the nanotubes axially and running the fiber through an alcohol allows the densification of the fiber even further. The nanotubes used, were synthesized at 1250 °C by chemical vapor deposition from a mixture which contained thiophene, ferrocene and a carbon source. Hydrogen was used as the carrier gas.

Using the same electrodeposition conditions as the ones that had been used for the yarns obtained by pulling from vertical CNT forests, fibers obtained by the oven drawn method were electrodeposited. As it can be observed from the SEM imagen shown on Figure 10, the resulting fibers had the same appearance as those prepared in Penn State University, and the cross section showed the same kind of brittle type of fracture as the one that had been observed in the previously synthesized fibers. All fibers were electrodeposited with 1 volt for different EDP times. The dispersion consisted of 100 ml water, 1M of $CuSO_4$, 0.01M of Triton-X surfactant and H_2SO_4 until a pH of 1 was reached. Apart from the fact, that the positive effect of surfactant usage during electrodeposition has been widely studied [42], we believed that using a surfactant would help the diffusion of ions inside the fiber by disrupting the surface tension of water and helping the wetting of the hydrophobic carbon nanotubes. The copper can be clearly seen as soon as the fiber is extracted from the dispersion. It is then cleaned with 2-propanol to make sure that any salt residues are cleaned.

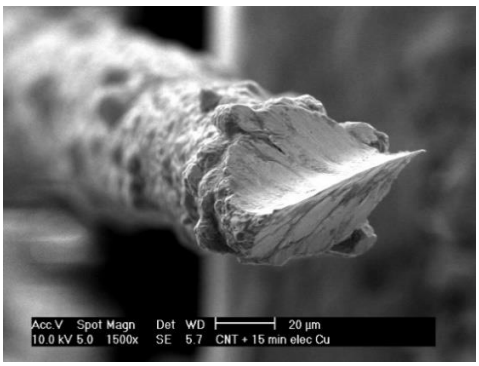

Figure 10: IMDEA CNT fiber after 15 minutes electrodeposition at 1V. The electrodeposition dispersion consisted of 100 ml water, 1M of CuSO4, 0.01M of Triton-X surfactant and H2SO4 until a pH of 1 was reached. The appearance of the cross section had great similarity to the one observed in the fibers that had been synthesized in Penn State University, exhibiting a brittle like fracture at the breaking point.

Using the Agilent power unit (reference in chapter 2, materials and methods) conductivity of these fibers as well as ampacity was measured again. Three different electrodeposition times were used; 5,10 and 15 minutes; and a voltage of 1V was applied to the fiber. Values for the diameters and electrode distance were determined accurately by SEM characterization, and the 3 different electrodeposition times presented conductivities of 2.7, 1.3 and 1.2 x 10^7 Sm^{-1} respectively, being the 5-minute electrodeposition time apparently more conducting that the longer deposition cycles. This result shows that the composite material exhibits good conductivity. Longer times of deposition creates a thicker layer of external copper but still offer lower conductivities. This is observed in the conductivity values that can be seen in Table 1, as even though the 5-minute electrodeposited fiber exhibited higher resistance values, the diameter was much smaller, causing the higher conductivity value.

Table 1: Conductivity and ampacity measurements of three different EDP times on the CNT fibers produced by IMDEA collaboration. Longer EDP times show a smaller resistance as it was expected due to the higher amounts of copper present. Although at first sight, 5 minutes shows a bigger resistance than the 10- and 15-minutes' electrodeposition times, conductivity also takes into account the diameter of the composite fiber. The diameter of the 5-minute fiber is significantly thinner, making therefore the conductivity overall higher. Measured with B2911A power unit.

Sample	Conductivity (Sm^{-1})	Ampacity (Acm^{-2})
5 minutes	$(2.7\pm0.2)\cdot10^7$	$(1.9\pm0.01)\cdot10^6$
10 minutes	$(1.3\pm0.1)\cdot10^7$	$(3.3\pm0.2)\cdot10^5$
15 minutes	$(1.2\pm0.1)\cdot10^7$	$(4.2\pm0.2)\cdot10^5$

Ampacity was measured for the same fibers and the results can be seen in Table 1 above. For the 10- and 15-minute electrodeposited fibers, the ampacity point wasn't reached, as the thickness of the composite material made the power unit insufficient to reach this ampacity point. This means that the current density was below the one required to reach the ampacity point. When compared to the bare copper fibers which were measured in the first chapters of this work, it is possible to observe that the ampacity in these composite materials was close to the one of pure copper.

For the 5-minute electrodeposited fiber, which was the only one of the samples which reached the ampacity point, the current density it withstood was the same as for the reference copper fiber. Complete characterization by SEM microscopy was done to the composite material after the ampacity point was reached. In the images, electromigration of copper can be clearly observed. It is surprising, that sometimes although the ampacity seems to have been reached (a sudden drop in current density), the actual fiber isn't completely broken, and carbon nanotubes still join both electrodes. At this point a sudden drop in conductivity is observed, although it is still unsure whether this is caused by the equipment not being able to detect such a sudden drop in current, or because no current is really passing through. However, it is interesting to notice, that drops of copper form at either side of this region showing how electromigration has made the copper ions diffuse away from this area. It is widely known that the adhesion of copper and carbon is poor, so it is likely that the diffusion of the copper from the failure point is also pulling the copper from the inside of the fiber towards the big drops at each edge of the failure point. An example of two different behaviors at the point of maximum current density can be seen in the images below (Figure 11).

This kind of behavior, had also been reported by Sundarama et al [43], who had continued the work done by Subramaniam et al [38] trying to replicate the same results in macroscopic sized fibers with the same results as the ones observed by our group. In their paper, two drops of copper also formed at both edges of the failure point when ampacity was reached, and such value was in the same order as pure copper, a value very far from the 100-fold increase which was observed at microscopic scales. These results completely agree to the ones that had been observed by our group throughout the thesis.

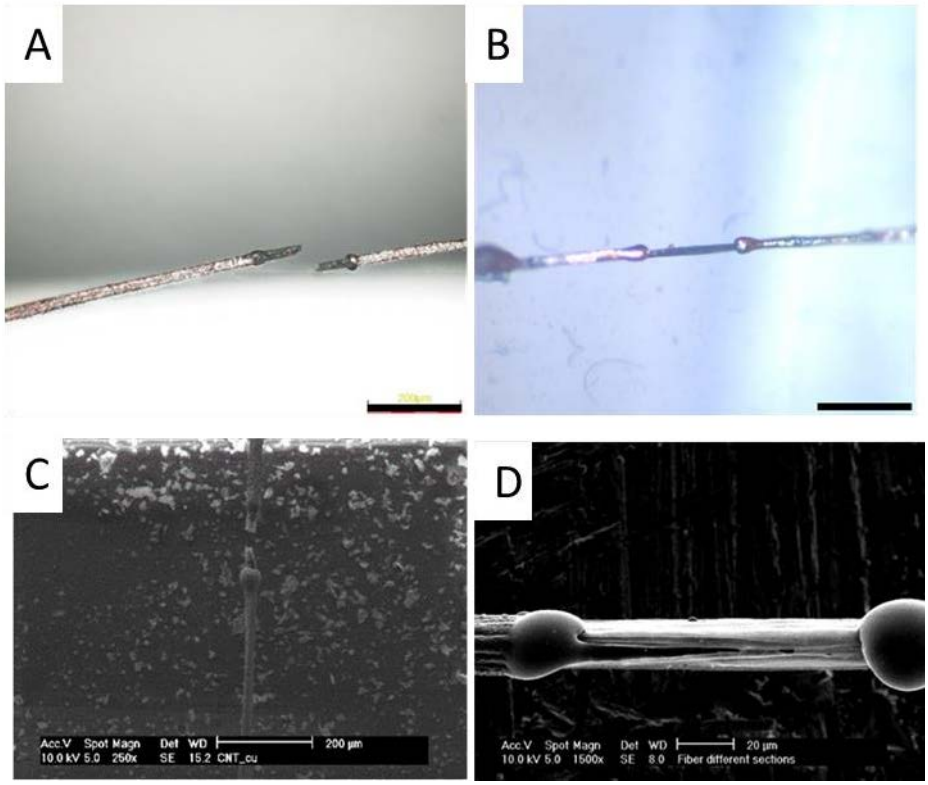

Figure 11: A) optical microscopy of the failure point of a CNT-Cu fiber, in which copper has diffused and the carbon nanotube has finally broken. B) shows a different optical microscopy where the copper has diffused in the same way, however the carbon nanotubes have resisted the maximum current density which means that both electrodes remain connected although with a high current drop. C) and D) shows the same types of failure mechanisms as the ones shown in the optical microscopies, being possible to observe in both cases the electromigration mechanisms of copper on the surface of the synthesized sample.

The insertion of nanotube fibers has been observed to increase mechanical properties in bibliography [44]–[46]. Although the main aim of this work is based on the electrical measurements of the material, and not on the mechanical properties, it was believed that these measurements would prove beneficial for a more complete characterization of the sample. To check if the copper-CNT hybrids exhibited better maximum tension in comparison to pure copper cables, a *Favimat*+ machine was used. Results obtained from the mechanical measurements showed a tensile strength of 232 MPa for a pure copper reference which agrees with bibliography results for coarse grained copper [47]. The 10 and 15-minute electrodeposited composite materials showed tensile strengths of 412 and 381 MPa respectively.

The results seemed promising, presenting a material which had the same conductivity as pure copper, better tensile strength, and theoretically a

better overall density. If a lower density could be achieved, this would mean that the main motivation of the thesis would have been accomplished, as this hybrid material would be able to reduce the overall weight of the lightning strike protection systems as it had been intended from the start. However, measuring density in such small fibers, with lengths close to 3 cm and a diameter of 15 micrometers, proved impossible by means of Archimedes, helium pycnometry or BET. As the theoretical idea had been proven in fibers, the group decided to move to bigger two-dimensional materials.

At this point it is important to remember, that one of the reasons why bigger fibers had not been done from the start was that huge currents would be required for reaching the ampacity point for bigger cross sections. This meant that a new power unit had to be acquired if 2-D materials were to be used, or an alternative technique for measuring ampacity would have to be developed. In parallel with the synthesis of 2-D CNT-Copper films, a laboratory lightning strike simulator, for measuring ampacity, was developed for the first time, to the best of our knowledge. For this end, a power unit which could withstand 600A (DC AMREL SPS10-600) had to be used. Indeed, it is difficult to compare the measurements obtained with both types of power unit, as the Amrel power unit has a much higher degree of error than those obtained with the Agilent power unit. However, it was impossible to obtain ampacity values any other way, as this was the only power unit available at the time, which could provide enough current density to our samples.

Thin CNT-Cu composite films. Copper electrodeposition in CNT Yarns.

Thin films of carbon nanotubes, as it has been explained, can be directly obtained from the reactor chamber the same way that fibers were obtained. However, instead of compacting these fibers with acetone, the fibers are left un-densified and placed on a flat substrate, forming this way a mat of oriented carbon nanotubes. If more layers are placed on top of each other, it is possible to obtain macroscopic thicknesses, although this wasn't tried during this work, as thinner materials were pursued. Once the mat is placed on a substrate, it is possible to insert it into a 2-propanol bath, creating a densified mat of oriented carbon nanotubes as seen in Figure 12.

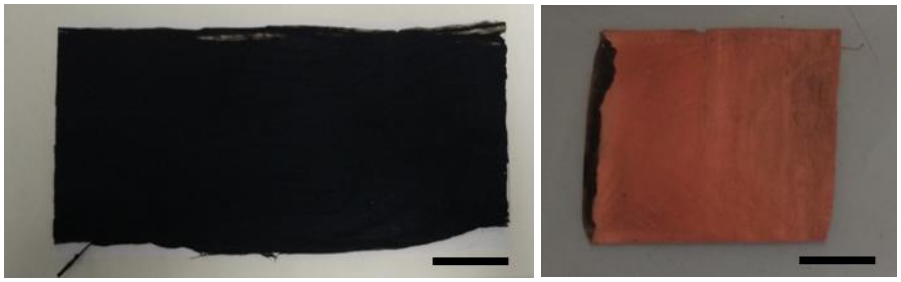

Figure 12: Left, Densified mat of carbon nanotubes (scale bar 5cm), right, CNT-Copper film (scale bar 1cm)

Exactly as it had been done to the carbon nanotube fibers, these mats could be inserted into the same electroplating solution that had been used with the fibers, consisting on copper salts, water, sulfuric acid and triton-X, using the same voltage and times (1Volt for 15 minutes) and a copper counter electrode of the same size (to avoid contaminants during the electrodeposition process due to oxidation of the counter electrode), it was possible to create a homogeneous carbon nanotube – copper hybrid material. This film was characterized by means of SEM and EDX as seen below in Figures 13 and 14.

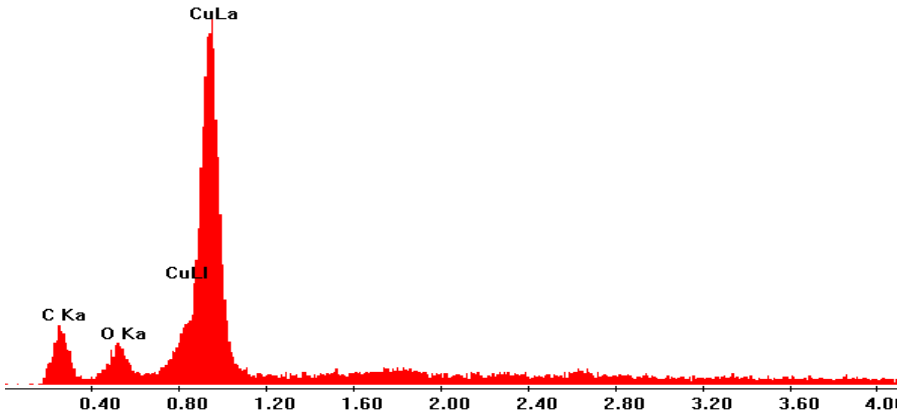

Figure 13: EDX of the CNT-Cu film. It is possible to observe how the main elements present in the material are copper and carbon, whilst small oxidation of the copper can also be observed.

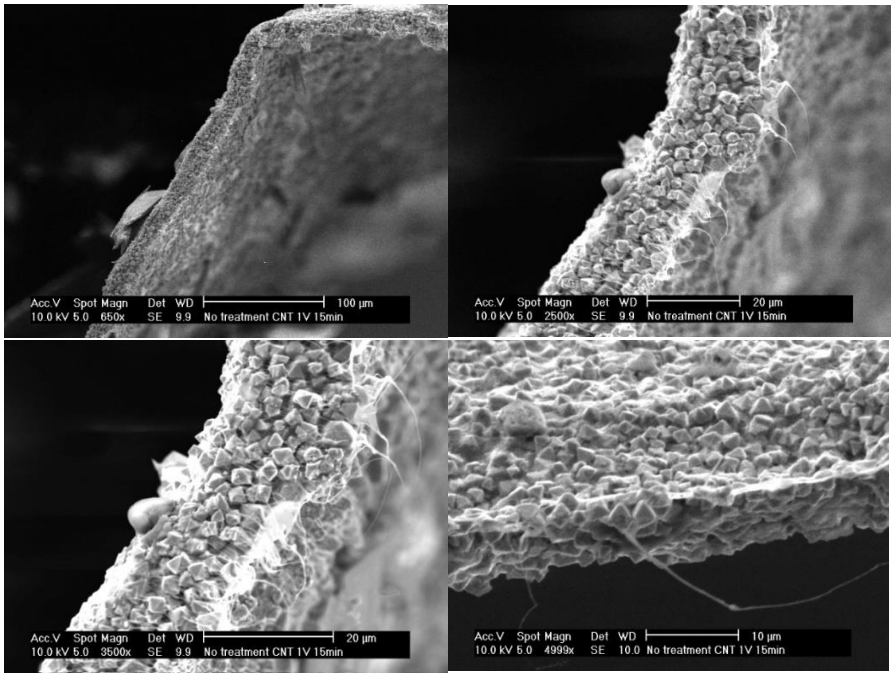

Figure 14: Different SEM microscopies of the different cross sections obtained from the CNT-Cu films. The copper has clearly penetrated into the interior of the film, creating a homogeneous hybrid material. Roughness of the copper grains was in the order of 1-2 um.

From the SEM and EDX characterizations, it was possible to conclude, that copper was indeed diffusing into the interior of the films, creating like this a CNT-Cu hybrid film. EDX showed that copper was the main element, whilst carbon and oxygen were also present on these films. Further annealing was done to these films, aiming to increase the grain size and thus improve conductivity. The annealing was done in a hydrogen atmosphere at 700°C for 1 hour, and results were optically visible at the macroscopic, as well as at the microscopic scale as seen in Figure 15.

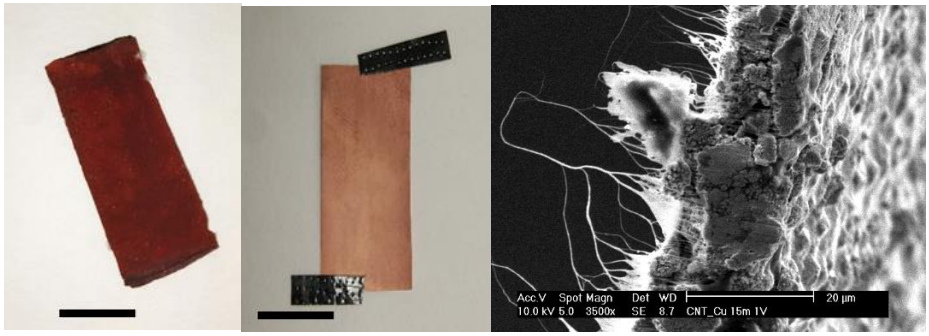

Figure 15: Left, CNT-Cu film before annealing, middle, the same film after annealing (scale bar 1cm), right, SEM microscopy of the cross-section area of a film after annealing. Bigger grains in the order of 10-15 micrometers can be observed which accounts for the reduction of the overall sample roughness.

Conductivities for the film, before and after annealing, were measured. Before annealing, conductivities of $1 \cdot 10^4$ Sm^{-1} $\pm$ $0.62 \cdot 10^3$ were obtained, whilst after the thermal process had been carried out, conductivities in the order of $2 \cdot 10^6$ Sm^{-1} $\pm$ $124 \cdot 10^3$ were achieved. These conductivities are somewhat lower when compared to the same hybrid material in its fiber form. X-ray diffraction was done to the films before and after annealing, to check if the oxidation of copper could be the reason for lower conductivities, however the results showed that a very small percentage of copper oxide was present on these films (approximately 5%), and it hardly varied after the thermal anneal although this process did eliminate the oxygen residues as seen in the figure below (Figure 16). This, means that it is very unlikely that oxides are the cause of the decrease in the overall conductivity, and points in the direction of the rearranging of the copper particles into bigger ones, which causes a decrease in the number of grain boundaries present and a decrease in the overall resistivity.

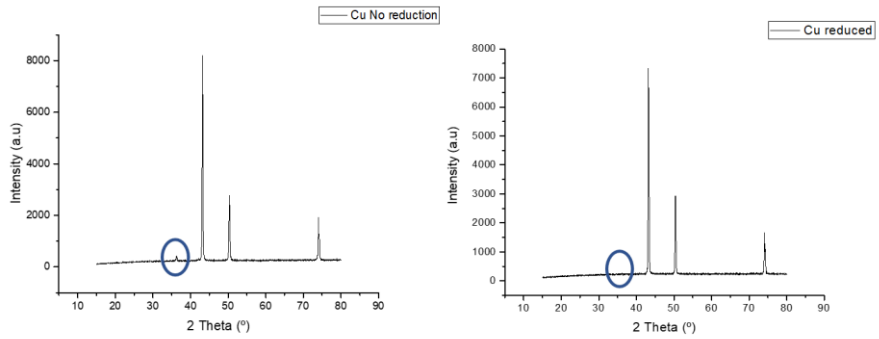

Figure 16: X-Ray diffraction of the CNT-Cu film, before (left) and after the thermal annealing (right). Oxygen, circled, is present before the thermal anneal, although in such small quantities that it is an unlikely cause for the increase in conductivity after annealing. After the thermal treatment, the same peak cannot be observed, showing that oxygen has been completely removed during the process.

The smaller conductivities are therefore likely to be cause by other factors other than the oxidation of the copper of the hybrid. One of the most plausible reasons could be due to the smaller carbon nanotube to copper ratio present in the fiber form as compared to the film hybrid, where a higher percentage of carbon nanotubes per meter can be found. This would reduce the overall conductivity, as CNTs have lower overall conductivities than a metal.

Having larger films allowed for the determination of the overall density of the material. Usual density determination test such as Archimedes test or helium pycnometry, proved incapable of measuring the density of these

films, therefore a different approach had to be used. Strips of the hybrid material, and pure copper strips with the same size were prepared. The volume was determined by SEM microscopy, to be as precise as possible with the thickness of the materials measured, and by means of optical microscopy to determine the larger width and length of the strip. All the strips were then measured, and density calculated from the weight and volume of each strip. 10 tests were carried out to determine a mean value of the hybrid and the copper strips' density. Results showed that copper had a density of 8.9 gcm^{-3}, the same as mentioned in bibliography, and the hybrid material exhibited densities in the order of 4.5 gcm^{-3} before the annealing process, and 5.9 gcm^{-3} after annealing had be carried out. The difference in the densities exhibited are most likely due to the reduction of free space inside the hybrid material once the thermal anneal is done, caused by the rearrangement of the copper particles within the fiber. However, even after the thermal treatment, the reduction of density when compared to pure copper was in the order of 34%.

Using the ampacity measuring cell together with the new DC AMREL SPS10-600 source, the ampacity measurements were carried out. At this point it is important to mention, that 4-point probe measurement was not possible due to the power unit setup. Instead, a 2-point probe measurement had to be done. The main reason for using 4-point measurements is to prevent error from the contact resistance as well as conducting line resistances. In order to diminish the impact of this kind of error in the 2-point probe measuring method which was used instead with the DC AMREL power unit, a thick, 1cm diameter copper cable was used. This thicker conducting line would have negligible resistance when compared to the sample's resistance, therefore allowing to measure with high degree of accuracy. Small steps of 0.05V at a time were applied until the sample test line reached the maximum current density, at which point the circuit breaker in the power unit opened. For comparative reasons, measurements were also carried out with pure copper films of the same thickness as the hybrid materials (Figure 17). From the results, several conclusions can be stablished; first, the current density that the hybrid material is able to withstand is in the same order of pure copper. Second, conductivities of the hybrid films are constant throughout the current densities applied unlike some small conductivity drops that has been observed in very thin copper films, where the copper crystal structure seems to rearrange at increasing current densities. When compared, it is easily seen that ampacity has not been improved by inserting carbon nanotubes into the material

although conductivity has not been affected negatively by this inclusion neither. Either way, it is safe to assume that although ampacity has not been improved, conductivity remains intact with a decrease in the overall density as it has been explained above. This material (although maybe not for the lightning strike protection systems which was the initial intended use), might be used as a substitute for conducting cables in places where the reduction of weight is of utmost importance, such as planes. Although many more tests should be carried out to prove the possibilities of these films, it is safe to assume that the objective and motivation of this thesis was fulfilled, finding a material which excels copper in density without sacrificing conductivity in the process. This work has led to a patent being published in the last months, proving the interest this hybrid material might have for industrial purposes in the aircraft industry (Patent reference: EP19382471)

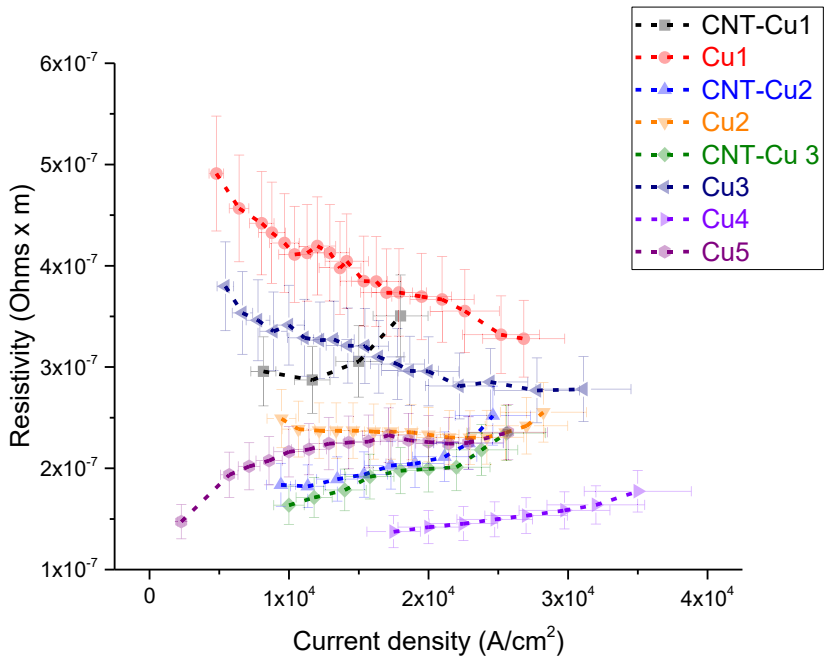

Figure 17: Current density against resistivity of CNT-Cu hybrid films and different samples of the same commercial pure copper film with 0.00135" thickness (onlinemetals) as described in materials and methods section in chapter 2. Resistivity values are in the same order as those exhibited by pure copper in most cases although ampacity (in the three different samples that were synthesized) was somewhat lower than the ampacity shown by pure copper. DC Amrel SP10-600 was used to obtain these measurements.

Unfinished work- Lightning simulation machine

Our group at Universidad Carlos III de Madrid, UC3M, is currently working in optimizing a method we have developed for measuring ampacity in thicker layers of material. The system consists on creating a home-made "lightning strike" laboratory, by using a set-up of 12 capacitors in parallel. The constructed example, consisted on 12 electrolytic capacitors, of 350V and 1000 μF, which together form a capacitor with a maximum voltage allowance of 350V and 12000 μF .The laminated sample is placed on a wooden surface, and a collector ring (made of thick copper) is placed on the outside of the sample to prevent any possible over-currents. A sharp copper electrode is placed above the surface of the sample and a drop of saltwater is used to create a conducting channel between tip and sample. It is important to notice, that the cross section of the connecting wires used is in the order of $1cm^2$, enough to reduce the voltage drop during the testing. A Rogowski probe is used to measure the current that passes through the electrode once the safety switch is turned on. As soon as the circuit is closed, the current will cause copper to migrate away from the contact zone creating a small gap that will become bigger together with the radial propagation of the current. The final size of the gap would give the user, the cross section of material that the current could not move, therefore giving a value of the maximum current density.

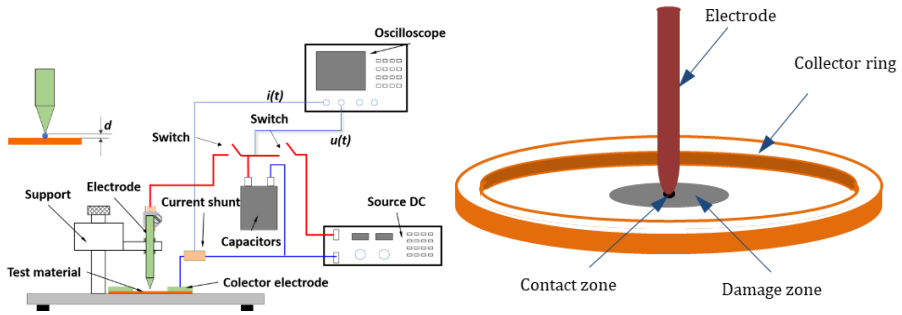

Figure 18: Set up of the lightning strike machine

The burn could be measured by means of SEM microscopy, but for an estimated calculation, photographs of the sample might also be taken. By means of image-J or any other image processing software, it is possible to calculate the area that has been migrated by the spark as seen in Figure 19.

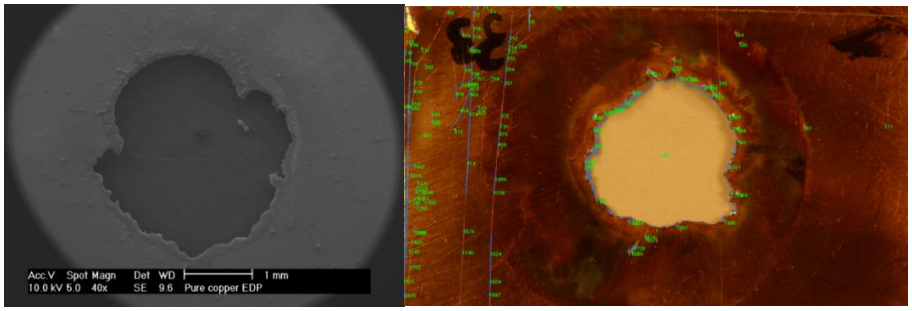

Figure 19: Left SEM microscopy of burn, right, image analysis for determining electromigrated area.

Many tests were carried out, using for this different voltages and samples. However, technical difficulties kept finding their way, so progress was usually slow. For instance, melting of the electrode tip was one of the initial setbacks that were encountered. The tip had to be replaced by a thinner tip (so that the density of charge in the contact area was bigger) but still the melting was causing material deposition on the sample, something that needs to be avoided. To avoid melting, the tip was separated from the sample, but the ionization of the air didn't happen, and therefore no spark was produced, so the addition of the water drop was necessary. Finally, the set-up begun to work, and the tests were finally possible. However, as this was late in the thesis, it was not possible to obtain a significant amount of data, to be able to correlate the ampacity to the burn marks' area. There were some trends observed during the last months, but there are too many variables to obtain an accurate result up to date. In line testing, the energy loss is minimized. By comparison, the lightning simulation machine that was developed during this work suffers from energy loss in the form of sound, light, heat and projection of material, so a deeper study of how to avoid these losses is completely necessary if someone is to correlate the mark left on the sample with its ampacity. This said, if enough time would have been placed on the optimization, this would probably be an outstanding alternative to the very expensive and demanding lightning machines [48] used by aircraft industry which cannot be used with smaller laboratory samples.

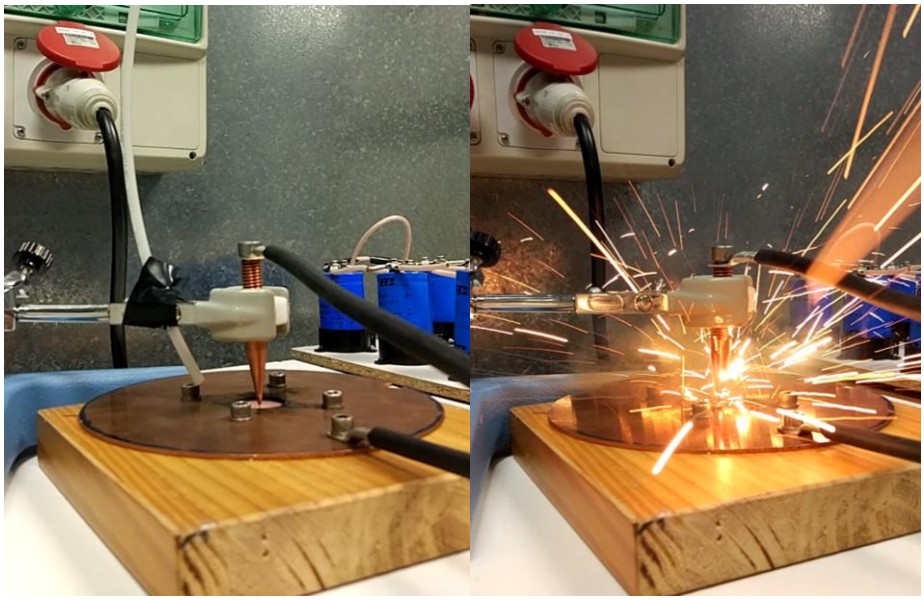

Figure 20: Two captions of the lightning strike test. Left, the sample is place in the sample holder and the tip is placed close to the sample. A drop of saltwater makes contact between the sample and the electrode. Right, the circuit is closed, discharging the capacitors in less than a second on top of the sample and causing a burn.

Chapter 5 conclusions

Carbon nanotubes with copper have been found to be a good alternative to pure copper as it was demonstrated by Subramaniam et al [38] first, presenting a material with one hundred times the ampacity and similar conductivity to copper. However, these tests that were carried out by Subramaniam were done at the nanoscale, presenting test lines with diameters in the order of 500 nm. This is a very important factor, as in such a thin structure, the contribution of grain boundaries is much smaller than in micro sized test lines, were the number of grain boundary defects is exponentially bigger with size. This factor, as it has been observed during the thesis, was also published years later by the same group, this time by Sundaram et al [34], where they discovered that the same outstanding ampacity could not be achieved at microscales, and in the best case scenario, only small improvements were observed. However, exactly as it was discovered during this thesis, the decrease in density even with the same ampacity could prove to be a huge benefit in substituting copper technology for industrial purposes.

Carbon nanotubes have other benefits in comparison to graphene or graphene oxide. First, the state of the art presents several synthesis methods to produce these carbon nanotubes in many forms and in industrial quantities. This is unthinkable to do with such a high purity material as graphene, making the synthesis of this material in industrial quantities impossible with modern techniques. Graphene, however, can be grown on the surface of many materials as a coating, which could prove beneficial for properties such as ampacity. This study was planned to be done during this thesis but was not tested due to time limitations. Graphene oxide on the other hand, is an interesting material as it can be synthesized in industrial quantities, and easily used for coating. However, it seems to possess no benefits for ampacity or conductivity at all.

Structures with carbon nanotubes also presents a very important advantage over the bidimensional carbon layers, and this is the porosity of the structures it makes. Due to their morphology, their packing is not as compact as the packing of graphene or graphene oxide when dry. This creates a porosity which can then be used for the insertion of copper ions and successful electrodeposition. This proved to be the most important factor, as copper could not be deposited inside the graphene oxide structures, no matter the many morphological changes they were subjected to.

Successful synthesis of a carbon nanotube-copper hybrid material has been achieved during this thesis, with a conductivity and ampacity as good as copper, but with a reduction of the overall density by 34%. This result concludes the thesis herein presented, having successfully achieved the main objective of the work.

Bibliography

[1] M. Su, B. Zheng, and J. Liu, "A scalable CVD method for the synthesis of single-walled carbon nanotubes with high catalyst productivity," *Chem. Phys. Lett.*, vol. 322, no. 5, pp. 321–326, May 2000.

[2] K. Hata, D. N. Futaba, K. Mizuno, T. Namai, M. Yumura, and S. Iijima, "Water-assisted highly efficient synthesis of impurity-free single-walled carbon nanotubes.," *Science*, vol. 306, no. 5700, pp. 1362–4, Nov. 2004.

[3] A. M. Cassell, J. A. Raymakers, J. Kong, and H. Dai, "Large Scale CVD Synthesis of Single-Walled Carbon Nanotubes," *J. Phys. Chem. B*, vol. 103, no. 31, pp. 6484–6492, Aug. 1999.

[4] E. V. Lobiak, E. V. Shlyakhova, L. G. Bulusheva, P. E. Plyusnin, Y. V. Shubin, and A. V. Okotrub, "Ni–Mo and Co–Mo alloy nanoparticles for catalytic chemical vapor deposition synthesis of carbon nanotubes," *J. Alloys Compd.*, vol. 621, pp. 351–356, Feb. 2015.

[5] Q. Zhao, Z. Xu, Y. Hu, F. Ding, and J. Zhang, "Chemical vapor deposition synthesis of near-zigzag single-walled carbon nanotubes with stable tube-catalyst interface," *Sci. Adv.*, vol. 2, no. 5, p. e1501729, May 2016.

[6] T. Maruyama *et al.*, "Single-walled carbon nanotube synthesis using Pt catalysts under low ethanol pressure via cold-wall chemical vapor deposition in high vacuum," *Carbon N. Y.*, vol. 96, pp. 6–13, Jan. 2016.

[7] J. K., L. Q., and F. S., "Spinning continuous carbon nanotube yarns," *Nature*, vol. 49, no. 1999, pp. 5246–5252, 2002.

[8] K. Liu *et al.*, "Carbon nanotube yarns with high tensile strength made by a twisting and shrinking method," *Nanotechnology*, vol. 21, no. 4, 2010.

[9] M. Zhang, K. R. Atkinson, and R. H. Baughman, "Multifunctional carbon nanotube yarns by downsizing an ancient technology," *Science (80-.).*, vol. 306, no. 5700, pp. 1358–1361, 2004.

[10] J. Hone *et al.*, "Electrical and thermal transport properties of magnetically aligned single wall carbon nanotube films," *Appl. Phys. Lett.*, vol. 77, no. 5, pp. 666–668, 2000.

[11] S. Muhl, R. Aguilar Osorio, and U. A. Martínez Huitle, "Transparent conductive carbon nanotube films," *Rev. Mex. Fis.*, vol. 63, no. 5, pp. 439–447, 2014.

[12] X.-H. Zhong *et al.*, "Continuous Multilayered Carbon Nanotube Yarns," *Adv. Mater.*, vol. 22, no. 6, pp. 692–696, Feb. 2010.

[13] B. Alemán, V. Reguero, B. Mas, and J. J. Vilatela, "Strong Carbon Nanotube Fibers by Drawing Inspiration from Polymer Fiber Spinning," *ACS Nano*, vol. 9, no. 7, pp. 7392–7398, Jul. 2015.

[14] J. J. Vilatela and A. H. Windle, "Yarn-Like Carbon Nanotube Fibers," *Adv. Mater.*, vol. 22, no. 44, pp. 4959–4963, Nov. 2010.

[15] B. Vigolo *et al.*, "Macroscopic Fibers and Ribbons of Oriented Carbon Nanotubes," *Science (80-.).*, vol. 290, no. 5495, pp. 1331–1334, Nov. 2000.

[16] L. M. Ericson *et al.*, "Macroscopic, Neat, Single-Walled Carbon Nanotube Fibers," *Science (80-.).*, vol. 305, no. 5689, pp. 1447–1450, Sep. 2004.

[17] M. Zhang, K. R. Atkinson, and R. H. Baughman, "Multifunctional Carbon Nanotube Yarns by Downsizing an Ancient Technology," *Science (80-.).*, vol. 306, no. 5700, pp. 1358–1361, Nov. 2004.

[18] K. Jiang, Q. Li, and S. Fan, "Spinning continuous carbon nanotube yarns," *Nature*, vol. 419, no. 6909, pp. 801–801, Oct. 2002.

[19] Y.-L. Li, I. A. Kinloch, and A. H. Windle, "Direct Spinning of Carbon Nanotube Fibers from Chemical Vapor Deposition Synthesis," *Science (80-.).*, vol. 304, no. 5668, pp. 276–278, Apr. 2004.

[20] K. Jiang, Q. Li, and S. Fan, "Nanotechnology: spinning continuous carbon nanotube yarns.," *Nature*, vol. 419, no. 6909, p. 801, 2002.

[21] M. Zhang, K. R. Atkinson, and R. H. Baughman, "Multifunctional carbon nanotube yarns by downsizing an ancient technology.," *Science (80-.).*, vol. 306, no. November, pp. 1358–1361, 2004.

[22] Q. Li *et al.*, "Sustained growth of ultralong carbon nanotube arrays for fiber spinning," *Adv. Mater.*, vol. 18, no. 23, pp. 3160–3163, 2006.

[23] K. Liu, Y. Sun, L. Chen, C. Feng, and X. Feng, "Controlled Growth of Super-Aligned Carbon Nanotube Arrays for Spinning Continuous

Unidirectional Sheets with Tunable Physical Properties," *Nano Lett.*, vol. 8, no. 2, pp. 700–705, 2008.

[24] Y. Nakayama, "Synthesis, nanoprocessing, and yarn application of carbon nanotubes," *Jpn. J. Appl. Phys.*, vol. 47, no. 10 PART 2, pp. 8149–8156, 2008.

[25] X. Lepr??, M. D. Lima, and R. H. Baughman, "Spinnable carbon nanotube forests grown on thin, flexible metallic substrates," *Carbon N. Y.*, vol. 48, no. 12, pp. 3621–3627, 2010.

[26] C. P. Huynh and S. C. Hawkins, "Understanding the synthesis of directly spinnable carbon nanotube forests," *Carbon N. Y.*, vol. 48, no. 4, pp. 1105–1115, 2010.

[27] R. Cruz-Silva *et al.*, "Super-stretchable graphene oxide macroscopic fibers with outstanding knotability fabricated by dry film scrolling," *ACS Nano*, vol. 8, no. 6, pp. 5959–5967, 2014.

[28] M. D. Lima *et al.*, "Biscrolling nanotube sheets and functional guests into yarns," *Science (80-.).*, vol. 331, no. 6013, pp. 51–55, 2011.

[29] X. Lepr??, R. Ovalle-Robles, M. D. Lima, A. L. El??as, M. Terrones, and R. H. Baughman, "Catalytic twist-spun yarns of nitrogen-doped carbon nanotubes," *Adv. Funct. Mater.*, vol. 22, no. 5, pp. 1069–1075, 2012.

[30] M. Zhang and R. Baughm, "Assembly of Carbon Nanotube Sheets," in *Electronic Properties of Carbon Nanotubes*, InTech, 2011.

[31] R. H. Baughman, "Towering forests of nanotube trees," *Nat. Nanotechnol.*, vol. 1, no. 2, pp. 94–96, Nov. 2006.

[32] A. A. Kuznetsov, A. F. Fonseca, R. H. Baughman, and A. A. Zakhidov, "Structural Model for Dry-Drawing of Sheets and Yarns from Carbon Nanotube Forests," *ACS Nano*, vol. 5, no. 2, pp. 985–993, Feb. 2011.

[33] J. Su, Y. Liu, M. Jiang, and X. Zhu, "Oxidation of copper during physical sputtering deposition : mechanism , avoidance and utilization."

[34] R. Sundaram, T. Yamada, K. Hata, and A. Sekiguchi, "Electrical performance of lightweight CNT-Cu composite wires impacted by surface and internal Cu spatial distribution," *Sci. Rep.*, vol. 7, no. 1, pp. 1–11, 2017.

[35] P. M. Hannula *et al.*, "Carbon nanotube-copper composites by electrodeposition on carbon nanotube fibers," *Carbon N. Y.*, vol. 107, pp. 281–287, 2016.

[36] D. J. Carbaugh, J. T. Wright, and F. Rahman, "Negative tone photolithography with photo-sensitised polymethyl methacrylate (PMMA)," *Microelectron. Eng.*, vol. 171, pp. 53–59, Mar. 2017.

[37] N. N. Le, T. C. Hue Phan, A. D. Le, T. M. Dung Dang, and M. C. Dang, "Optimization of copper electroplating process applied for microfabrication on flexible polyethylene terephthalate substrate," *Adv. Nat. Sci. Nanosci. Nanotechnol.*, vol. 6, no. 3, p. 035007, May 2015.

[38] C. Subramaniam *et al.*, "One hundred fold increase in current carrying capacity in a carbon nanotube-copper composite.," *Nat. Commun.*, vol. 4, p. 2202, Jan. 2013.

[39] K. Koziol *et al.*, "High-Performance Carbon Nanotube Fiber," *Science (80-.).*, vol. 318, no. 5858, pp. 1892–1895, Dec. 2007.

[40] M. Zhang, K. R. Atkinson, and R. H. Baughman, "Multifunctional Carbon Nanotube Yarns by Downsizing an Ancient Technology," *Science (80-.).*, vol. 306, no. 5700, pp. 1358–1361, Nov. 2004.

[41] B. Vigolo *et al.*, "Macroscopic fibers and ribbons of oriented carbon nanotubes.," *Science*, vol. 290, no. 5495, pp. 1331–4, Nov. 2000.

[42] C. Guo, Y. Zuo, X. Zhao, J. Zhao, and J. Xiong, "Effects of surfactants on electrodeposition of nickel-carbon nanotubes composite coatings," *Surf. Coatings Technol.*, vol. 202, no. 14, pp. 3385–3390, Apr. 2008.

[43] R. Sundaram, T. Yamada, K. Hata, and A. Sekiguchi, "Electrical performance of lightweight CNT-Cu composite wires impacted by surface and internal Cu spatial distribution," *Sci. Rep.*, vol. 7, no. 1, pp. 1–11, 2017.

[44] J. N. Coleman, U. Khan, W. J. Blau, and Y. K. Gun'ko, "Small but strong: A review of the mechanical properties of carbon nanotube-polymer composites," *Carbon N. Y.*, vol. 44, no. 9, pp. 1624–1652, 2006.

[45] E. T. Thostenson *et al.*, "Aligned multi-walled carbon nanotube-reinforced composites: processing and mechanical characterization," *J. Phys. D. Appl. Phys.*, vol. 35, no. 16, pp. L77–L80, 2002.

[46] C. Velasco-Santos, A. L. Martínez-Hernández, F. T. Fisher, R. S. Ruoff, and V. M. Castaño, "Improvement of Thermal and Mechanical

Properties of Carbon Nanotube Composites through Chemical Functionalization," *Chem. Mater.*, vol. 15, no. 23, pp. 4470–4475, 2003.

[47] K. L. Lei Lu. Yongfeng Shen, Xianhua Chen, Lihua Qian, "Ultrahigh Strength and High Electrical Conductivity in Copper," *Science (80-.).*, vol. 304, no. 5669, pp. 422–426, Apr. 2004.

[48] "Lightning Testing and Protection | NTS." [Online]. Available: https://www.nts.com/services/testing/lightning/. [Accessed: 02-Aug-2019].

Chapter 6: Final conclusions and future work

There are some conclusions that could be obtained from this work, and these will be summarized below, separately for each chapter.

Chapter 3 conclusions

- Electrophoretic deposition technique seems to be a promising technique for depositing charged particles such as graphene oxide platelets because it is quick, cost effective, scalable and could therefore be used for industrial purposes.
- Direct current electrophoretic deposition of graphene oxide on a copper electrode, causes oxidation as it has been demonstrated during this chapter. This is an important drawback that could be avoided completely by using pulse reverse electrophoretic deposition.
- When using pulse reverse electrophoretic deposition to deposit graphene oxide on the surface of copper, the conductivity achieved is the one given by the copper matrix and was never found to be higher. This is due to graphene oxide being heavily oxidized which makes conductivity of the layers very low, and therefore causing electrons to be conducted through the metal matrix. This causes conductivity to remain constant, always exhibiting the same conductivity as pure copper.
- Adding graphene oxide on the surface of the copper electrode causes a minimal increase in thickness, with almost no change in the overall density of the material (as compared to the initial bare copper).

Chapter 4 conclusions

- Graphene oxide dispersions can be used to synthesize, by means of hydrothermal synthesis, reduced graphene oxide fibers.

- During hydrothermal synthesis of graphene oxide, the oxygenated groups are reduced in the form of carbon dioxide, and thus causes the reduced graphene oxide platelets to re-stack into a 3D structure.
- The shape that the structure adopts, depends completely on the container used during the hydrothermal synthesis. If a small capillary of 100 micrometers is used, the fiber formed will have the same diameter when wet. After drying, the size of the fiber will shrink by about two thirds of the initial diameter.
- Even though hydrothermal synthesis reduces most of the oxygenated species in graphene oxide, the conductivity of such fibers is in the order of $3 \cdot 10^2$ Sm^{-1}, far below values exhibited by metals.
- Electrodeposition of copper on the surface of these fibers achieved conductivities up to $1 \cdot 10^6$ Sm^{-1}, values close to those exhibited by pure copper. However, copper was observed to remain in the exterior of the fiber, creating a ring like structure that coated the reduced graphene oxide core. Diffusion of copper ions int the interior of such fibers is very low, and most of the electrodeposition happens in the outside of the fibers where the concentration of copper ions is greater.
- If the fibers are frozen (liquid nitrogen), before they are able to dry, water will remain in the interior of such fibers. If lyophilization is then used, sublimation of the water crystals will induce microporosity in the core of these fibers.
- The structure of porous fibers has been found to be highly unreproducible. Even after using the same dispersions, capillaries, conditions and freeze-drying process, the inner structure of such fibers is completely different.
- Conductivity values of porous reduced graphene oxide fibers after undergoing electrodeposition reached values of $1 \cdot 10^6$ Sm^{-1}, achieving however a very heterogenous deposition throughout the inner core, and being most of the copper concentrated on the outside of the porous fiber.
- The high un-reproducibility of both, the reduced graphene oxide fiber's structure, and the electrodeposition of copper throughout the fiber, makes this technique unlikely to be used for industrial purposes. However, if a high specific surface area fiber is required, this could be a good alternative for smaller scale devices.

Chapter 5 conclusions

- Spinning from vertically aligned nanotube forests is a technique which consists on pulling from one of the vertically aligned nanotubes, which due to Van der Waal forces would attract the one next to it, and so forth, creating like this, yarns of chained carbon nanotubes. If instead of a single nanotube, a whole section of the vertical forest is pulled at the same time, the yarn would have the same size as the chosen section. The length of such yarns depends on how big the carbon nanotube forest is.
- It has been possible to obtain a forest of horizontally oriented carbon nanotubes by depositing layer after layer of oven pulled carbon nanotube yarns. The nanotubes used, were synthesized at 1250 °C by chemical vapor deposition from a mixture which contained thiophene, ferrocene and a carbon source, and using hydrogen as the carrier gas.
- When these yarns were twisted to form fiber like structures, the conductivity was found to be in the order of 1 Sm^{-1}. If instead of twisting the fibers, these were introduced into 2-propanol, the quick drying process caused the compaction of the yarns into fiber like structures, with conductivities up to $1 \cdot 10^3$ Sm^{-1}. This difference was due to the twisted fibers having high amounts of free space in their interior, whilst alcohol-drying lead to a reduction of the inner space.
- Electrodeposition on the twisted fibers (and equally on yarns) was not possible, due to the low conductivities these structures exhibited. Alcohol drying of these structures increased the conductivity and electrodeposition could be used. By electrodepositing these carbon nanotube fibers, conductivities up to $2 \cdot 10^6$ Sm^{-1} were achieved.
- SEM microscopies and EDX mapping proved that due to the porosity of these carbon nanotube fibers, copper ions could penetrate easily into the interior of the fiber during electrodeposition, which lead to a homogeneous copper-carbon nanotube hybrid material being synthesized.
- The oven drawn technique is similar to the vertical forest pull technique, with the difference that the initial carbon nanotube pull is done in the interior of the reactor's furnace. An aerogel of carbon nanotubes exists within such chamber, and the pull begins a chain

reaction of carbon nanotubes attracting the next, by Van der Waal forces, producing a continuous yarn of oriented nanotubes. Exactly like forest spun yarns, these yarns can be compacted by means of alcohol drying, improving conductivity by two orders of magnitude.

- Electrodeposition on oven drawn fibers was found to be effective for producing hybrid carbon nanotube – copper fibers, and the conductivity of such structures reached values of pure copper, $2 \cdot 10^7$ Sm^{-1}.
- Density measurements of microfibers, are, up to date, highly complicated, and in most cases, laboratory equipment is not able to measure with such degree of accuracy and resolution. New techniques for measuring density of microfibers should be searched for, as there is a lack of knowledge in this field. BET, Archimedes' test or helium pycnometry are just a few of the techniques that were used for this end during this thesis, with no success due to the size and weight of this material.
- Carbon nanotube films can be produced, by aligning parallel to each other, yarns of oven drawn carbon nanotubes. Thickness of these films can be finely tuned by adjusting the number of yarns placed. The orientation can be finely tuned by changing the drawing velocity.
- Films can also be compacted by means of alcohol drying producing films with a conductivity close to $1 \cdot 10^3$ Sm^{-1}. These 15-20 um films can be electrodeposited just like the fibers, and copper was seen to penetrate throughout the carbon nanotube matrix homogeneously. Copper grains can be clearly observed in these cases, and conductivities are in the order of $1 \cdot 10^4$ Sm^{-1} due to the many grain boundaries present. Apparent density of this initial material, as measured by the macroscopic dimensions of the specimen and its weight, is in the order of 4.5 gcm^{-3}, half of the one observed in copper.
- When these films are further annealed at 700 Cº in a reducing atmosphere, the conductivity rises to $2 \cdot 10^6$ Sm^{-1} and ampacity reaches values of $2.5 \cdot 10^4$ Acm^{-2}, values exhibited by ultra-thin copper films. After annealing, the grain boundaries are reduced in number, and the density rises to 5.9 gcm^{-3}. This, when compared to pure copper, translates into a density reduction of around 35%, whilst maintaining conductivity and ampacity in the same order of magnitude as pure copper.

- These results show that this material can be a very good alternative for industry. Initially, lightning strike protection, and thus, ampacity, was searched for. However, it was observed that conductivity values were outstanding with respect to density (and to copper), and therefore the potential uses of such material have increased exponentially. Electrical cabling, for instance, could be one of the many uses given to these materials in aeronautical industry.